Chapter 2

GENERALIZED TRANSITION STATE THEORY

Donald G. Truhlar, Alan D. Isaacson, and Bruce C. Garrett

TABLE OF CONTENTS

"Generalized Transition State Theory," D. G. Truhlar, A. D. Isaacson, and B. C. Garrett, in Theory of Chemical Reaction Dynamics, edited by M. Baer (CRC Press, Boca Raton, FL, 1985), pp. 65-137.

I. INTRODUCTION

The calculation of reliable thermal rate constants for elementary gas-phase chemical reactions has been a subject of great interest since the advent of quantum mechanics. Examples of current areas for which thermal rate information is indispensable include combustion chemistry and atmospheric chemistry, especially in the study of pollutants. In this chapter we shall concentrate on generalized transition-state theory (GTST) calculations of the rates of bimolecular reactions of the general form:

$$A + B \rightarrow C + D \tag{1a}$$

where A, B, C, and D are atoms or molecules. We will also consider the high-pressure limit of unimolecular reactions, such as unimolecular decomposition:

$$A \rightarrow C + D \tag{1b}$$

or isomerization:

$$A \rightarrow C \tag{1c}$$

The extension of the methods presented here to reaction Equations 1b or c at low pressures requires the additional consideration of energy-transfer activation steps; this extension will not be treated.

The scope of this chapter can be illustrated by a simple example, the reaction of an oxygen atom with an OH radical. This reaction has been studied experimentally at low pressure where the dominant mechanism is atom transfer:

$$O + OH \rightarrow H + O_2 \tag{1d}$$

Although the stable intermediate HO_2 must be formed temporarily, the pressure is low enough that stabilizing collisions are rare and one can ignore the side reaction:

$$O + OH + M \rightarrow HO_2 + M \tag{1e}$$

The methods presented in this chapter can be used to study reaction Equation 1d or its reverse in the low-pressure limit where only binary collisions need be considered, or to study reaction Equation 1e or its reverse in the high-pressure limit where they become second and first order, respectively; however, these methods are insufficient to study the competition between these routes at intermediate pressures. In transition state theory (TST) the fundamental assumption (discussed in more detail below) is that all transition state species have been created directly from reactants and will directly convert to products. The transition state approximation to the rate is the rate of formation of transition states so the products are not explicitly involved in the calculation. Thus, identical, TST calculations would be performed and identical results would be obtained for the binary-collision rate constant for reaction Equation 1d and for the high-pressure limit of the rate constant for reaction Equation 1e.

The calculation of a rate constant requires a knowledge of the potential energies of the reacting system; thus, we assume that a Born-Oppenheimer potential energy surface is available for the system under consideration. It is very important to keep in mind that the accuracy of the computed results is limited by the accuracy of the potential energy surface. The collision theory approach for obtaining the thermal rate constant involves a Boltzmann

average of the energy-dependent reaction cross section,[1,2] which can be approximated with either classical trajectory calculations (recently reviewed by one of the authors and Muckerman;[2,3] see also Chapter 1 of Volume III) or quantum mechanical coupled-channel calculations (see, e.g., two reviews [4,5]). Unfortunately, even if truly accurate potential energy surfaces were available, accurate cross section calculations are not practical for three-dimensional studies of reactions that involve more than three atoms. In fact, quantal cross sections or rate constants that are numerically converged for a given potential energy surface are available only for the H + H_2 reaction.[6,7] An alternative to collision theory is provided by TST. Since this theory, especially in its conventional formulation, is relatively easy to apply, this approach has become quite popular, and it is discussed in several monographs and texts.[8-15] From the standpoint of classical dynamics, the fundamental assumption of TST is that the net rate of forward reaction at equilibrium is given by the flux of trajectories across a predetermined surface in phase space in the product direction.[16] This surface must divide reactants from products. In conventional TST, this phase space dividing surface is chosen to be a function of just the coordinates (not momenta) and is located in such a way that it passes through the saddle point of the potential energy surface, which is the highest energy point on the minimum energy path (MEP) from reactants to products. A consequence of the fundamental assumption is that classical TST will only provide the exact classical rate constant if every trajectory passing through the dividing surface toward products crosses it only once.[17] In other words, if the dividing surface were located at a perfect bottleneck to reaction, to which trajectories, having left, never returned, then classical TST would yield the exact classical rate constant. However, there often exist trajectories which do cross the dividing surface more than once. Some examples of such trajectories for the collinear Cl + HD system on the Stern-Persky-Klein potential energy surface[18,19] are shown in Figure 1; further discussions are provided elsewhere.[20,21] Since such recrossing trajectories lead to an equilibrium flux across the dividing surface that exceeds the net reaction rate, the classical TST rate constant will overestimate the exact classical result when recrossing occurs. Stated another way, this says that classical TST provides an upper bound to the true classical rate constant.

There are several reasons why the classical upper bound of conventional TST is unsatisfactory. First, the amount by which classical conventional TST overestimates the true classical rate can be large, and it can be expected to increase with increasing temperature. For example, for the collinear reaction Cl + HD → ClH + D, the conventional classical TST rate constants are larger than the exact classical values by factors of 1.1 at 300 K, 2.8 at 1500 K, and 9.6 at 4000 K.[21] Second, accurate information about the potential energy surface for the reacting system, including the height of the barrier to reaction, is not often available. In fact, a widely used procedure is to estimate such information by adjusting the surface parameters so that conventional TST reproduces experimental rate constants, activation energies, or kinetic isotope effects. Hence, the dynamical errors in conventional TST are compensated for by errors in the empirically derived potential energy surface. However, the most serious difficulty with the classical upper bound is that quantal effects play a major role in most chemical reactions.

The fact that classical TST yields an upper bound to the true classical rate constant suggests that one way of improving the results would be to vary the location of the dividing surface through which the equilibrium flux in the product direction is calculated in order to obtain the minimum rate constant.[21-29] In this way, one obtains the lowest upper bound to the true classical rate constant within the space of variations of the dividing surface, which in this context is labeled a generalized transition state. The method used in the present chapter is to consider a one-parameter family of dividing surfaces perpendicular to a prespecified reaction coordinate, which is a degree of freedom along which we may measure progress from reactants to products. We variationally optimize the dividing surface parameter for a

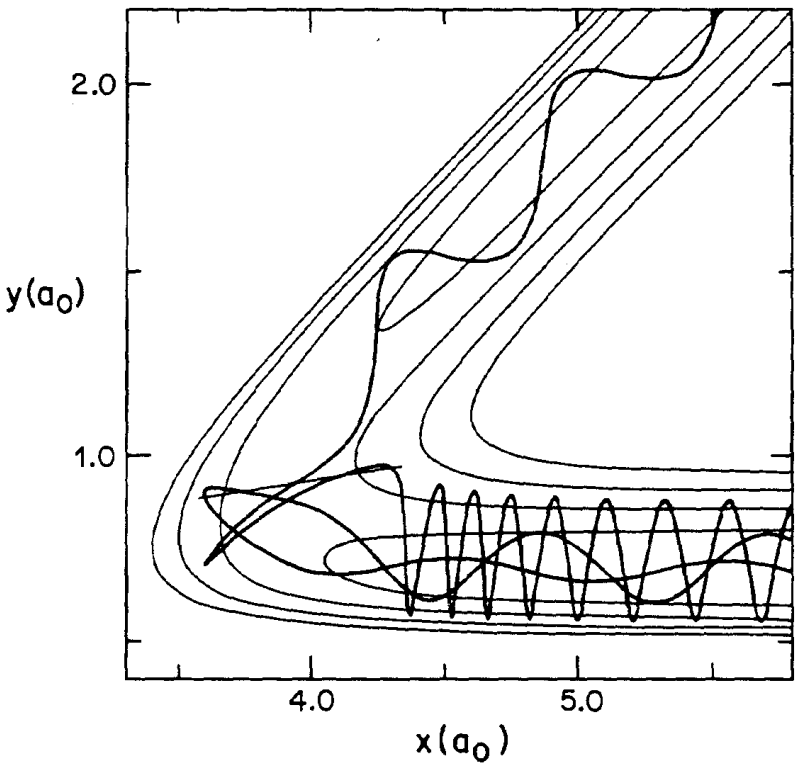

FIGURE 1. Two trajectories (heavy curves) for the collinear reaction Cl + HD → ClH + D on the Stern-Persky-Klein surface[18,19] superimposed on potential energy surface contours (lighter curves). The trajectories start at the lower right, cross the conventional transition state (indicated by a straight line through the saddle point) more than once, and either do not react (return to lower right) or eventually react (exit interaction region toward top of figure). The abscissa x is the distance from Cl to the center of mass of HD; the ordinate y is the HD internuclear distance scaled so that the reduced mass for y motion is the same as for x motion.

calculation in which the motion across the dividing surface is treated classically (but other degrees of freedom except possibly rotation, for which the classical approximation is usually adequate, are quantized), and then we use this calculation as a foundation on which to add quantal effects on reaction-coordinate motion. The most complete calculation we perform is to find the variationally best dividing surface for each total energy;[20,21] this is called microcanonical variational theory (μVT). For some reactions it may be desirable to go beyond this and find the variationally best dividing surface for each total energy and angular momentum. For most reactions, though, it is sufficient to find the best single compromise dividing surface for all energies and angular momenta contributing significantly to the rate constant at each given temperature. The latter procedure is called canonical-ensemble variational TST, or simply canonical variational theory (CVT). This approach has proved to be a practical method for calculating thermal rate constants for atom-diatom reactions[20,30-47] and has also been applied successfully to the OH + $H_2 \rightleftharpoons H_2O$ + H reaction and its isotopic analogs using a general polyatomic formalism.[39,48] In this chapter we present the equations necessary for calculating the rate constant by both μVT and CVT, with the simpler CVT equations considered first. We shall also present the equations for improved canonical variational theory (ICVT).[34] This method is a threshold-corrected version of CVT that may give comparable accuracy to μVT at low enough temperatures while requiring only

a slightly more involved calculation than CVT. The methods in this chapter may also be used to perform conventional TST calculations as a special case similar to CVT; the only difference is that the dividing surface is positioned at the highest saddle point rather than being determined by the minimization of the rate constant.

As mentioned above, it is not accurate to calculate reaction rate constants in classical terms. A proper description of chemical reactions requires the inclusion of quantum mechanical effects, especially at lower temperatures. Such effects are usually incorporated into conventional TST as follows.[8-15] First, a reaction coordinate is separated out, with motion along this coordinate treated classically. The remaining degrees of freedom of the transition state are then assigned quantized energy levels just as in the case of a bound state. This implies that one must deal with quantized energy levels and that the transition state contains zero-point energy. In addition, quantum effects on the reaction coordinate are treated by multiplying the rate constant by a transmission coefficient, which primarily corrects for the degree to which the reaction proceeds by tunneling through the barrier to reaction rather than by classically surmounting it. As mentioned in the previous paragraph, we adopt a similar approach in variational transition state theory (VTST). A major topic of discussion in this chapter concerns the details of how quantum mechanical effects can be incorporated in a consistent manner in both conventional TST and VTST by procedures of this kind. Once these effects are included in the VTST calculations, one no longer obtains a strict bound by varying the transition state location to minimize the calculated rate constant. Nevertheless, the evidence obtained to date indicates that this kind of approach to including quantum effects is capable of providing rate constants of useful accuracy for a given potential energy surface. Furthermore, the VTST formulation often offers significant improvement over the results of conventional TST. (See reviews[5,20,39,46,47] and four more recent papers.[42,43,49,50]) In many cases, an important element in this success is the ability to reliably calculate tunneling contributions, and the present chapter contains a detailed discussion of this topic.

Another topic that is discussed in this chapter is anharmonicity, which is important in TST because the quantized degrees of freedom of the generalized transition state corresponding to vibrations of the reacting system are bound by a potential energy surface that is, in general, anharmonic. There have been several studies[30,39,48,51-56] of the effect of anharmonicity on conventional TST and /or VTST calculations. These studies show that in many (but not all) cases rate constants computed with anharmonic vibrations differ significantly from the harmonic results. Thus, a practical method for including anharmonicity in the calculation of the vibrational energy levels is needed, and the inclusion of anharmonicity in a practical manner in conventional TST and in VTST calculations is discussed in this chapter.

This chapter does not attempt to review the entire literature of TST or even of generalized TST. The goal here is to explain the general features of the theory and to illustrate them by describing in detail some of the methods we use in our own calculations. Although there has been a large amount of fundamental work applying TST to one-dimensional systems (collinear reactions), the present chapter is concerned almost entirely with reactions in a three-dimensional world. We give some examples and references involving collinear reactions, but the treatment is general and all equations apply to reactions involving any number of atoms in the fully three-dimensional world.

Section II describes those parts of a generalized TST rate-constant calculation that are the same for a classical or quantal world, namely finding the saddle point, calculating the reaction path, normal modes, generalized normal modes, and moments of inertia, and numerical procedures for finding the variational transition state; Section III discusses the rest of a CVT rate-constant calculation for quantized bound degrees of freedom and classical reaction-coordinate motion; Section IV discusses the incorporation of quantum effects on the reaction-

coordinate motion; Section V gives formulas for improving on the CVT calculation by using ICVT or μVT to obtain a less recrossed dividing surface; Section VI discusses improving any of the variational results by using the unified statistical theory or unified dynamical theory to estimate the recrossing of the variationally optimized dividing surface; Sections VII and VIII contain concluding remarks.

This chapter also includes an appendix in which TST is related to an exact collision theory treatment involving cross sections. We hope that this will contribute to a better understanding of the assumptions of TST. A second appendix contains a derivation of the cut-off rotational partition function and sum of states that are needed for ICVT calculations. The final appendix is an alphabetical list of abbreviations.

II. CLASSICAL CANONICAL VARIATIONAL THEORY

A. General Theory

In this section, the basic procedures for the application of CVT to the general thermal reaction of Equation 1a, 1b, or 1c are presented. We begin with a definition of the coordinate system. Assume that there are a total of N atoms in the reacting system (with N_A in reactant A, etc.) and let i = 1,2,...,N label the atoms. Suppose $R_{i\gamma}$, for γ = x, y or z, are the laboratory-frame cartesian coordinates of atom i with respect to the center of mass of the system. We employ a mass-scaled coordinate system[48] defined by

$$x_{i\gamma} = (m_i/\mu)^{1/2}R_{i\gamma}\,, \qquad i = 1,2,\ldots,N;\ \gamma = x, y, z \tag{2}$$

where m_i is the mass of atom i and μ is an arbitrary mass. Our convention for reaction Equation 1a is that μ is the reduced mass of reactant relative translational motion:

$$\mu = m_A m_B/(m_A + m_B) \tag{3a}$$

where m_A and m_B are the masses of reactants A and B, respectively. For reaction Equation 1b we take:

$$\mu = m_C m_D/(m_C + m_D) \tag{3b}$$

and for reaction Equation 1c we take μ equal to the mass of one of the atoms in the system. The motivation for the choice of coordinate system in Equation 2 can be seen by considering the kinetic energy of nuclear motion, which simplifies from:

$$T = {}^1/_2 \sum_{i=1}^{N} m_i \sum_{\gamma} (dR_{i\gamma}/dt)^2 \tag{4}$$

in cartesian coordinate space to:

$$T = {}^1/_2\mu \sum_{i=1}^{N} \sum_{\gamma} (dx_{i\gamma}/dt)^2 \tag{5}$$

in mass-scaled cartesian coordinates, where t denotes time. Thus, the kinetic energy of nuclear motion is diagonal (i.e., contains no cross terms) as a quadratic form in the momenta with the same mass for all $x_{i\gamma}$ coordinates. That is, the same mass (μ) is associated with motion in any direction, so that motion of the many-atom system governed by the potential energy surface $V([R_{i\gamma}])$ is equivalent to the motion of a point of mass, μ, governed by the

potential $V[x_{i\gamma}]$). As discussed below, this property of the mass-scaled coordinate system greatly simplifies the calculation of vibrational energies and partition functions, because the normal coordinates of vibration,[57] in which the kinetic energy and the potential energy through quadratic terms are simultaneously diagonal, can be obtained by a linear transformation involving only the potential energy.

Conveniently, for any coordinate system in which the kinetic energy is diagonal as a quadratic form in the momenta and in which the same mass is associated with motion in any direction, the path of steepest descent from the saddle point to reactants and products, obtained by following the direction of the negative of the potential gradient (producing a path which is everywhere perpendicular to equipotential surfaces of potential energy), will be the same.[58] Furthermore, the steepest-descents path in such a coordinate system is very suitable for dynamical interpretations.[59-61] It corresponds to the "intrinsic" reaction coordinate, i.e., to the zero-kinetic energy trajectory given by the solution of Hamilton's classical equations of motion for a system whose instantaneous motion is continuously damped to an infinitesimal speed.[60,61] This path will be called the minimum energy path (MEP) in the present chapter, and we will usually take this path as the reference path used to define the sequence of dividing surfaces.

The present choice of coordinate system is quite similar to the conventional mass-weighted coordinates [57] used in vibrational spectroscopy, in which each $R_{i\gamma}$ coordinate is multiplied by $m_i^{1/2}$. The advantage of the mass-scaled coordinates used here is that distances have units of length, whereas distances in the mass-weighted coordinate system have units of (mass)$^{1/2}$ length. A third example of a set of coordinates in which the nuclear kinetic energy is diagonal and the same mass is associated with motion in any direction is the mass-scaled Jacobi coordinate system,[2,21,58] which is very convenient for describing collisions in collinear atom-diatom systems (denoted here by a + bc). In this case, one coordinate is the distance from the atom (a) to the center of mass of the diatom (bc), while the other coordinate is the bc internuclear distance scaled by $(\mu_{bc}/\mu)^{1/2}$, where the diatomic reduced mass (μ_{bc}) is

$$\mu_{bc} = (m_b m_c)/(m_b + m_c) \tag{6}$$

Figure 2 illustrates the potential energy surfaces and MEPs in mass-scaled Jacobi coordinates for three systems that will be discussed later in this chapter.

The reaction coordinate(s) is defined as the signed distance along the reference path. As mentioned above, we usually take the reference path to be the MEP. Then, if there is at least one saddle point along the MEP, s is measured from the highest saddle point (or earliest, if there are two or more of equal height). For reaction Equation 1a values of $-\infty$, 0, and ∞ refer to reactants, saddle point, and products, respectively. The reactant, saddle point, and product values of s are denoted s^R, 0, and ∞ for reaction Equation 1b, and they are denoted s^R, 0, and s^P for reaction Equation 1c. For reactions of the form of Equation 1a or 1b that do not have a saddle point, one must follow the path of steepest descent by starting with A and B (or C and D) at large but finite separations; in such cases $s = 0$ has no special meaning.[47] In CVT, the generalized transition state (GTS) dividing surface through which the equilibrium flux is computed is assumed to be a function only of coordinates and not of momenta. For systems with four or more atoms or for three-atom systems with noncollinear reference paths,* we take the GTS to be a hypersurface in $x_{i\gamma}$ coordinates which is parametrized by the value of s at which it intersects the reference path. We further require the GTS to be perpendicular to the MEP at and near the point of intersection, but far from the

* Although the procedures discussed in this chapter are general and could be applied to atom-diatom reactions with linear MEPs, we have used many special procedures for that simplest of all cases. Only a few of these are discussed in the present chapter; others are discussed in References 21, 33, 34 and 58.

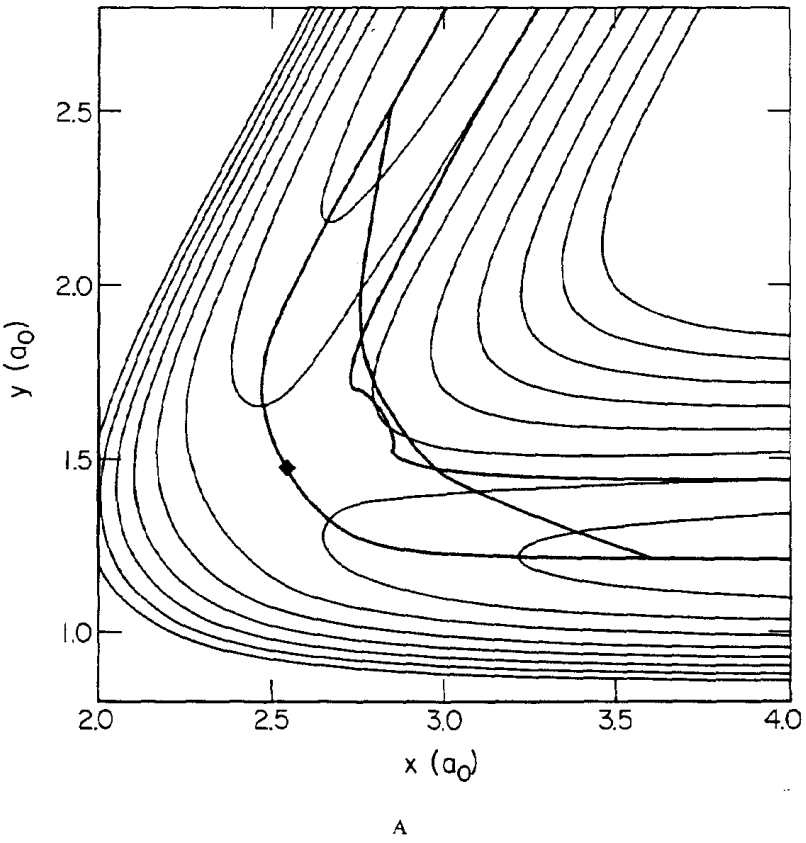

FIGURE 2. Potential energy contours, MEPs, and tunneling paths for three collinear atom-diatom reactions plotted in scaled and skewed coordinates obtained by mass-scaling the Jacobi coordinates as described in Figure 1. In each part, the solid diamond indicates the location of the saddle point, and the heavy curve passing through the saddle point is the MEP. (A) Contours for the H + H_2 reaction on surface no. 2 of Reference 168 are from 4 to 32 kcal/mol spaced every 4 kcal/mol. The MCP is the path on the concave side of the MEP. The optimum LAG tunneling path (α = 0.432) for a total energy of 8.8 kcal/mol starts and ends on the MEP and crosses the MCP in the saddle point region. (B) Contours for the Cl + HD reaction on the potential of References 18 and 19 are from 3 to 21 kcal/mol spaced every 3 kcal/mol. Tunneling paths for α = 0, 1/3, 2/3, and 1 at a total energy of 8 kcal/mol are shown. The α = 0 path is the MEP and the α = 1 path is the straight-line path. (C) Contours for the Cl + HCl reaction on the potential of Reference 49 are from 4 to 16 kcal/mol spaced every 2 kcal/mol. The straight line between the MEP in the reactant and product channels is the LCG tunneling path between the reaction-coordinate turning points for a total energy of 7.8 kcal/mol.

intersection with the MEP, we allow the GTS to bend if necessary in order to truly divide reactants from products up to the lowest dissociation energy of the system.

In certain circumstances it may be desirable to calculate the equilibrium flux through dividing surfaces which are orthogonal to paths other than the MEP. For example, if the potential energy surface is very flat in the region of the saddle point, following the gradient is numerically difficult because it is small, and it might be more convenient to choose an arbitrary smooth path through this region than to follow the gradient. Another example of a case in which the MEP might not be the best path to follow arises when a system exhibits multiple saddle points separated by low barriers.[44] The present discussion does not deal with reference paths other than the MEP; for completely general choices of the reaction path,

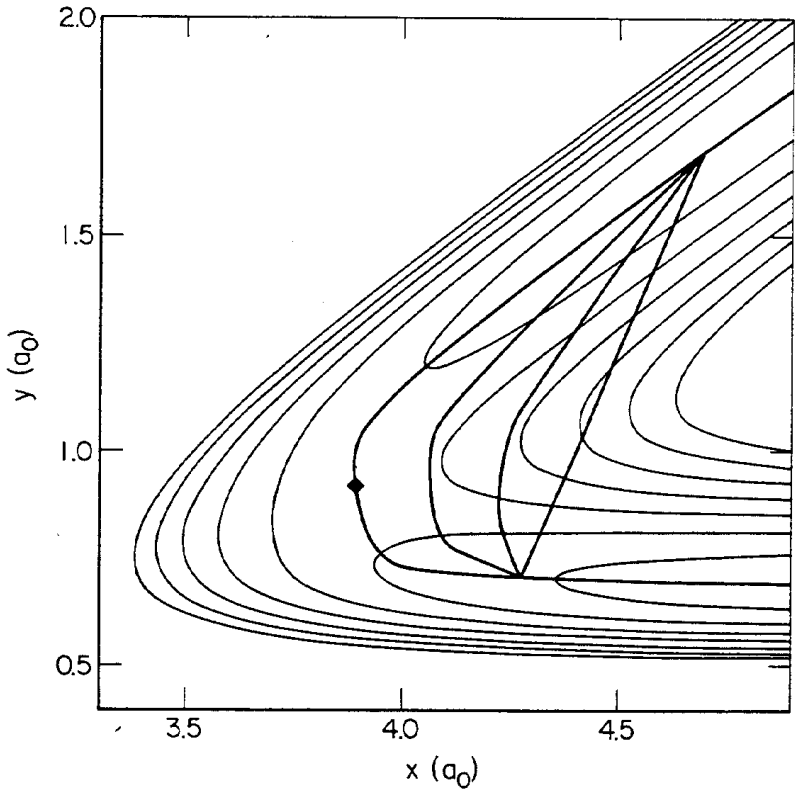

FIGURE 2B

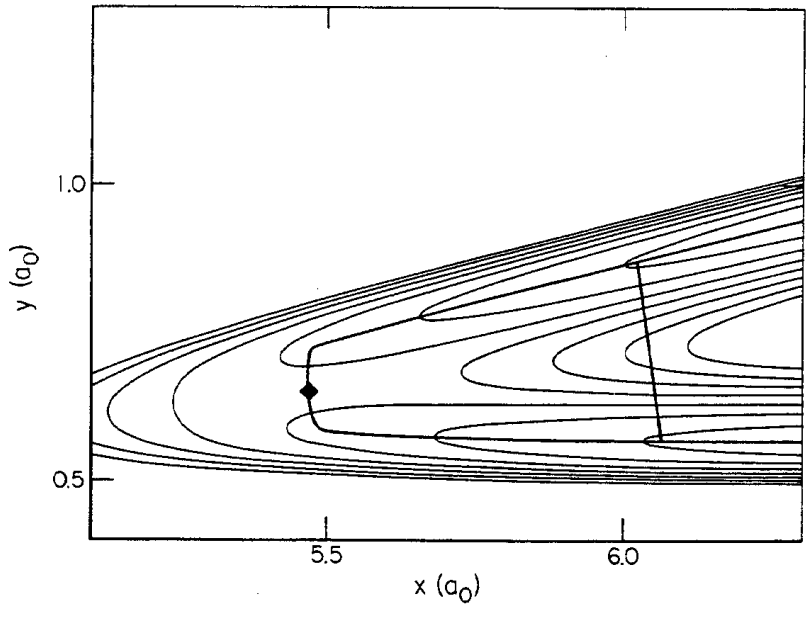

FIGURE 2C

one requires a more general expression for the reaction-path Hamiltonian, as discussed elsewhere.[62,63] (See also further work.[64,65]) In the rest of this chapter we will assume that the reference path is always taken as the MEP.

If, as just discussed, we take the reference path as the MEP and set $s = 0$, the above definition of the GTS provides the conventional TST dividing surface. For a canonical ensemble of reacting classical mechanical systems characterized by a temperature T, the conventional TST rate constant $k_C^{\ddagger}(T)$ is the equilibrium one-way flux coefficient of phase-space trajectories through this dividing surface in the product direction. This may be calculated as the net density of forward-crossing states per unit time divided by the density of reactant states per unit volume, and the resulting approximate expression for the thermal rate constant may be stated in terms of equilibrium partition functions of the reactants and a quasiequilibrium partition function of the transition state as follows:

$$k_C^{\ddagger}(T) = \frac{\sigma}{\beta h} \frac{Q_C^{\ddagger}(T)}{\Phi_C^{R}(T)} \exp(-\beta V^{\ddagger}) \tag{7a}$$

Here β is $(k_B T)^{-1}$, where k_B is Boltzmann's constant, h is Planck's constant, and $Q_C^{\ddagger}(T)$ is the conventional transition state classical partition function with its zero of energy at the saddle point. $\Phi_C^{R}(T)$ is the reactants classical partition function per unit volume for reaction Equation 1a or the unitless reactant classical partition function for reaction Equation 1b or 1c; in any case, its zero of energy is at the overall zero of energy, which corresponds to infinitely separated reactants, each at its own classical equilibrium position, i.e., V_{MEP} ($s = -\infty$) = 0, for reaction Equation 1a, or to the reactant classical equilibrium position for reaction Equation 1b or 1c, i.e., V_{MEP} ($s = s^R$) = 0. These classical partition functions are phase-space integrals involving $\exp(-\beta V)$, so that the fact that $Q_C^{\ddagger}(T)$ is calculated with its zero of energy at the saddle point gives rise to the exponential factor in Equation 7a, where $V^{\ddagger}$ is the classical potential energy of the saddle point measured from the overall zero of energy. In both these partition functions, the rotational symmetry numbers have been set to unity because the symmetry factor (σ) in Equation 7a represents the reaction path multiplicity, i.e., the number of equivalent reaction paths from reactants to products.[12] For example, in the case of an atom-diatom collision, $\sigma = 2$ if the diatom is homonuclear but $\sigma = 1$ if the diatom is heteronuclear. In addition, note that neither $Q_C^{\ddagger}(T)$ nor $\Phi_C^{R}(T)$ contains a contribution from overall translation of the system. We could include this contribution in both the numerator and denominator of Equation 7a, but it would cancel.

If desired we can include a transmission coefficient in Equation 7a. This yields:

$$k_C^{\ddagger/Y}(T) = \kappa_C^{\ddagger/Y}(T)\, k_C^{\ddagger}(T) \tag{7b}$$

where the transmission coefficient $\kappa_C^{\ddagger/Y}(T)$ may be used to account for effects such as quantum mechanical tunneling along the reaction coordinate. Y is a generic label that denotes the method used to calculate the transmission coefficient. This is discussed in Section IV; in this section we set $\kappa_C^{\ddagger Y}(T)$ to unity.

With regard to applying Equations 7a and 7b, or the generalized TST expressions discussed below to high-pressure unimolecular reactions, it may be useful to make an extra comment about the treatment of rotation. Since we have included all degrees of freedom in $Q_C^{\ddagger}(T)$ and $\Phi_C^{R}(T)$, we have implicitly assumed that all degrees of freedom exchange energy freely in the energized reactant. The standard terminology for this is that all modes are active. It is more common in the theory of unimolecular reactions to assume that all vibrations are active but that rotations are adiabatic. The reader is referred to standard references, e.g., Setser's review[66] and references therein, for the changes this makes in Equation 7a; rotational effects in unimolecular reactions will not be discussed further in this chapter.

Notice that although we have defined the TST rate constants in dynamical terms (flux through a dividing surface), the resulting rate expression has an appealing quasiequilibrium (or quasithermodynamic) interpretation. We define a transition state quasiequilibrium constant by

$$K_C^{\ddagger}(T) = \frac{Q_C^{\ddagger}(T)}{\Phi_C^R(T)} \exp(-\beta V^{\ddagger}) \tag{7c}$$

so the rate constant becomes

$$k_C^{\ddagger}(T) = \sigma(\beta h)^{-1} K_C^{\ddagger}(T) \tag{7d}$$

[*Note:* Since $\Phi_C^R(T)$ has different units for reaction Equation 1a than for reaction Equation 1b or 1c, so does $K_C^{\ddagger}(T)$. In particular, $K_C^{\ddagger}(T)$ has units of inverse concentration (volume per molecule) for reaction Equation 1a but is unitless for reaction Equation 1b or 1c.] The quantity $(\beta h)^{-1}$ in Equation 7d is sometimes called the universal transition state frequency factor. Equation 7d gives the same rate constant we would obtain if we postulated that transition states are in equilibrium with reactants and they unimolecularly convert to products with the rate constant $(\beta h)^{-1}$ for each of σ symmetry-related elementary reactions. (Actually, it is more correct to say that transition states are in "quasiequilibrium" with reactants since transition states are localized on a surface, i.e., they have one less degree of freedom than chemical species.) This equilibrium postulate is employed in the most popular derivations of TST in elementary textbooks, but it is important to emphasize that the theoretically most justifiable derivation of Equation 7a or 7d does not rest on this simple picture. In the collision theory derivation, the factor $(\beta h)^{-1}$ is just an accumulation of physical constants arising from the calculation of the flux through a dividing surface. Because the relationship of TST to collision theory is very important, it is discussed further in an appendix to this chapter.

If we now consider a GTS which intersects the MEP at some nonzero value of s, we can define a generalized TST rate constant $k_C^{GT}(T,s)$ at temperature T for this dividing surface by a straightforward extension of Equation 7a:[21]

$$k_C^{GT}(T,s) = \frac{\sigma}{\beta h} \frac{Q_C^{GT}(T,s)}{\Phi_C^R(T)} \exp[-\beta V_{MEP}(s)] \tag{8}$$

where $V_{MEP}(s)$ is the classical potential energy at point s on the MEP relative to the overall zero of energy, and $Q_C^{GT}(T,s)$ is the classical partition function for the GTS dividing surface with its zero of energy at $V_{MEP}(s)$ and with all rotational symmetry numbers set to unity. As discussed in Section I, for a fixed temperature the lowest upper bound on the true classical rate constant for the assumed set of GTS dividing surfaces is found by varying the location of the GTS in order to minimize $k_C^{GT}(T,s)$. Thus, the CVT rate constant $[k_C^{CVT}(T)]$ is given by

$$k_C^{CVT}(T) = \min_s k_C^{GT}(T,s) \tag{9a}$$

$$= k_C^{GT}[T,s_C^{CVT}(T)] \tag{9b}$$

where $s_C^{CVT}(T)$ is the location of the CVT transition state for temperature T.

Another interpretation of the CVT rate constant can be seen by generalizing[1,21,30,48,67,68] the quasithermodynamic formulation of conventional TST. In this approach, quasiequilibrium between the reactants and systems at the GTS dividing surface at s is described by the equilibrium constant:

$$K_C^{GT}(T,s) = \frac{Q_C^{GT}(T,s)}{\Phi_C^R(T)} \exp[-\beta V_{MEP}(s)] \tag{10}$$

where the exponential factor again arises from the fact that the zero of energy for the GTS partition function is at $V_{MEP}(s)$, while the zero of energy for the reactants partition function is at the overall zero of energy. The standard-state free energy change $\Delta G_C^{GT,0}(T,s)$ for the formation of the GTS at s from reactants is then given in terms of the equilibrium constant by

$$\Delta G_C^{GT,0}(T,s) = -RT \ln [K_C^{GT}(T,s)/K^0] \tag{11}$$

where R is the gas constant and K^0, the value of the reaction quotient evaluated at the standard state, is taken to be 1 cm^3 per molecule for reaction Equation 1a or simply unity for reaction Equation 1b or 1c. Rewriting Equation 11 gives:

$$K_C^{GT}(T,s) = K^0 \exp[-\Delta G_C^{GT,0}(T,s)/RT] \tag{12}$$

and a comparison of Equations 8, 10, and 12 shows that the GTS rate constant is given by

$$k_C^{GT}(T,s) = \frac{\sigma}{\beta h} K^0 \exp[-\Delta G_C^{GT,0}(T,s)/RT] \tag{13}$$

where, by combining Equations 10 and 11, we have:

$$\Delta G_C^{GT,0}(T,s) = RT\left[\beta V_{MEP}(s) - \ln \frac{Q_C^{GT}(T,s)}{\Phi_C^R(T)K^0}\right] \tag{14}$$

Equation 13 shows that the minimum in $k_C^{GT}(T,s)$, which occurs (by definition) at $s_C^{CVT}(T)$, corresponds to a maximum in $\Delta G_C^{GT,0}(T,s)$, the generalized free energy of activation curve. Thus, CVT is equivalent to the maximum free energy of activation criterion.[1,21,30,48,67,68] These considerations also demonstrate that CVT is more internally consistent than conventional TST in that the criterion for the conventional dividing surface involves only the potential energy, whereas the criterion for the CVT dividing surface involves both "entropic" effects associated with the $Q_C^{GT}(T,s)/\Phi_C^R(T)$ factor (as well as zero-point effects when quantum partition functions are used, as in Section III) and energetic effects associated with the $\exp[-\beta V_{MEP}(s)]$ factor. Both theories include both factors in calculating the free energy of activation (and hence, the rate constant) for a given dividing surface, but only CVT involves both factors in choosing the dividing surface. In addition, CVT is more accurate. For example, Figure 3 shows the classical free energy of activation curves[21] at various temperatures for the collinear reaction Cl + HD → ClH + D on the same potential energy surface[18,19] as used for Figure 1. At 4000 K, the CVT dividing surface is located about 0.3 a_0 later than the conventional transition state. This decreases the amount by which TST overestimates the true classical collinear rate constant from a factor of 9.6 for the conventional theory to a factor of 4.9 for CVT. Similarly, at 1500 K the error is reduced from a factor of 2.8 to a factor of 1.9.[21]

B. Practical Procedures

We now turn to a discussion of practical procedures for evaluating the quantities needed for calculating $k_C^{CVT}(T)$ from a given potential energy surface.

The saddle point, if any exists, is found by a Newton-Raphson search[69] for the solution of $\nabla V(\mathbf{R}) = 0$ in a $(3N - \eta)$-dimensional subspace of the **R** coordinate system, where η

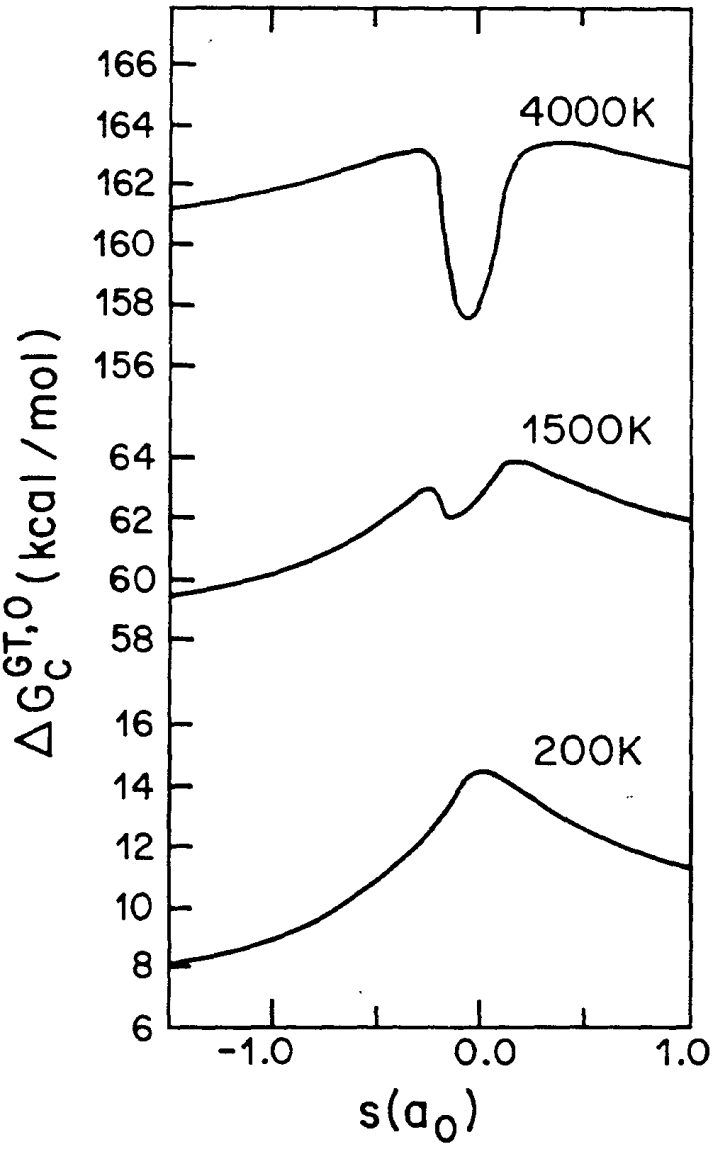

FIGURE 3. Classical generalized standard-state free energy of activation for collinear Cl + HD → ClH + D as a function of reaction coordinate at three temperatures. The standard state is 1 molecule and per centimeter, anharmonicity is included by the Morse I approximation. The saddle point is located at s = 0.

= 6 for a nonlinear transition state and $\eta = 5$ for a linear one. Here the point **R** is the 3N-dimensional column vector of cartesian coordinates $R_{i\gamma}$ and the gradient $\nabla V(\mathbf{R})$ is the 3N-dimensional column vector of first derivatives $\partial V(\mathbf{R})/\partial R_{i\gamma}$ evaluated at **R**. To remove η degrees of freedom corresponding to overall translations and rotations of the system, the $(3N - \eta)$-dimensional subspace of independent cartesian coordinate variations can be defined by fixing (somewhat arbitrarily) the values of η of the $R_{i\gamma}$ coordinates. For example, in the nonlinear case we could require that atom 1 be at the origin, atom 2 lie on the x axis, and atom 3 lie in the xy plane. This leaves a restricted set of $3N - \eta$ coordinates represented by $\mathbf{R}'$ in which to consider variations. Starting from a reasonable guess for the position of the saddle point, an improved guess $(\mathbf{R}'_{j+1})$ is obtained from the previous guess $(\mathbf{R}'_j)$ by

$$\mathbf{R}'_{j+1} = \mathbf{R}'_j - [\mathbf{M}(\mathbf{R}'_j)]^{-1}\nabla V(\mathbf{R}'_j) \tag{15}$$

where $\mathbf{M}(R'_j)$ is the $(3N - \eta) \times (3N - \eta)$ restricted matrix of second derivatives of the potential $\partial^2 V(\mathbf{R})/\partial R_{i\gamma}\partial R_{i'\gamma'}$ evaluated at $\mathbf{R}'_j$, and $\nabla V(\mathbf{R})'_j$ is the $(3N - \eta)$-dimensional restricted vector of first derivatives $\partial V(\mathbf{R})/\partial R_{i\gamma}$ evaluated at $\mathbf{R}'_j$. In practice, whenever possible, we compute the gradient of the potential analytically. This is straightforward when V itself is analytic, and the direct calculation of analytic derivatives has recently also become practical for *ab initio* energy calculations.[70,71] The elements of $\mathbf{M}$ are obtained by a two-point central difference method involving the analytic gradient:

$$\left.\frac{\partial^2 V(\mathbf{R})}{\partial R_{i\gamma}\partial R_{i'\gamma'}}\right|_{\mathbf{R}'_j} = \frac{1}{2\delta}[\nabla V(\mathbf{R}'_j + \delta\mathbf{e}_{i\gamma}) - \nabla V(\mathbf{R}'_j - \delta\mathbf{e}_{i\gamma})]_{i'\gamma'} \tag{16}$$

for a small stepsize δ (typically 0.0001 a_0), where $\mathbf{e}_{i\gamma}$ is the unit vector in the $R_{i\gamma}$ direction. Iterative use of Equation 15 until all the coordinates are constant thus provides an efficient method for converging on the saddle point position. This approach, which is based on a Taylor expansion of $\nabla V(\mathbf{R})$ through linear terms about a point where $\nabla V(\mathbf{R})$ is zero, is similar to, though somewhat simpler than, the method described by McIver and Komornicki,[72] which is based on a Taylor expansion of $|\nabla V(\mathbf{R})|^2$ through quadratic terms about a point where it goes to zero. Next, to properly define the mass-scaled $x_{i\gamma}$ coordinates of the saddle point, we redefine the 3N-dimensional set of cartesian coordinates $R_{i\gamma}$ such that the center of mass of the system lies at the origin. This is accomplished by subtracting the cartesian coordinates of the center of mass from the saddle point position $R_{i\gamma}$:

$$R^{\ddagger}_{i\gamma} = R_{i\gamma} - \left(\sum_{j=1}^{N} m_j R_{j\gamma}\right) \Big/ \left(\sum_{j=1}^{N} m_j\right), \quad \begin{matrix} i = 1,2,\ldots,N; \\ \gamma = x,y,z \end{matrix} \tag{17}$$

The saddle point geometry in $x_{i\gamma}$ coordinates ($\mathbf{x}^{\ddagger}$) is then found from Equation 2.

If the surface has a saddle point, the MEP is obtained by following the potential gradient in the "downhill" direction, starting at the saddle point. Since the gradient in $x_{i\gamma}$ coordinates $[\nabla V(\mathbf{x})]$ is zero at the saddle point, a first step off the saddle point must be taken in order to follow the steepest-descents path. At the saddle point the direction of the MEP is given by the unbound normal mode[61] associated with an imaginary frequency (i.e., a negative force constant) because it is along this direction that the potential has a true barrier. Thus, in order to find the direction of the MEP at the saddle point, a normal-mode analysis must be performed there. An extra benefit of this approach is that this information can also be used to calculate $Q^{\ddagger}_C(T)$. That is, since the normal modes form an orthogonal set,[57] the bound modes are perpendicular to the direction of the reaction coordinate at the saddle point, and hence span the conventional transition state in the region of the saddle point. Thus, the bound normal modes at the saddle point are useful in evaluating $Q^{\ddagger}_C(T)$; further details are discussed in Section III, where we consider the quantized partition function $Q^{\ddagger}(T)$. Note that a subscript C denotes a completely classical quantity, and its absence denotes quantized vibrations or quantized vibrations and rotations.

Taking the saddle point as our local zero of energy and using the fact that all the first derivatives are zero there, the potential energy for small displacements from the saddle point $\mathbf{x}^{\ddagger}$ can be approximated by

$$V(\mathbf{x} - \mathbf{x}^{\ddagger}) \cong {}^1/_2(\mathbf{x} - \mathbf{x}^{\ddagger})^{\dagger}\,\mathbf{F}(\mathbf{x}^{\ddagger})(\mathbf{x} - \mathbf{x}^{\ddagger}) \tag{18}$$

where † denotes a transpose and $\mathbf{F}(\mathbf{x}^{\ddagger})$ is the $3N \times 3N$ force constant matrix in mass-scaled coordinates evaluated at $\mathbf{x}^{\ddagger}$:

$$F_{i\gamma,i'\gamma'}(\mathbf{x}^{\ddagger}) = \partial^2 V(\mathbf{x})/\partial x_{i\gamma}\partial x_{i'\gamma'}|_{x^{\ddagger}} \quad , \; i,i' = 1,2,\ldots,N; \; \gamma,\gamma' = x,y,z \tag{19}$$

and higher-order terms in $(\mathbf{x} - \mathbf{x}^{\ddagger})$ have been neglected. We note in passing that the elements of $\mathbf{F}(\mathbf{x})$ are related to the elements of the matrix $\mathbf{M}$ evaluated at the corresponding cartesian point $\mathbf{R}$ as shown in Equation 16 by

$$F_{i\gamma,i'\gamma'}(\mathbf{x}) = \frac{\mu}{(m_i m_{i'})^{1/2}} M_{i\gamma,i'\gamma'}(\mathbf{R}) \tag{20}$$

To define a set of normal coordinates $\{Q_m, \; m = 1,2,\ldots,3N\}$, which are linear combinations of the components of $(\mathbf{x} - \mathbf{x}^{\ddagger})$ corresponding to directions of independent motions through second order in the displacements, we require that both the kinetic and potential energies be diagonal in $\{Q_m\}$.[57] In such a case, the set of 3N equations for nuclear motion:

$$\frac{d}{dt}\frac{\partial T}{\partial(dQ_m/dt)} + \frac{\partial V}{\partial Q_m} = 0 \quad , \quad m = 1,2,\ldots,3N \tag{21}$$

simplifies to:[73]

$$\frac{d^2Q_m}{dt^2} + k_m Q_m = 0 \quad , \quad m = 1,2,\ldots,3N \tag{22}$$

which have solutions:

$$Q_m(t) = t_m^{\ddagger} \sin(k_m^{1/2}t + \delta_m) \quad , \quad m = 1,2,\ldots,3N \tag{23}$$

where $t_m^{\ddagger}$ is the turning point of mode m. Equation 23 shows that these modes describe harmonic motion with all the atoms moving in phase, and so they are the normal modes we desire. But since the kinetic energy T is already diagonal in the $x_{i\gamma}$ coordinates and hence in the components of $(\mathbf{x} - \mathbf{x}^{\ddagger})$, the linear combinations we seek, corresponding to the normal-mode directions, can be obtained just by diagonalizing the matrix $\mathbf{F}$.[57,73] That is, we perform the unitary transformation (which does not change the diagonal character of T):

$$\mathbf{L}(\mathbf{x}^{\ddagger})^{\dagger} \, \mathbf{F}(\mathbf{x}^{\ddagger})\mathbf{L}(\mathbf{x}^{\ddagger}) = \mathbf{\Lambda}(\mathbf{x}^{\ddagger}) \tag{24}$$

where $\mathbf{L}(\mathbf{x}^{\ddagger})$ is a unitary matrix whose columns $\mathbf{L}_m(\mathbf{x}^{\ddagger})$ provide the linear combinations of the components of $(\mathbf{x} - \mathbf{x}^{\ddagger})$ corresponding to the normal-mode directions at the saddle point and $\mathbf{\Lambda}(\mathbf{x}^{\ddagger})$ is a diagonal matrix with eigenvalues $\lambda_m(0)$, which are the normal-mode force constants at the saddle point, and are related to the normal-mode frequencies $\omega_m(0)$ at the saddle point by

$$\omega_m(0) = [\lambda_m(0)/\mu]^{1/2} \quad , \quad m = 1,2,\ldots,3N \tag{25}$$

Out of the 3N eigenvalues $\lambda_m(0)$, $3N - \eta - 1$ are positive and correspond to bound modes, one is negative and corresponds to the unbound mode (i.e., the reaction coordinate), and η are zero, corresponding to overall translations and rotations. The unbound mode has an imaginary frequency $(\omega^{\ddagger})$ given by Equation 25 and a direction provided by the eigenvector $\mathbf{L}_F(\mathbf{x}^{\ddagger})$.

Beginning at the saddle point $\mathbf{x}^{\ddagger} = \mathbf{x}(s = 0)$, we next compute a set of geometries $[\mathbf{x}(s_j)]$ and classical potential energies $[V_{MEP}(s_j)]$ along the MEP by taking steps of length δs. Since $\mathbf{L}_F(\mathbf{x}^{\ddagger})$ gives the direction of the MEP at the saddle point, the first step from the saddle point is taken in the direction $\pm\mathbf{L}_F(\mathbf{x}^{\ddagger})$:

$$\mathbf{x}(s_1 = \pm\delta s) = \mathbf{x}(0) \pm \delta s\, \mathbf{L}_F(\mathbf{x}^\ddagger) \tag{26}$$

where the choice of sign dictates whether we head toward products or toward reactants. Once we step off the saddle point, $\nabla V[\mathbf{x}(s)]$ is no longer zero, so that subsequent steps can be taken in the direction of the negative of the normalized gradient:

$$\mathbf{x}(s_j = s_{j-1} \pm \delta s) = \mathbf{x}(s_{j-1}) - \delta s \frac{\nabla V[\mathbf{x}(s_{j-1})]}{|\nabla V[\mathbf{x}(s_{j-1})]|} \tag{27}$$

where $\nabla V(\mathbf{x})$ is the 3N-dimensional vector of first derivatives $\partial V(\mathbf{x})/\partial x_{i\gamma}$ evaluated at $\mathbf{x}$ which is given in terms of the analytic cartesian derivatives evaluated at the corresponding cartesian point $\mathbf{R}$ by

$$\partial V/\partial x_{i\gamma}|_{\mathbf{x}} = (\mu/m_i)^{1/2}\, \partial V/\partial R_{i\gamma}|_{\mathbf{R}} \tag{28}$$

To maintain accuracy and stability of the results, quite small steps (typically around 0.0001 a_0) must usually be taken. Otherwise, the calculated points $\mathbf{x}(s_j)$ will oscillate about the true path, especially when the potential "flattens out" outside the region of strong interaction. The calculation of the reaction path, which typically needs to be carried out to a distance of a few bohr in each direction from the saddle point, thus involves a large number of potential energy and gradient evaluations. For this reason, it is highly desirable that V and ∇V be analytic functions of $\mathbf{R}$. In cases where this is not feasible or in which the evaluation of V and ∇V is time-consuming (as in *ab initio* calculations), it may be more efficient to use larger steps and then refine the guess to the point on the MEP.[74,75]

For atom-diatom systems with collinear MEPs, we use special procedures. The gradient is followed as described above until it begins to oscillate. Incorrect oscillation of the computed gradient vector is checked by comparing its values at the current and previous steps; if the cosine of the angle between the two vectors is less than 0.9, the gradient is considered to oscillate too much. In this case, the coordinates and gradient vector are reset to values from several steps back (typically ten steps). Incorrect oscillation of the computed gradient may occur in regions where the potential flattens out, e.g., in the asymptotic regions. A check is made to see if the system is in an asymptotic region by comparing the current calculated value of the gradient vector with that for the asymptotic region; if the angle between these two vectors is less than some small value (typically 0.05 to 0.5°), the system is assumed to be in the asymptotic region. In the asymptotic regions the gradient vector is no longer followed, but steps are taken along the direction of the asymptotic vector. After each step a search is performed to find the minimum of the potential normal to the asymptotic vector, and the point on the MEP is set at this minimum.

In the case that the potential has flattened out but the system is not in the asymptotic region, the following procedure is used. First, a check is made to see if the system is in a van der Waals well by searching for the location at which the first derivatives vanish. If a van der Waals well is found, the gradient is followed into the well from a point in the asymptotic region. If a van der Waals well is not found, the MEP is found by finding the minimum of the potential along an arc of constant radius from the last point found on the MEP. This procedure is continued to the point at which the reaction path information is saved, then an attempt is made to follow the gradient in the usual fashion again.

For cases with two or more saddle points or a saddle point and a well, or, in general, two or more nonasymptotic stationary points (i.e., points where all the first derivatives vanish) on the MEP, the MEP must be constructed by parts, following the gradient down from saddle points, and, when the potential is attractive at long range, from asymptotic points, into wells, and then joining the segments to create a continuous reference path.

In order to calculate the equilibrium flux through GTS dividing surfaces other than the conventional one and obtain $Q^{GT}(T,s)$, a normal-coordinate analysis for the bound-mode frequencies and directions needs to be carried out at regular intervals (Δs) (typically every 0.01 a_0) along the MEP. Since in general the first derivatives of the potential at points on the MEP are not zero except at the saddle point, the procedure used for this part of the calculation is different from the above calculation of the saddle point normal modes. The procedure we use is based on a recent paper on the reaction-path Hamiltonian by Miller et al.[76] We first consider the case of a nonlinear system; the linear case is dealt with below. As above, suppose $\mathbf{x}(s)$ is a point on the MEP. Then, for general points $\mathbf{x}$ near $\mathbf{x}(s)$, the potential can be approximated by

$$V(\mathbf{x}) = V[\mathbf{x}(s)] + \nabla V[\mathbf{x}(s)] \cdot [\mathbf{x} - \mathbf{x}(s)] + {}^1/_2[\mathbf{x} - \mathbf{x}(s)]^\dagger \mathbf{F}(s) [\mathbf{x} - \mathbf{x}(s)] \quad (29)$$

where $\mathbf{F}(s)$ is the force constant matrix of Equation 19 evaluated at $\mathbf{x}(s)$, and where higher-order terms in $[\mathbf{x} - \mathbf{x}(s)]$ have been neglected. By suitable linear combinations of the components $[\mathbf{x} - \mathbf{x}(s)]_{i\gamma}$, displacements $[\xi_m(s)]$ may be obtained in directions orthogonal to $\nabla V[\mathbf{x}(s)]$, in which case the second term in Equation 29 is zero, so that the potential is quadratic (but not necessarily diagonal) in the displacements $\xi_m(s)$. Thus, normal coordinates $[Q_m(s)]$ for vibrations orthogonal to the MEP can be found by projecting out of $\mathbf{F}(s)$ those contributions that come from motion along the reaction coordinate prior to diagonalization. In addition, since motion along the reaction coordinate is, in general, coupled to overall translations and rotations of the system, the normal coordinates must be chosen in such a way that they are also orthogonal to the six directions corresponding to infinitesimal translations and rotations. Normal modes orthogonal to the reaction path at $\mathbf{x}(s)$ are thus found by diagonalizing the projected force constant matrix:[76]

$$\mathbf{F}^P(s) = [\mathbf{1} - \mathbf{P}(s)]\mathbf{F}(s)[\mathbf{1} - \mathbf{P}(s)] \quad (30)$$

with the elements of the projector $\mathbf{P}$ given by

$$P_{i\gamma,i'\gamma'}(s) = v_{i\gamma}(s)v_{i'\gamma'}(s) + (m_A + m_B)^{-1}(m_i m_{i'})^{1/2}\,\delta_{\gamma\gamma'} + \sum_{\substack{\alpha,\beta,\alpha',\beta' \\ =x,y,z}} \epsilon_{\alpha\beta\gamma}x_{i\beta}(s)[\mathbf{I}_0^x(s)^{-1}]_{\alpha\alpha'}\epsilon_{\alpha'\beta'\gamma'}x_{i'\gamma'}(s) \quad (31)$$

where

$$v_{i\gamma}(s) = -\nabla V[\mathbf{x}(s)]_{i\gamma}/|\nabla V[\mathbf{x}(s)]| \quad (32)$$

$\delta_{\gamma\gamma'}$ is the Kronecker delta and $\epsilon_{\alpha\beta\gamma}$ is the completely antisymmetric unit pseudotensor of rank 3:[77]

$$\epsilon_{\alpha\beta\gamma} = \begin{cases} 0, & \alpha\beta\gamma \text{ not all distinct} \\ 1, & \alpha\beta\gamma \text{ an even permutation of xyz} \\ -1, & \alpha\beta\gamma \text{ an odd permutation of xyz} \end{cases} \quad (33)$$

and $\mathbf{I}_0^x(s)$ is the 3×3 moment of inertia tensor at $\mathbf{x}(s)$:[78]

$$\mathbf{I}_0^x(s) = \sum_{i=1}^{N} \begin{pmatrix} x_{iy}^2 + x_{iz}^2 & -x_{ix}x_{iy} & -x_{ix}x_{iz} \\ -x_{ix}x_{iy} & x_{ix}^2 + x_{iz}^2 & -x_{iy}x_{iz} \\ -x_{ix}x_{iz} & -x_{iy}x_{iz} & x_{ix}^2 + x_{iy}^2 \end{pmatrix} \quad (34)$$

The first term in Equation 31 projects onto the direction along the reaction path, the second onto the three directions corresponding to overall translations, and the third onto the three directions corresponding to overall rotations. The projector $[\mathbf{1} - \mathbf{P}(s)]$ thus provides a projected force constant matrix $\mathbf{F}^P(s)$ for which motion along these seven directions has been removed.

In a linear system, there are only two degrees of freedom corresponding to overall rotations, and hence there is an additional bound internal degree of freedom. In addition, due to the symmetry of the system, the projector in Equation 30 has a much simpler form in this case. Assuming that the system lies along the z axis, the elements of the projector $\mathbf{P}$ are given by[76]

$$P_{i\gamma,i'\gamma'}(s) = v_{i\gamma}(s)v_{i'\gamma'}(s)\delta_{\gamma z}\delta_{\gamma' z} + (m_A + m_B)^{-1}(m_i m_{i'})^{1/2}\,\delta_{\gamma\gamma'} + \frac{x_{iz}(s)x_{i'z}(s)}{I(s)}(\delta_{\gamma\gamma'} - \delta_{\gamma z}\delta_{\gamma' z}) \tag{35}$$

where $I(s)$ is the moment of inertia, which is given in mass-scaled coordinates by

$$I(s) = \mu \sum_{i=1}^{N} [x_{iz}(s)]^2 \tag{36}$$

The matrix $\mathbf{F}^P(s)$ is then diagonalized through the unitary transformation:

$$[\mathbf{L}^{GT}(s)]^{\dagger}\,\mathbf{F}^P(s)[\mathbf{L}^{GT}(s)] = \mathbf{\Lambda}(s) \tag{37}$$

which yields $\eta + 1$ zero eigenvalues, corresponding to overall translation and rotation and motion along the reaction coordinate, and $3N - \eta - 1$ positive eigenvalues $\lambda_m(s)$ corresponding to the bound modes of the GTS orthogonal to the reaction path at s. These generalized normal modes have frequencies $\omega_m(s)$ given by

$$\omega_m(s) = [\lambda_m(s)/\mu]^{1/2}, \qquad m = 1,2,\ldots 3N \tag{38}$$

and directions $\mathbf{L}_m^{GT}(s)$ given by the corresponding columns of $\mathbf{L}^{GT}(s)$. The modes obtained from Equation 37 should be called generalized normal modes since true normal modes are defined only at stationary points (e.g., minima or saddle points) of potential energy surfaces; for convenience, though, we will simply call them normal modes. In addition, since the system has a total of $F \equiv 3N - \eta$ internal degrees of freedom, we also find it convenient in this chapter to order the orthogonal modes obtained from Equation 37 such that the first $F - 1$ modes are the bound normal modes at s, and mode F is the reaction coordinate. This convention differs from one of our original papers on polyatomic systems,[48] in which the reaction coordinate was taken to be mode 3N.

The above discussion has assumed that an analytic representation of the potential energy surface is available and has described the calculation of second derivatives and vibrational frequencies from this surface. An alternative procedure is to calculate the second derivative matrix directly as part of the electronic structure calculations; a recent discussion of this approach, with references to earlier examples, is given by Osamura et al.[79] In some cases, however, it is uneconomical either to calculate enough points to allow an analytic fit to the surface or to accurately follow the MEP and compute second derivatives along it. In such cases an alternative is to use global interpolation based on analytic fits to information calculated only in the vicinities of reactants, saddle points, and products[80] or based on assumed range parameters.[81-84]

The generalized normal-mode frequencies discussed above are used in the computation of $Q_C^{GT}(T,s)$ as discussed in Reference 21, or in the computation of $Q^{GT,O}(T,s)$ as discussed in Section III. The calculation of the classical rate constant $k_C^{GT}(T,s)$ or the rate constant $k^{GT}(T,s)$, corresponding to quantization of the reactants and the generalized transition state, for a GTS at s [or, equivalently, the generalized free energy of activation $\Delta G_C^{GT,0}(T,s)$ or $\Delta G^{GT,O}(T,s)$] also requires the reactants partition function per unit volume $\Phi_C^R(T)$ or $\Phi^R(T)$ for reaction Equation 1a or the unitless reactants partition function for reaction Equation 1b or 1c. $\Phi_C^R(T)$ is discussed in Reference 21. As shown in Section III, $\Phi^R(T)$ is obtained from the properties (i.e., the equilibrium positions and energies and the normal modes) of reactants A and B for reaction Equation 1a or of reactant A for reaction Equation 1b or 1c. Starting with a reasonable guess for the geometry of reactant A, its equilibrium position is found quite efficiently by a Newton-Raphson search in a restricted $(3N_A - \eta_A)$-dimensional cartesian subspace for the point where $\nabla V(\mathbf{R}) = 0$ by the procedure discussed above for locating the saddle point. Here η_A is six if A is nonlinear and five if it is linear. Once the center of mass of reactant A is placed at the origin through the use of an equation analogous to Equation 17, a $3N_A$-dimensional set of mass-scaled coordinates defined by Equation 2 is used to obtain the $3N_A - \eta_A$ bound normal-mode frequencies and directions for reactant A in exactly the same manner discussed above for obtaining the normal modes at the saddle point. For reaction Equation 1a, this procedure is then repeated for reactant B. Of course, if a reactant is an atom, such calculations are unnecessary. The special case of a diatomic molecule can be treated by a Morse potential. For Morse parameters D_e and β_M [Herzberg[85] calls this β, but we wish to distinguish it from $(k_BT)^{-1}$] and equilibrium interatomic distance r_e, the vibrational frequency and moment of inertia of a diatomic molecule are given by[85]

$$\omega_e = \beta_M \left(\frac{2D_e}{\mu_{bc}}\right)^{1/2} \tag{39a}$$

and

$$I = \mu_{bc} r_e^2 \tag{39b}$$

where μ_{bc} is given by Equation 6.

Given the partition functions $Q_C^{GT}(T,s)$ and $\Phi_C^R(T)$, the generalized free energy of activation curve $\Delta G_C^{GT,0}(T,s)$ is computed from Equation 14. The maximum of this curve, located at $s_C^{CVT}(T)$, is obtained by interpolation from a quartic fit to $\Delta G_C^{GT,0}(T,s)$ at five values of s nearest the maximum. That is, $\Delta G_C^{GT,0}(T,s)$ is fit in the region of the maximum to the form:

$$\Delta G_C^{GT,0}(T,s) \cong a(T)s^4 + b(T)s^3 + c(T)s^2 + d(T)s + e(T) \tag{40}$$

where the coefficients of the fit are determined from the values of $\Delta G_C^{GT,0}(T,s)$ at five points $s_i, s_{i+1}, \ldots, s_{i+4}$ around the maximum by solving the set of five simultaneous equations:

$$\Delta G_C^{GT,0}(T,s_n) = a(T)s_n^4 + b(T)s_n^3 + c(T)s_n^2 + d(T)s_n + e(T),$$
$$n = i, i+1, \ldots, i+4 \tag{41}$$

by standard methods. Here we assume that the five s values are in general not equally spaced, as occurs, e.g., when refinements are made in the calculation of the MEP. The position of the maximum in $\Delta_C^{GT,0}(T,s)$ is then approximated by the analytic solution[86] to the cubic equation:

$$0 = \frac{d}{ds} \Delta G_C^{GT,0}(T,s) \cong 4a(T)s^3 + 3b(T)s^2 + 2c(T)s + d(T) \quad (42)$$

yielding $s_C^{CVT}(T)$. The value of $\Delta G_C^{GT}[T,s_C^{CVT}(T)]$ is then found from Equation 40, and the CVT rate constant of Equation 9a is calculated from Equation 13. For comparison, the conventional TST rate constant $[k_C^{\ddagger}(T)]$ is obtained from $\Delta G_C^{GT,0}(T,s = 0)$ by Equation 13 also.

III. QUANTUM EFFECTS ON BOUND DEGREES OF FREEDOM

In Section II the calculation of the CVT rate constant was discussed from a purely classical mechanical standpoint, in which the motion of the system along the reaction coordinate is treated classically and the partition functions for the reactant and transition state degrees of freedom are given by classical phase-space integrals. However, as noted in Section I, the incorporation of quantum mechanical effects is indispensable for obtaining reliable rate constants for real reactions in that the effects of quantized energy levels (especially the existence of zero-point energies) as well as dynamical effects, such as barrier penetration, can be large. These effects must therefore be included in CVT in order to obtain rate constants which can be compared meaningfully with experiment. Since the fundamental assumption of TST relies on simultaneously specifying the momentum and position of the system along the reaction coordinate, the inclusion of quantum mechanics in TST leads to an ambiguous result.[27] As noted in Section I, the quantization of conventional TST is usually accomplished by the assumption of a separable reaction coordinate with *ad hoc* quantization of the energy levels for the remaining bound degrees of freedom of the transition state and for the reactants, together with the use of a multiplicative transmission coefficient to include other effects arising from motion along the reaction coordinate.[8-15,58] This is also the approach used here. As also noted in Section I, when quantum mechanics is included in this fashion, TST no longer provides a rigorous upper bound to the true quantal equilibrium rate constant for a given potential energy surface (unlike the classical case), so that the variational optimization of this quantized TST rate constant (as in CVT) might be questioned. In actuality, however, we have found that this quantization scheme does lead to accurate numerical results, and it provides a useful basis for discussion and interpretation of rate constants in a quantum mechanical world.[2,20,30-50,58,87-92] For example, the quantized conventional TST rate constants for the collinear reactions Cl + HD → ClH + D and Cl + DH → ClD + H computed from the Stern-Persky-Klein potential energy surface[18,19] predict a collinear HD/DH intramolecule isotope effect (i.e., the ratio of the rate of Cl + HD → ClH + D to that of Cl + DH → ClD + H) of 1.59 at 300 K, as compared to the CVT and accurate quantal results of 0.53 and 0.68, respectively.[34,39,58,93] This large difference between the conventional and CVT results is due to the greater effect of varying the dividing surface for the reaction of Cl with the H end of HD than for reaction with the D end. Conventional TST thus predicts the wrong direction for the HD/DH kinetic isotope effect, which points out the danger of using conventional TST in fitting surfaces to experimental data, since artificial errors are introduced into the empirically derived surface in order to compensate for the errors made by conventional TST.[37]

A. Separable, Harmonic Approximation

As described above, the first step in the quantization of TST is the replacement of the classical partition functions in Equation 8 by their quantum mechanical analogs. The generalized transition state quantal partition function $[Q^{GT}(T,s)]$ thus involves a summation of Boltzmann factors over the s-dependent quantized electronic-vibrational-rotational energy levels of the degrees of freedom orthogonal to the reaction coordinate at s. If we neglect

the couplings between electronic, vibrational, and rotational energies, the GTS partition function can be written as the product of partition functions for the electronic, vibrational, and rotational degrees of freedom as follows:

$$Q^{GT}(T,s) = Q_{el}^{GT}(T,s)\, Q_{vib}^{GT}(T,s)\, Q_{rot}^{GT}(T,s) \tag{43}$$

where $Q_{vib}^{GT}(T,s)$ and $Q_{rot}^{GT}(T,s)$ are the values appropriate to the ground electronic state. The quantum mechanical electronic partition function is given by

$$Q_{el}^{GT}(T,s) = \sum_{\alpha} d_{\alpha}^{GT}(s) \exp\{-\beta[\epsilon_{el}^{GT}(\alpha,s) - V_{MEP}(s)]\} \tag{44}$$

where $\alpha = 0,1,\ldots,d_{\alpha}^{GT}(s)$ is the degeneracy, and $\epsilon_{el}^{GT}(\alpha,s)$ is the energy of electronic state α measured from the overall zero of energy, with $\epsilon_{el}^{GT}(\alpha = 0,s) = V_{MEP}(s)$. Because the spacings between electronic energy levels are generally large, the summation in Equation 44 usually converges rapidly; ordinarily, only the energetically lowest electronic multiplet needs to be considered. In addition, we usually take the generalized transition state electronic partition function to be independent of s, i.e., $Q_{el}^{GT}(T,s)$ is set to $Q_{el}^{GT}(T)$. Since the rotational energy levels are generally closely spaced, little accuracy is lost if we approximate the quantal rotational partition function by the corresponding classical one.[78] This approach has been shown to give an error in the CVT rate constant of not more than about 1% for atom-diatom reactions.[30] For a linear GTS, the classical rotational partition function is given by

$$Q_{rot}^{GT}(T,s) = \frac{2I(s)}{\hbar^2\beta} \tag{45}$$

where I(s) is the moment of inertia in mass-scaled coordinates given in Equation 36. For a nonlinear GTS, the classical rotational partition function is given by

$$Q_{rot}^{GT}(T,s) = \left[\left(\frac{2}{\hbar^2\beta}\right)^3 \pi I_A(s) I_B(s) I_C(s)\right]^{1/2} \tag{46}$$

where the product of the three principal moments of inertia (which are related to the eigenvalues of the moment of inertia tensor $\mathbf{I}_0^x(s)$ of Equation 34) can be evaluated readily from

$$I_A(s)I_B(s)I_C(s) = \mu^3 \det[\mathbf{I}_0^x(s)] \tag{47}$$

Note that the symmetry number is absent from the rotational partition function, since it is incorporated into the symmetry factor σ of Equation 8.

The projected force constant matrix of Miller et al.,[76] discussed in Section II, provides a set of frequencies $\{\omega_m(s), m = 1,\ldots,F-1\}$ for the bound modes of the GTS at s. From these frequencies, we can construct a harmonic approximation to the potential energy for general points **x** near **x**(s) by

$$V(s,Q_1,\ldots,Q_{F-1}) = V_{MEP}(s) + {}^1/_2\mu \sum_{m=1}^{F-1} [\omega_m(s)Q_m(s)]^2 \tag{48}$$

where $Q_m(s)$ is the normal-mode coordinate for mode m when the system coordinates are **x**, i.e.,

$$Q_m(s) = [\mathbf{x} - \mathbf{x}(s)] \cdot \mathbf{L}_m^{GT}(s) \tag{49}$$

The vibrational energy levels for this potential are given by

$$\epsilon_{vib}^{GT}(n_1,n_2,\ldots,n_{F-1},s) = \sum_{m=1}^{F-1} (n_m + {}^1/_2)\hbar\omega_m(s) \tag{50}$$

Thus, in the harmonic approximation, the vibrational partition function is separable:

$$Q_{vib}^{GT}(T,s) = \prod_{m=1}^{F-1} Q_{vib,m}^{GT}(T,s) \tag{51}$$

where the vibrational partition function for mode m is

$$Q_{vib,m}^{GT}(T,s) = \sum_{n_m} \exp[-\beta\epsilon_{vib,m}^{GT}(n_m,s)] \tag{52}$$

with the vibrational energy of level n, $\epsilon_{vib,m}^{GT}(n_m,s)$, measured from the bottom of the local vibrational well [i.e., at $V_{MEP}(s)$]. The summation in Equation 52 should be terminated with the last term for which $\epsilon_{vib,m}^{GT}(n_m,s)$ is less than the lowest dissociation energy of the system.[17,21,94] However, assuming that the contributions from higher energy levels are negligible for the temperature being considered, the summation can be extended formally to include all harmonic levels $\epsilon_{vib,m}^{GT}(n_m,s) = (n_m + {}^1/_2)\hbar\omega_m(s)$, in which case Equation 52 can be replaced by the analytic result:

$$Q_{vib,m}^{GT}(T,s) = \exp[-\hbar\omega_m(s)\beta/2]\{1 - \exp[-\hbar\omega_m(s)\beta]\}^{-1} \tag{53}$$

The reactant partition function per unit volume can be factored as

$$\Phi^R(T) = \Phi_{rel}^{A,B}(T)Q^A(T)Q^B(T) \tag{54a}$$

for reaction Equation 1a and for reaction Equations 1b and 1c we have

$$\Phi^R(T) = Q^A(T) \tag{54b}$$

In Equation 54a, $\Phi_{rel}^{A,B}(T)$ is the relative translational partition function per unit volume given by

$$\Phi_{rel}^{A,B}(T) = (2\pi\mu/\beta h^2)^{3/2} \tag{55}$$

and in Equations 54a and 54b $Q^A(T)$ and $Q^B(T)$ represent the partition functions for the internal degrees of freedom of species A and B, respectively. If reactant A is a molecule, $Q^A(T)$ is treated in a similar fashion to the GTS partition function, except that an additional vibrational mode must be considered (giving a total of $F_A = 3N_A - \eta_A$ total vibrational modes for reactant A):

$$Q^A(T) = Q_{el}^A(T)Q_{vib}^A(T)Q_{rot}^A(T) \tag{56}$$

where $Q_{el}^A(T)$ is given by

$$Q_{el}^A(T) = \sum_{\alpha} d_\alpha^A \exp[-\beta\epsilon_{el}^A(\alpha)] \tag{57}$$

in terms of the degeneracies d_α^A and term values $\epsilon_{el}^A(\alpha)$, with $\epsilon_{el}^A(\alpha = 0) = 0$. $Q_{rot}^A(T)$ is approximated classically using the equilibrium moments of inertia given in Equations 36 or 47 but with only the atoms of reactant A considered, and $Q_{vib}^A(T)$ is given in the separable-mode approximation by

$$Q_{vib}^A(T) = \prod_{m=1}^{F_A} \left\{ \sum_{n_m} \exp[-\beta \epsilon_{vib,m}^A(n_m)] \right\} \tag{58}$$

where the vibrational energies $\epsilon_{vib,m}^A(n_m)$ are measured from the overall zero of energy and are evaluated in the harmonic approximation from the frequencies obtained by a standard normal-mode analysis for reactant A. In this case, a result similar to that of Equation 53 can be obtained. Of course, if reactant A is an atom, then $Q^A(T)$ is given by $Q_{el}^A(T)$ alone. Similar considerations apply to reactant B.

Having incorporated quantal effects in the partition functions for the bound degrees of freedom, we obtain the hybrid (i.e., quantal bound degrees of freedom, classical reaction-coordinate motion) generalized TST rate constant $k^{GT}(T,s)$. By analogy to Equations 9a and 9b we denote the value of the reaction coordinate that minimizes $k^{GT}(T,s)$ as $s^{CVT}(T)$ and we denote the minimum value of $k^{GT}(T,s)$ as $k^{CVT}(T)$.

In Section IV we will make extensive use of the vibrationally adiabatic ground-state potential curve $V_a^G(s)$. This is defined by

$$V_a^G(s) = V_{MEP}(s) + \epsilon_{int}^G(s) \tag{59}$$

where $\epsilon_{int}^G(s)$ is the total vibrational zero-point energy:

$$\epsilon_{int}^G(s) = \sum_{m=1}^{F-1} \epsilon_{vib,m}^{GT}(n_m = 0,s) \tag{60}$$

In the harmonic approximation:

$$\epsilon_{int}^G(s) = {}^1/_2\hbar \sum_{m=1}^{F-1} \omega_m(s) \tag{61}$$

B. Inclusion of Anharmonicity

Up to this point, we have presented procedures for the calculation of the reaction rate constant under the assumption that the vibrational modes of the reactants and the GTS can be treated harmonically. These procedures are based on the harmonic approximation to the potential energy along the reaction path, given by Equation 48, which leads to the separable vibrational partition function of Equation 51 and to the zero-point energies used in calculating the vibrationally adiabatic ground-state potential curve $V_a^G(s)$ of Equation 59. In general, however, the vibrational degrees of freedom of the reactants and the GTS are bound by an anharmonic potential which contains terms in normal coordinates of order higher than two. Since these higher-order terms affect the quantized vibrational energy levels of the bound modes, substantial differences can be obtained between CVT rate constants computed from harmonic and anharmonic vibrations. For stretches, anharmonicity effects are most important for tight transition states and at low temperatures, where small fractional changes in the zero-point energies of high-frequency modes can significantly affect the results. The anharmonicity of bending vibrations, however, may have a greater effect at high temperatures. Another important kind of anharmonicity, which is harder to treat,[54] is mode-mode coupling, i.e., cross terms. Cross terms couple vibrational modes to each other and also to rotational modes.

As an example of anharmonicity effects we note that for the three-dimensional Cl + HD → ClH + D reaction using the Stern-Persky-Klein[18,19] potential energy surface, the rate constants calculated with the harmonic approximation are 25 to 42% larger than those obtained by including Morse anharmonicity in the bound stretching motion and quartic anharmonicity in the bends.[39] Moreover, for a set of atom-diatom reactions that we have modeled with rotated Morse bond-energy-bond-order potential energy surfaces, the harmonic approximation for the transition state bend overestimates the quadratic-quartic approximation[95] for the conventional TST rate constant by an average factor of 1.5 at 600 K.[30,31,54] Effects associated with anharmonicity of bending degrees of freedom are significantly larger than this average for some of the cases studied, especially at high temperature.[54] As a final example of the effect of including anharmonicity in the calculation of quantal CVT rate constants, we consider the reaction $OH + H_2 \rightarrow H_2O + H$, which has been studied[48] using an analytic potential energy surface obtained by Schatz and Elgersma[96] by a fit to the accurate extended basis set configuration-interaction electronic structure calculations of Walch and Dunning.[97] For this reaction, it was observed that the harmonic approximation to the CVT/SCSAG rate constant, which is described in Section IV and which is the most accurage available calculation for this reaction, overestimates the anharmonic result obtained within the independent normal-mode (INM) framework presented below by factors of 2.27 at 298 K and 1.32 at 2400 K. The first of these results indicates that the inclusion of anharmonicity may affect the calculated rate constants for polyatomic reactions to a somewhat larger extent than has been found in typical atom-diatom studies at room temperature.

The first and largest part of this section gives detailed expressions for including Morse and quartic anharmonicity in the INM approximation.[48] This is followed by brief discussions of several possible alternative ways to treat anharmonicity.

To include vibrational anharmonicity in polyatomic CVT calculations, we require an approach which allows for the practical calculation of anharmonic vibrational energy levels, so that the vibrational partition function can be computed without undue effort. In the INM approximation we accomplish this by neglecting the mode-mode couplings and including anharmonicity in an approximate manner for each of the normal modes of the reactants and the GTS. To be specific, in this section we will consider the vibrational degrees of freedom of the GTS. Within the INM framework, the separable approximation for the vibrational partition function and total zero-point energy, as given by Equations 51 and 60, is still valid, so it is sufficient to consider a single mode m at s, with a corresponding normal coordinate $Q_m(s)$ given by Equation 49. The potential energy along this mode is given by

$$V_m[s,Q_m(s)] = {}^1/_2 k_{mm}(s)[Q_m(s)]^2 + k_{mmm}(s)[Q_m(s)]^3 + k_{mmmm}(s)[Q_m(s)]^4 + \ldots \quad (62)$$

where $k_{mm}(s)$, $k_{mmm}(s)$, $k_{mmmm}(s)$, etc. are called the principal normal-coordinate force constants to denote that all subscripts are the same. {A nonprincipal force constant would be the coefficient in a cross term like $k_{smmm'}(s)s[Q_m(s)]^2Q_{m'}(s)$ or $k_{mmm'm'}(s)[Q_m(s)]^2[Q_{m'}(s)]^2$}. The principal normal-mode force constants are related to the second, third, fourth, etc. directional derivatives of the potential energy along the normal-mode direction. That is, the quadratic normal-mode force constant $[k_{mm}(s)]$ is given by the eigenvalue $\lambda_m(s)$ of the projected force constant matrix defined below Equation 37, while the higher-order force constants are obtained from numerical directional derivatives of the analytic gradient:

$$k_{mmm}(s) = \frac{1}{6\delta^2}\{\nabla V[\mathbf{x}(s) + \delta \mathbf{L}_m^{GT}(s)] + \nabla V[\mathbf{x}(s) - \delta \mathbf{L}_m^{GT}(s)] - 2\nabla V[\mathbf{x}(s)]\} \cdot \mathbf{L}_m^{GT}(s) \quad (63)$$

$$k_{mmmm}(s) = \frac{1}{48\delta^3}\{\nabla V[\mathbf{x}(s) + 2\delta \mathbf{L}_m^{GT}(s)] - 2\nabla V[\mathbf{x}(s) + \delta \mathbf{L}_m^{GT}(s)] + 2\nabla V[\mathbf{x}(s) - \delta \mathbf{L}_m^{GT}(s)] - \nabla V[\mathbf{x}(s) - 2\delta \mathbf{L}_m^{GT}(s)]\} \cdot \mathbf{L}_m^{GT}(s) \quad (64)$$

etc. for some small stepsize δ (typically 0.0001 a_0).

We next need to compute vibrational energy levels for the one-dimensional potential given by Equation 62, so that the vibrational partition function for mode m can be calculated from Equation 52. From collinear atom-diatom studies,[39,58] it was found that a satisfactory approach to treating the bound stretching motions is provided by replacing the general potential of Equation 62 by a Morse function:[85]

$$V_{M,m}[s,Q_m(s)] = D_e(s)\{\exp[-\beta_{M,m}(s)\, Q_m(s)] - 1\}^2 \quad (65)$$

where $D_e(s)$ is the local dissociation energy for the vibrational potential on the potential energy surface:

$$D_e(s) = D - V_{MEP}(s) \quad (66)$$

(where D represents the lowest dissociation energy of the system) and where the range parameter $\beta_{M,m}(s)$ is chosen so that the Morse potential has the correct force constant at its minimum:

$$\beta_{M,m}(s) = [k_{mm}(s)/2D_e(s)]^{1/2} \quad (67)$$

We refer to this method of choosing $D_e(s)$ and $\beta_{M,m}(s)$ as the Morse approximation I.[21,48,58] The energy levels of this potential are given by[85]

$$\epsilon_{vib,m}^{GT}(n,s) = \hbar\omega_m(s)(n + {}^1/_2)[1 - x_{M,m}(s)(n + {}^1/_2)] \quad (68)$$

where n is the level index, $\omega_m(s)$ is the harmonic frequency given by Equation 38, and $x_{M,m}(s)$ is the unitless Morse anharmonicity constant given by

$$x_{M,m}(s) = \hbar\omega_m(s)/4D_e(s) \quad (69)$$

Although this is not the only method of fitting the vibrational potential to a Morse function, it has the advantage that the energy levels will always increase monotonically up to the dissociation energy D, so that the vibrational partition function can be computed straightforwardly. It should be pointed out that rate constants obtained using Morse approximation I in quantal atom-diatom studies[58] and in the study of the OH + H_2 system[48] agreed well with those obtained by fitting the Morse function to the second and third derivatives of the true potential at its minimum.

Vibrational modes that have no cubic anharmonicity [i.e., $k_{mmm}(s) = 0$] cannot be well approximated by a Morse model. Examples of such modes include bending motions of linear systems, out-of-plane bends of planar systems, and certain stretching motions (such as the asymmetric stretch in the water molecule). A practical prescription is to treat the modes for which $k_{mmm}(s)$ is nonzero by Morse approximation I, while the modes having zero cubic anharmonicity are treated by a quadratic-quartic model, which has been shown to fit non-series-expanded bend potentials much more accurately than the harmonic model does for atom-diatom systems.[54] In the quadratic-quartic model, the potential of Equation 62 is truncated after the quartic term, yielding:

$$V_{qq,m}[s,Q_m(s)] = {}^1/_2 k_{mm}(s)[Q_m(s)]^2 + k_{mmmm}[Q_m(s)]^4 \tag{70}$$

(For atom-diatom reactions, the quadratic-quartic potential is written more conveniently — and more accurately — in terms of the bending angle rather than the normal coordinate. In the INM approximation we use normal coordinates, but we will discuss the coordinate question again below.) Accurate approximations to the energy levels for the quadratic-quartic potential of Equation 70 can be determined by a perturbation-variation method which yields:[54,95]

$$\epsilon^{GT}_{vib,m}(n,s) = {}^1/_2(\eta_n^2 + \eta_n^{-2})\epsilon_n^0(s) + k_{mmmm}(s)\eta_n^{-4}\epsilon_n^1(s) \tag{71}$$

where $\epsilon_n^0(s)$ is the harmonic energy of level n:

$$\epsilon_n^0(s) = \hbar\omega_m(s)(n + {}^1/_2) \tag{72}$$

$$\epsilon_n^1(s) = 3\hbar^2(2n^2 + 2n + 1)/4[\mu\omega_m(s)]^2 \tag{73}$$

and where η_n^2 is determined by solving:

$$\eta_n^6 - \eta_n^2 - 2c_{1,n} = 0 \tag{74}$$

with

$$c_{1,n} = 2k_{mmmm}(s)\epsilon_n^1(s)/\epsilon_n^0(s) \tag{75}$$

Since Equation74 is a cubic equation in η_n^2, it can be solved to give:[86]

$$\eta_n^2 = \begin{cases} 2\cos(\theta_n/3)/3^{1/2}, & c_{1,n}^2 < 1/27 \\ (c_{1,n} + c_{2,n})^{1/3} + (c_{1,n} - c_{2,n})^{1/3}, & c_{1,n}^2 \geq 1/27 \end{cases} \tag{76}$$

where

$$\theta_n = \arccos(3^{3/2}c_{1,n}) \tag{77}$$

and

$$c_{2,n} = \left[c_{1,n}^2 - \frac{1}{27}\right]^{1/2} \tag{78}$$

Using the anharmonic energy levels given in Equation 68 or 71, the anharmonic vibrational partition function for mode m is determined by Equation 52, where the summation is terminated with the last term for which $\epsilon^{GT}_{vib,m}(n_m,s) \leq D$. Within the INM framework assumed here, the total anharmonic vibrational partition functions are given by Equations 51 and 58 for the GTS and reactants, respectively. From these, anharmonic approximations to $k^{\ddagger}(T)$ and $k^{CVT}(T)$ may be calculated. Since anharmonicity affects the zero-point energies of the vibrational modes, the vibrationally adiabatic potential $V_a^G(s)$ given by Equation 59 will also be affected, resulting in different values for the transmission coefficients discussed in the next section. The small curvature approximation transmission coefficient (see Section IV) is additionally affected by changes in the values of the turning points for the anharmonic potentials.

In some cases it may be appropriate to treat hindered internal rotors by special techniques. These have been discussed by several authors.[98-103]

The neglect of cross terms in the INM approximation may lead to significant quantitative errors in some cases. The importance of cross terms can be minimized by using curvilinear coordinates.[104] For atom-diatom collisions this is our standard procedure,[30,33,34,54,55] but for TST calculations with more than three atoms we have so far retained the normal-mode approximation because of its convenience. As discussed above, normal modes are linear combinations of (mass-scaled or mass-weighted) atomic cartesians; hence, they are not curvilinear. A second advantage of curvilinear coordinates, in addition to the fact that cross terms tend to be smaller, is that principal force constants can often be predicted reasonably accurately by simple models in curvilinear coordinates.[104] An example of the advantage of modeling the anharmonicity in curvilinear internal coordinates rather than cartesian normal coordinates is provided by the work of Morino et al.[105] on NH_3. They classify the force constants in internal coordinate space as "principal" for terms with all subscripts the same, and "subsidiary" for terms coupling two or more internal coordinates. Going beyond the "anharmonic valence force field", which includes the principal but not the subsidiary force constants in internal coordinates, they modeled the potential energy surface for NH_3 by an anharmonic valence force field through quartic terms plus an H-H van der Waals interaction. This yields nonzero values for only 6 of the 14 independent cubic force constants in internal coordinate space, but the evidence from experiment is that the omitted force constants are all smaller than the largest principal cubic force constant by at least an order of magnitude. In fact, in internal coordinate space, 13 of the 14 independent cubic force constants are more than an order of magnitude smaller than the largest principal one, whereas in normal-coordinate space the largest cubic force constant is not a principal one and only 5 of the 14 independent cubic force constants are more than an order of magnitude smaller than the largest cubic force constant. Thus, anharmonicity is much easier to model in internal coordinates, but, if the calculations are to be completed in normal coordinate space, they are more difficult because the transformation from the modeling space of internal coordinates to the computational space of normal coordinates is nonlinear and in the general case somewhat unwieldy.

If the mode-mode couplings are included by any method in any coordinate system, and if the vibrational energy levels are then represented as

$$\epsilon_{vib}^{GT}(\mathbf{n},s) = \sum_{m} \hbar\omega_m(s)\,[(n_m + {}^1/_2) - x_m(s)(n_m + {}^1/_2)^2] - \sum_{m}\sum_{\substack{m' \\ m' \neq m}} \chi_{mm'}(s)(n_m + {}^1/_2)(n_{m'} + {}^1/_2) \tag{79}$$

where $\mathbf{n}$ denotes the set of quantum numbers $\{n_m, m = 1,2,\ldots,F-1\}$, one can still obtain reasonably simple analytic approximations to the vibrational partition functions and free-energy contributions by power series methods and by the definition of effective frequencies that take into account the leading anharmonic corrections under the assumption that anharmonic terms are small.[106-112]

Another procedure for estimating the partition functions without assuming separable normal modes is the Pitzer-Gwinn method.[101,113-115] This approximation scheme is based on the fact that the ratio of anharmonic to harmonic quantal partition functions, with the zero of energy at the local zero-point level, is given correctly by the classical approximation in both the low- and high-temperature limits. The approximation is to assume that this ratio is given correctly by the classical limit at all temperatures. Then the quantum mechanical anharmonic partition function needed for the rate constant calculation can be calculated from four quan-

tities, all of which are more easily obtained, namely, the quantal and classical harmonic partition functions, the anharmonic zero-point energy, and the classical anharmonic partition function. The harmonic quantities may be obtained analytically.[116] The quantal zero-point energy may be calculated by perturbation theory.[52,117-119] The classical anharmonic partition function may be evaluated by Gauss-Hermite[115] or Monte Carlo[120-126] numerical integration of the phase-space integral. Monte Carlo methods may also be applied to evaluate semiclassical partition functions directly.[113]

In evaluating bound-state partition functions for equilibrium-constant calculations, Bron and Wolfsberg[118] found that the main correction due to vibrational anharmonicity at room temperature arose from the anharmonicity correction to the zero-point energy. Thus, in some cases it may be adequate to include anharmonicity only as far as its effect on zero-point energies.

In principle, the partition functions could also be calculated by direct summation of Boltzmann factors involving energy levels computed from accurate quantum mechanical variational calculations, quantum mechanical perturbation theory, or a spectral method based on a Fourier transform of a quantum mechanical time correlation function.[104,127] This will generally be too expensive since energy levels are required up to high quantum numbers at each s. Furthermore, perturbation theory is expected to break down for high quantum numbers and sometimes even for low quantum numbers.

Other promising approaches for evaluating partition functions for coupled oscillator systems are thermodynamic perturbation theory[128-135] and variational approaches based on trace inequalities for the partition function.[131-138] So far, these techniques have not been applied in the context of rate calculations.

We will discuss the evaluation of the sum of states $N^{GT}(E,s)$ in Section V. The density of states may be evaluated by numerical differentiation of $N^{GT}(E,s)$, and the partition function may be evaluated by a Laplace transform of the density of states.[94] However, if one wishes to calculate both $Q^{GT}(T,s)$ and $N^{GT}(E,s)$, it may be more convenient to evaluate $Q^{GT}(T,s)$ directly and obtain $N^{GT}(E,s)$ by inverse Laplace transformation.[94]

IV. QUANTUM EFFECTS ON REACTION-COORDINATE MOTION

The treatment given in Section III provides a "hybrid" quantized GTS rate constant, in that, while motions in the GTS degrees of freedom orthogonal to the reaction path are treated quantum mechanically, motion along the reaction coordinate is still treated classically. By analogy to the classical theory of Section II, it seems physically reasonable that a better dynamical bottleneck can be obtained by variationally optimizing the location of the GTS dividing surface to minimize the rate constant calculated with quantized vibrations but classical reaction-coordinate motion. As discussed near the end of Section III.A, this yields $k^{CVT}(T)$, the hybrid analog[34,58] of the classical result defined by Equation 9a. Since this result still neglects tunneling, $k^{CVT}(T)$ often underestimates the true quantal rate constant, especially at low temperatures.[2,34] One convenient way to correct this deficiency is to use a multiplicative transmission coefficient $\kappa(T)$ as in Equation 7b:

$$k^{CVT/Y}(T) = \kappa^{CVT/Y}(T)k^{CVT}(T) \tag{80}$$

to account for the dynamical quantum effects of reaction-coordinate tunneling and nonclassical reflection, as well as the nonseparability of such effects from other degrees of freedom because of the curvature of the reaction path, which couples reaction-coordinate motion with vibrational motions. It is important that the transmission coefficient be consistent with the way the quantized partition functions are defined above.

For conventional TST we use:

$$k^{\ddagger/Y}(T) = \kappa^{\ddagger/Y}(T)k^{\ddagger}(T) \tag{81}$$

where

$$k^{\ddagger}(T) = k^{GT}(T,s = 0) \tag{82}$$

for the case of a conventional transition state located at a saddle point. The simplest and most common method of approximating reaction-coordinate tunneling in conventional TST is by the semiclassical Wigner correction to lowest order in $\hbar$, which yields:[139,140]

$$\kappa^{\ddagger/W}(T) = 1 + \frac{1}{24}|\hbar\omega^{\ddagger}\beta|^2 \tag{83}$$

where $\omega^{\ddagger}$ is the imaginary frequency at the saddle point. For this correction to be valid, contributions to tunneling must come only from the saddle point region of the potential energy surface, where the transverse vibrational frequencies do not vary appreciably and the potential along the reaction path is well approximated as an inverted parabola. In addition to these severe restrictions, the reaction-path curvature must have a negligible effect, and the scattering by the parabola must be treated accurately by truncation at the $(\hbar\beta)^2$ term. For these reasons, use of the Wigner correction is justifiable only at very high temperatures where it is near unity; when it differs appreciably from unity, the assumptions of its derivation are not satisfied and it is often found to be inaccurate.[28,87,141]

To include dynamical quantum effects more consistently and accurately than can be done with the Wigner expansion, we must distinguish between two extreme kinds of dynamical behavior, one of which is expected for systems with small reaction-path curvature and the other of which is expected for systems with large reaction-path curvature. For the former we may assume that the dominant quantal correction to reaction-coordinate motion comes from tunneling through the saddle point region. To treat this we describe the motion of the system in an approximate way as one-dimensional motion along the reaction coordinate governed by an effective one-dimensional potential and an effective reduced mass. The potential is obtained by assuming that the bound degrees of freedom orthogonal to the reaction coordinate adjust adiabatically (i.e., remain in the same quantum state) as the system moves along the reaction path.[59,142-145] This approach is based on the assumption that motion in the vibrational, rotational, and electronic degrees of freedom is fast compared with the motion of the system along the reaction path, and, although not strictly true, it is the most consistent way of including one-dimensional tunneling in the hybrid quantal rate constant defined above.[34,59,142,145-151] Within the Born-Oppenheimer approximation used in calculating the potential energy surface, the electronic motion is already taken to be adiabatic, and since the lowest-energy state has no rotational energy, only vibrational adiabaticity has an explicit effect on the effective potential. Furthermore, at low temperatures, where tunneling is most important, a quantized system is in its ground state, so that the one-dimensional adiabatic potential governing the reaction-path motion is taken to be the vibrationally adiabatic ground-state potential energy curve of Equation 59. Thus, neglecting the curvature of the reaction path, the motion of the system is described by the Hamiltonian:

$$\mathcal{H}(s,p_s) = \frac{1}{2\mu}p_s^2 + V_a^G(s) \tag{84}$$

where p_s is the momentum conjugate to the reaction coordinate s. Equation 84 shows that the vibrational adiabatic approximation reduces the full quantum scattering problem to the one-dimensional motion of a point of mass (μ) on the adiabatic potential curve $V_a^G(s)$. Based

on the adiabatic theory of reactions with a proper zero-point energy correction for the implicit threshold energy $V_a^G[s_*^{CVT}(T)]$ of the hybrid quantal CVT rate constant,[20,33,34] the adiabatic ground-state CVT transmission coefficient is given by the ratio of the thermally averaged quantal transmission probability P(E) to the thermally averaged classical transmission probability for the same vibrationally adiabatic barrier:[34,58,59]

$$\kappa^{CVT/SAG}(T) = \frac{\int_0^\infty P^{SAG}(E)\exp(-\beta E)dE}{\int_0^\infty \theta\{E - V_a^G[s_*^{CVT}(T)]\}\exp(-\beta E)dE} \tag{85a}$$

$$= \frac{\int_0^\infty P^{SAG}(E)\exp(-\beta E)dE}{\int_{V_a^G[s_*^{CVT}(T)]}^\infty \exp(-\beta E)dE} \tag{85b}$$

$$= \beta\exp\{V_a^G[s_*^{CVT}(T)]\}\int_0^\infty P^{SAG}(E)\exp(-\beta E)dE \tag{85c}$$

where $\theta(x)$ is the Heaviside unit-step function. We will see that the fact that the integrals in Equations 85a to c extend to infinity also allows for the inclusion of nonclassical reflection at energies above the barrier. (Strictly speaking, the integrals should only extend up to the lowest dissociation energy of the system. As before, the presence of the Boltzmann weighting factor in the integrand allows us to use the more convenient infinite upper limit for the integral since the added contributions are assumed to be negligible at the temperatures under consideration.) Although the transmission probability [P(E)] in Equation 85a to c could be obtained by a quantum mechanical calculation, it is much more convenient to use semiclassical methods,[151-157] which generally have been found to yield results within 10% of the accurate quantal values.[34,35,157] Thus, by $P^{SAG}(E)$ in Equations 85a to c we mean the one-dimensional uniformized semiclassical approximation to the one-dimensional transmission probability at total energy E through the vibrationally adiabatic ground-state potential $V_a^G(s)$.[34,157] Note that later in this section, after we introduce reaction-path curvature effects, it will be convenient to rename the present approximation $P^{MEPSAG}(E)$. If V^{AG} denotes the maximum value of $V_a^G(s)$, then for $E < V^{AG}$ the uniform semiclassical approximation to the transmission probability is given by

$$P^{SAG}(E) = \{1 + \exp[2\theta(E)]\}^{-1} \tag{86}$$

where the imaginary-action integral $\theta(E)$ is

$$\theta(E) = \hbar^{-1}\int_{s_<}^{s_>}\{2\mu[V_a^G(s) - E]\}^{1/2}ds \tag{87}$$

which is just 2π times the action integral between the classical turning points $s_<$ and $s_>$ [the locations at which $V_a^G(s) = E$] for reaction-coordinate motion along the tunneling path through the classically forbidden region. In order to perform the Boltzmann average in Equation 85c, the tunneling probability must also be approximated for $E > V^{AG}$, for which the effects of nonclassical reflection should be incorporated. If the barrier in $V_a^G(s)$ is assumed to be parabolic in the region of the maximum, then it can be shown semiclassically that for energies above but near the barrier:[152]

$$P^{SAG}(V^{AG} + \Delta E) \cong 1 - P^{SAG}(V^{AG} - \Delta E) \tag{88}$$

where $\Delta E = E - V^{AG}$. Since $P^{SAG}(V^{AG})$ given by Equation 86 is $^1/_2$, Equation 88 provides a continuous extension of the transmission probability for energies above V^{AG}. In addition, the presence of the Boltzmann factor in the integrand of Equation 85c allows for the use of Equation 88 at energies well above the barrier, since the contributions from such energies are assumed to be small. Thus, denoting the quantal threshold energy by E_0:

$$E_0 = \max[V_a^G(s = -\infty), V_a^G(s = +\infty)] \tag{89}$$

the full semiclassical prescription for the transmission probability is

$$P^{SAG}(E) = \begin{cases} 0, & E < E_0 \\ \{1 + \exp[2\theta(E)]\}^{-1}, & E_0 \leq E \leq V^{AG} \\ 1 - P^{SAG}(2V^{AG} - E), & V^{AG} \leq E \leq 2V^{AG} - E_0 \\ 1, & 2V^{AG} - E_0 < E \end{cases} \tag{90}$$

The semiclassical approximation to the transmission coefficient is obtained by substituting Equation 90 into Equation 85c, which can be written conveniently as

$$\kappa^{CVT/SAG}(T) = \exp\{V_a^G[s_*^{CVT}(T)] - V^{AG}\} \times \left\{1 + 2\beta \int_{E_0}^{V^{AG}} P^{SAG}(E) \sinh[\beta(V^{AG} - E)]dE\right\} \tag{91}$$

If the integration of the imaginary-action integral $\theta(E)$ is carried out along the MED as indicated above, the resulting semiclassical transmission coefficient is denoted by $\kappa^{CVT/MEPSAG}(T)$. It is indeed reasonable to evaluate the imaginary-action integral along the MEP in the absence of reaction-path curvature, since in that case there are no internal centrifugal forces that would tend to make the system leave the MEP.[158,159] However, it is also possible to modify the tunneling path in order to include the effects of reaction-path curvature, which have been found to be important in obtaining reliable results in many cases.[34,39,48,58,87,91,151,159,160] For example, accurate quantal calculations of the rate constants for the collinear $H + H_2$ and $D + D_2$ reactions demonstrate that the transmission coefficients obtained by measuring the vibrationally adiabatic barrier along the MEP are not accurate.[34,147-149] One generally successful approach to incorporating curvature for atom-diatom collisions with collinear MEPs is to choose the tunneling path in the classically forbidden region as the path of concave-side zero-point energy turning points for the mode coupled to the reaction coordinate by reaction-path curvature.[34,55,58,87,151] This path, which was shown through numerical trials by Marcus and Coltrin[151] to be the optimum tunneling path for collinear $H + H_2$ by analytically continuing the classical mechanical least-action principle into the domain of complex momenta, corresponds to "cutting the corner" of the potential energy surface (cf. Figure 2), and can be understood in the sense that in the classically forbidden region the kinetic energy is negative (corresponding to the momentum being imaginary), leading to a negative internal centrifugal effect, i.e., motion toward the inside of the MEP ("corner cutting") rather than toward the outside ("bobsledding").[142,161-166] Within the semiclassical adiabatic approximation, the effective potential is $V_a^G(s)$ if the tunneling path remains within the ground-state vibrational amplitude around the MEP.[151] Thus, the shortening of the path by corner cutting simply contracts the effective barrier for the tunneling calculation, i.e., makes it thinner, and there is less exponential damping for a given total energy. Hence, a larger value of $P^{SAG}(E)$ is obtained than for tunneling along

the MEP. The path chosen as just described is called the Marcus-Coltrin path (MCP), and transmission coefficients obtained in this manner are denoted by $\kappa^{CVT/MCPSAG}(T)$. As an example of the MCP, consider the three-dimensional D + H_2 and H + D_2 reactions.[33] In these cases, the MEP is collinear, so there is no curvature coupling of the reaction coordinate to the bending modes and the tunneling path is chosen to be the path of outer turning points of the bound stretching mode; this leads to good agreement with experiment.[33] To generalize the physical model that underlies the MCP to many-dimensional systems that have curvature coupling of the reaction coordinate to more than one bound degree of freedom, we and Skodje have developed a new approximation called the small-curvature (SC) approximation.[39,91,159] This approximation is based on an alternative approach in which we treat the effect of reaction-path curvature by using an effective mass for reaction-coordinate motion. That is, if ξ measures the distance along an arbitrary tunneling path, then the imaginary-action integral becomes

$$\theta(E) = \hbar^{-1} \int_{\xi<}^{\xi>} \{2\mu[V_a^G(\xi) - E]\}^{1/2} \, d\xi \tag{92}$$

However, since ξ is related to s through a metric factor $M(s)$ by

$$d\xi = M(s) \, ds \tag{93}$$

Equation 92 can be rewritten as

$$\theta(E) = \hbar^{-1} \int_{s<}^{s>} \{2\mu_{eff}(s)[V_a^G(s) - E]\}^{1/2} \, ds \tag{94}$$

where

$$\mu_{eff}(s) = \mu[M(s)]^2 \tag{95}$$

To describe the SC approximation in detail, recall that the harmonic approximation to the potential energy for points near the reaction path can be written in terms of the reaction coordinate s and the F − 1 orthogonal normal-mode coordinates $Q_m(s)$ as in Equation 48. (Anharmonic effects are considered below after the complete presentation of the harmonic limit.) For a discussion of dynamical effects, we thus need to express the kinetic energy in these same coordinates. For the case of zero total angular momentum (for which we can neglect rotation-vibration coupling), the kinetic energy is given by[76]

$$\begin{aligned} T(s,p_s,Q_1,\ldots,Q_{F-1},P_1,\ldots,P_{F-1}) &= \frac{1}{2\mu} \sum_{m=1}^{F-1} P_m^2(s) \\ &+ \frac{1}{2\mu} \frac{\left[p_s - \sum_{m=1}^{F-1} \sum_{m'=1}^{F-1} Q_m(s) P_{m'}(s) B_{mm'}(s) \right]^2}{\left[1 + \sum_{m=1}^{F-1} Q_m(s) B_{mF}(s) \right]^2} \end{aligned} \tag{96}$$

where $P_m(s)$ and p_s are the momenta conjugate to $Q_m(s)$ and s, respectively,

$$B_{mm'}(s) = \sum_{i=1}^{N} \sum_{\gamma} \left[\frac{d}{ds} L_{i\gamma,m}^{GT}(s) \right] L_{i\gamma,m'}^{GT}(s) \tag{97}$$

and

$$B_{mF}(s) = -[\text{sign}(s)] \sum_{i=1}^{N} \sum_{\gamma} \frac{dv_{i\gamma}(s)}{ds} L^{GT}_{i\gamma,m}(s) \tag{98}$$

where $v_{i\gamma}(s)$ is the $i\gamma$ component of the normalized gradient vector defined in Equation 32. [In another notation,[34,91] $\kappa_m(s)$ is used to denote $B_{mF}(s)$ so the denominator of the last term in Equation 96 becomes $1 - \boldsymbol{\kappa}(s) \cdot \mathbf{Q}(s)]^2$. Here the quantities $B_{mm'}(s)$ are Coriolis-like couplings between the modes arising from the twisting of the normal modes about the MEP [with $B_{mm}(s) = 0$], while $B_{mF}(s)$ is the component of the reaction-path curvature:

$$\kappa(s) = \left\{ \sum_{m=1}^{F-1} [B_{mF}(s)]^2 \right\}^{1/2} \tag{99}$$

along the direction of mode m at s, which is chosen such that the product $Q_m(s)B_{mF}(s)$ is negative when $Q_m(s)$ is taken on the concave side of the MEP. If we neglect the Coriolis-like couplings [which do not appear in the Marcus-Coltrin path method since $P_m(s) = 0$ at a turning point of mode m] and treat the motion in the vibrational degrees of freedom adiabatically (i.e., averaged over a vibrational period), the Hamiltonian of Equation 84 for the one-dimensional motion of the system along the reaction coordinate is replaced by

$$\mathcal{H}(s,p_s) = \frac{<A>(s)}{2\mu} p_s^2 + V_a^G(s) \tag{100}$$

where $< A >(s)$ denotes the appropriate average of $[1 + \sum_{m=1}^{F-1} Q_m(s)B_{mF}(s)]^{-2}$ over the vibrational degrees of freedom along the tunneling path. Thus, the effective mass $\mu_{eff}(s)$ can be thought of as the ratio of μ to $< A >(s)$, so that the quantity $[M(s)]^2$ of Equation 95 can be viewed as an approximation to $[< A >(s)]^{-1}$, hence providing an effective mass for motion measured along the MEP. Of course, for tunneling along the MEP, as in $\kappa^{CVT/MEPSAG}(T)$, the curvature is ignored, so that $< A >(s) = 1$ and $\mu_{eff}^{MEP}(s) = \mu$. If the tunneling path is chosen to be the Marcus-Coltrin path of concave-side turning points, as in $\kappa^{CVT/MCPSAG}(T)$, the metric factor $M(s)$ in Equation 93 relating an element of length $(d\xi)$ along the tunneling path to an element of length (ds) along the MEP can be shown by analytic geometry to be[91]

$$M(s) = \left\{ [1 + \sum_{m=1}^{F-1} B_{mF}(s)t_m(s)]^2 + \sum_{m=1}^{F-1} [dt_m(s)/ds]^2 \right\}^{1/2} \tag{101}$$

where $t_m(s)$ is the value of the mass-scaled normal coordinate $Q_m(s)$ at the zero-point energy turning point of mode m on the concave side of the MEP, which in the harmonic approximation is given by $\pm [\hbar/\mu\omega_m(s)]^{1/2}$, where the sign is chosen to be opposite that of $B_{mF}(s)$ [Recall that the sign of $B_{mF}(s)$ is chosen such that the product $B_{mF}(s)t_m(s)$ is negative]. Thus, curvature lowers the effective mass of Equation 95:

$$\mu_{eff}^{MCP}(s) = \mu \left\{ [1 + \sum_{m=1}^{F-1} B_{mF}(s)t_m(s)]^2 + \sum_{m=1}^{F-1} [dt_m(s)/ds]^2 \right\} \tag{102}$$

and hence lowers the barrier penetration integral $\theta(E)$ in Equation 94 and raises the tunneling probability $P^{SAG}(E)$ in Equation 86. For cases in which the curvature is large, however, the magnitude of the first summation in Equation 102 can be larger than one (i.e., the sum can

be less than -1), corresponding to a breakdown of the reaction-path coordinate system which allows the tunneling path to "wrap around" on itself (see, e.g., Figure 1 of Reference 58). To avoid this difficulty, we treat the MCP effective mass in Equation 102 as an expansion in the SC limit and we "unexpand" it to remove the singularity in the coordinate system to infinity. In addition, if the curvature component $B_{mF}(s)$ for mode m is zero, we require that this mode have no effect on the effective mass. This yields:[39,48,91]

$$\mu_{eff}^{SC}(s) = \mu \prod_{m=1}^{F-1} \min \begin{cases} \exp\{-2a_m(s) - [a_m(s)]^2 + [dt_m(s)/ds]^2\} \\ 1 \end{cases} \tag{103}$$

where

$$a_m(s) = -B_{mF}(s)t_m(s) = |B_{mF}(s)t_m(s)| \tag{104}$$

Use of the SC effective mass $[\mu_{eff}^{SC}(s)]$ leads to the SC approximation to the semiclassical adiabatic ground-state transmission coefficient, $\kappa^{CVT/SCSAG}(T)$. Though this method could be applied to large-curvature systems without singularities, we have found that it is most accurate for systems with small to intermediate curvature. In fact, it has already been shown to give reasonably reliable results in atom-diatom studies,[39,91,159] while still being sufficiently practical for polyatomic systems.[39,48]

The curvature components $B_{mF}(s)$ appearing in Equation 104 are computed from Equation 98 at each of the locations (here assumed to be equispaced) along the MEP at which a generalized normal-mode analysis is performed, with the derivative of the gradient obtained by one-sided numerical differencing with a step size δs equal to that used for computing the MEP (typically 0.0001 a_0):

$$dv_{i\gamma}(s)/ds = \{v_{i\gamma}(s) - v_{i\gamma}[s - \delta s \text{ sign}(s)]\}/\delta s \tag{105}$$

A numerical method which is more stable with respect to step size δs is to use central differences to compute this derivative. We have incorporated this improvement in our studies of atom-diatom reactions and have obtained significantly better stability. The turning-point derivative terms $[dt_m(s)/ds]^2$ are computed at s by a two-point central-difference method using the turning-point results obtained at adjacent locations at which the normal modes are found:

$$[dt_m(s)/ds]^2 = \{[t_m(s + \Delta s) - t_m(s - \Delta s)]/2\Delta s\}^2 \tag{106}$$

where Δs denotes the separation between the equispaced normal-mode analyses (typically 0.01 a_0). For the first (s_1) and last (s_M) points on the MEP from the saddle point at which a normal-mode analysis is performed, the turning-point derivative term is obtained by Lagrangian interpolation:[86]

$$[dt_m(s_1)/ds]^2 = \{[-3t_m(s_1) + 4t_m(s_2) - t_m(s_3)]/(s_3 - s_1)\}^2 \tag{107a}$$

$$[dt_m(s_M)/ds]^2 = \{[t_m(s_{M-2}) - 4t_m(s_{M-1}) + 3t_m(s_M)]/(s_M - s_{M-2})\}^2 \tag{107b}$$

Since $\nabla V = 0$ at the saddle point, the curvature components cannot be determined accurately there by the method described above. Instead, the effective mass at the saddle point is found from a linear interpolation between the two closest values of $\mu_{eff}^{SC}(s)$:

$$\mu_{eff}^{SC}(s = 0) = [\mu_{eff}^{SC}(s = +\Delta s) + \mu_{eff}^{SC}(s = -\Delta s)]/2 \tag{108}$$

For convenience, the effective mass $[\mu_{eff}^{SC}(s)]$ and adiabatic potential $[V_a^G(s)]$ are fit by cubic spline functions. The imaginary-action integral $\theta(E)$ of Equation 94 is then obtained by quadrature as follows.[157] First, the limits of integration $s_<$ and $s_>$ are found by Newton root searches for points where

$$V_a^G(s) - E = 0 \tag{109}$$

between two close points on either side of the crossings. (Although $s_<$ and $s_>$ could have been obtained from the solutions of cubic equations involving the spline coefficients, the present approach is more general.) Next, by a suitable change of variables, we reduce the integration interval to the region $[-1,1]$, for which we choose a set of $2n + 1$ quadrature points g_i and weights w_i by Kronrod's improved Gaussian quadrature method.[167] This method provides both an n-point Gauss-Legendre estimate and a $(2n + 1)$-point quadrature estimate such that n of the nodes of the latter are restricted to be the same as in the former, thus providing a convenient convergence test of the quadrature size. Rather than performing the numerical integration with the points g_i, faster convergence can be obtained in some cases by an alternate choice of quadrature variable y_i, given by

$$g(y) = (2/\pi)[y(1 - y^2)^{1/2} + \arcsin y] \tag{110}$$

which is based on approximating $V_a^G(s)$ as a symmetric parabola between $s_<$ and $s_>$. The quadrature points y_i are obtained from the g_i values by inverting Equation 110 numerically with Newton's method of iteration, which gives the $(j + 1)$ iterate for y_i in terms of the *jth* iterate as

$$y_i^{(j+1)} = {}^1/_2 y_i^{(j)} - [2 \arcsin y_i^{(j)} - \pi g_i]/4\{1 - [y_i^{(j)}]^2\}^{1/2} \tag{111}$$

Applying this quadrature scheme to the imaginary-action integral of Equation 94 yields:

$$\theta(E) \cong (\pi A/4\hbar) \sum_{i=1}^{2n+1} W_i\{2\mu_{eff}(s_i)[V_a^G(s_i) - E]\}^{1/2} \tag{112}$$

where

$$s_i = A(1 + y_i) + s_< \tag{113}$$

with

$$A = (s_> - s_<)/2 \tag{114}$$

and

$$W_i = w_i(1 - y_i^2)^{-1/2} \tag{115}$$

In Equation 112, $\mu_{eff}(s)$ is taken to be μ for tunneling along the MEP or $\mu_{eff}^{SC}(s)$ for the SC approximation. Although extra computational effort is required for generating the y_i and W_i values, note that for a given quadrature size these quantities need be determined only once. In atom-diatom studies, $(2n + 1)$ values of less than 20 are often sufficient for convergence to 1% or better between the n- and $(2n + 1)$-point results, although a $(2n + 1)$ value of 61 was needed for similar convergence for the $OH + H_2$ system. In practice, the semiclassical tunneling calculations are not the most expensive part of the calculation, so we often use

$(2n + 1)$ equal to 41 to 61 to ensure good convergence with less checking. Some potential functions have more than one local maximum, so that at certain total energies there is more than one classically forbidden region. In such a case, the overall imaginary-action integral is taken to be the sum of the results obtained by a $(2n + 1)$-point quadrature in each classically forbidden region.

The semiclassical transmission probability $P^{SAG}(E)$ is obtained from $\theta(E)$ by Equation 86, and the Boltzmann average for the transmission coefficient $\kappa^{CVT/SAG}(T)$ in Equation 91 is performed with straight numerical integration using Kronrod's method. The numbers of quadrature points required to converge the integral over energy are similar to those required to converge the integral over s as discussed above. Within the assumptions discussed above, the quantal CVT rate constant is obtained from the hybrid quantal one by

$$k^{CVT/MEPSAG}(T) = k^{CVT}(T)\, \kappa^{CVT/MEPSAG}(T) \tag{116}$$

when the tunneling path is taken to be the MEP (i.e., curvature is neglected), and by

$$k^{CVT/SCSAG}(T) = k^{CVT}(T)\, \kappa^{CVT/SCSAG}(T) \tag{117}$$

when tunneling is calculated under the SC approximation.

The parabolic approximation for nonclassical reflection, as embodied in Equation 88 and the third line of Equation 90, may be justified as a mapping of the SCSAG tunneling probabilities onto the semiclassical solution for one-dimensional scattering by a parabolic potential. One could argue, though, that at energies above the barrier maximum it is physically inappropriate to base the results on $P^{SCSAG}(E)$, which depends on $\mu_{eff}^{SC}(s)$, since the tunneling-path model that leads to $\mu_{eff}^{SC}(s)$ does not apply at energies above the barrier maximum.[159] An alternative model for nonclassical reflection is to replace the third line of Equation 90 by

$$P(E) = 1 - P^{MEPSAG}(E) \quad , \quad V^{AG} \leq E \leq 2V^{AG} - E_0 \tag{118}$$

If the SCSAG model is used for tunneling and Equation 118 is used for nonclassical reflection, we call it the SC tunneling semiclassical adiabatic ground-state (SCTSAG) model to emphasize that $\mu_{eff}^{SC}(s)$ is used only for tunneling energies.[159] The SCTSAG method yields rate constants very similar to those obtained by the SCSAG method, but slightly larger and usually slightly more accurate.

To include anharmonicity in the MEPSAG, SCSAG, or SCTSAG transmission coefficient, we first replace the harmonic $V_a^G(s)$ by the anharmonic one. In addition, since the SCSAG and SCTSAG transmission coefficients involve the distance from the curved reaction path to the vibrational ground-state classical turning point on its concave side, we must use the anharmonic value for the turning-point distance. For a Morse oscillator with the potential given in Equation 65, the concave-side turning point of the ground-state level is found as follows. Define:

$$z(s) = \pm[\epsilon_{vib,m}^{GT}(n_m = 0, s)/D_e(s)]^{1/2} \tag{119}$$

where the sign of $z(s)$ is given by

$$\text{sign}[z(s)] = -\text{sign}[B_{mF}(s)]\text{sign}[k_{mmm}(s)] \tag{120}$$

Then the concave-side turning point for this mode is given by

$$t_m(s) = \frac{1}{\beta_{M,m}(s)} \ln[1 + z(s)]\text{sign}[k_{mmm}(s)] \tag{121}$$

For a quadratic-quartic oscillator corresponding to the potential of Equation 70, the concave-side turning point is found by solving the equation $V_{qq,m}[s,Q_m(s)] = \epsilon^{GT}_{vib,m}(n_m = 0,s)$, which is quadratic in $[Q_m(s)]^2$. This yields:

$$t_m(s) = \pm\{-k_{mm}(s) + [k^2_{mm}(s) + 16k_{mmmm}(s)\epsilon^{GT}_{vib,m}(n_m = 0, s)]^{1/2}/4k_{mmmm}(s)\}^{1/2} \tag{122}$$

where the sign of $t_m(s)$ is chosen to be opposite that of $B_{mF}(s)$.

As mentioned below Equations 85a to c, instead of finding the tunneling probability by the uniform semiclassical approximation, we could solve the effective one-dimensional Schrödinger equation numerically. For the MCP and SC approximations this involves a contracted adiabatic barrier.[39,58,87] Although the numerical quantal solution is, in principle, more accurate than the semiclassical one, the differences for realistic potentials are not great.[34,157] Since the numerical quantal solution is much more expensive, we prefer the uniform semiclassical method.

As noted above, the CVT/SCSAG and CVT/SCTSAG methods generally provide significantly more reliable results than does the CVT/MEPSAG method. A recent review of several cases is presented in Reference 39. For example, in the collinear H + H_2 reaction, the CVT,[58] CVT/MEPSAG,[34] and CVT/SCSAG[39] rate constants calculated for the potential energy surface of Truhlar and Kuppermann[148] underestimate the accurate quantal results[148] for this surface at 200 K by factors of 29, 14, and 1.3, respectively. At 400 K, the corresponding factors are 2.0, 1.8, and 1.2, respectively. (The results quoted in this paragraph include the effects of anharmonicity. The CVT results used for this comparison are the hybrid ones; in contrast, we note that the *classical* CVT rate constant underestimates the accurate results by factors of 7.4×10^4 at 200 K and 67 and 400 K.[21]) Similar effects are observed for the H + H_2 reaction in three dimensions, namely the CVT,[33,55] CVT/MEPSAG,[39] and CVT/SCSAG[39] rate constants calculated for the realistic Porter-Karplus surface no. 2[168] underestimate the accurate quantal values[6] (see also Reference 55) for this surface by factors of 23, 7.1, and 1.6, respectively, at 300 K, and by factors of 2.2, 1.7, and 1.1, respectively, at 600 K. These results demonstrate that in order to obtain reliable rate constants, quantum effects must be properly and consistently incorporated into the theory. In particular, tunneling corrections must be employed that account for reaction-path curvature. As another example we consider the reaction OH + $H_2 \rightarrow H_2O$ + H. Our CVT/SCSAG calculations[48] for this system, based on the Schatz-Elgersma analytic representation[96] of the *ab initio* Walch-Dunning potential energy surface[97] and including anharmonicity, agree with the recently recommended experimental results,[169] based on an evaluation of all available data, to within a factor of 1.6 at all temperatures in the range 298 to 2400 K. Over this range the rate constant varies by a factor of 2000, and $\kappa^{CVT/SCSAG}$ varies by a factor of 17.3. The use of conventional TST or the neglect of anharmonicity or reaction-path curvature significantly worsens the agreement with experiment.

It is important to emphasize that the SCSAG method, which is based on the SC approximation, works quite well for H + H_2, for which the effect of reaction-path curvature is large. Nevertheless, we classify the reaction-path curvature itself as small to intermediate for this reaction. Large reaction-path curvature is often encountered in the tunneling region in systems with small skew angles. We define the skew angle β for a multidimensional system as the angle between the gradient $\nabla V[\mathbf{x}(s)]$ in the product channel and the gradient in the reactant channel. [We use β for the skew angle for consistency with our published

work. We assume there will be no confusion with $(k_B T)^{-1}$ which β represents in other contexts in this chapter.] For the bimolecular reaction AX + B → A + BX, where A, X, and B are comprised of one or more atoms, the skew angle is defined by

$$\cos \beta = [m_A m_B/(m_A + m_X)(m_B + m_X)]^{1/2} \tag{123}$$

where m_A, m_X, and m_B are the masses of the A, X, and B moieties, respectively. The reaction-path curvature and skew angle are related as follows: The tangent vector to the reaction coordinate at $\mathbf{x}(s)$ is $\dot{\mathbf{x}}(s)$, where an overdot denotes a derivative with respect to s, i.e.,

$$\dot{\mathbf{x}}(s) = d[\mathbf{x}(s)]/ds \tag{124}$$

From the definition of s as the arc length along the reaction path, it follows that $\dot{\mathbf{x}}(s)$ is a unit vector.[170-173] It is related to $\mathbf{v}(s)$ of Equation 32 by

$$\dot{\mathbf{x}}(s) = +\text{sign}(s)\, \mathbf{v}(s) \tag{125}$$

For the present discussion $\dot{\mathbf{x}}(s)$ is more convenient because it is a continuous function of s, whereas $\mathbf{v}(s)$ changes sign discontinuously at $s = 0$. The curvature vector is defined by

$$\boldsymbol{\kappa}(s) = d[\dot{\mathbf{x}}(s)]/ds = \ddot{\mathbf{x}}(s) \tag{126}$$

The magnitude $\kappa(s)$ of $\boldsymbol{\kappa}(s)$ is the curvature of the reaction path at $\mathbf{x}(s)$, and the unit vector in the direction of $\boldsymbol{\kappa}(s)$ is the principal normal of the reaction path.[170-173] The projections of $\boldsymbol{\kappa}(s)$ along the normal-mode coordinates are the negatives of the quantities in Equation 98 (see the remark in brackets after Equation 98). Defining the values of $\mathbf{x}(s)$ in the reactant and product channels as $\mathbf{x}^R$ and $\mathbf{x}^P$, respectively, the skew angle is related to the curvature by

$$[\int_{-\infty}^{\infty} \boldsymbol{\kappa}(s)ds] \cdot \dot{\mathbf{x}}^R = (\dot{\mathbf{x}}^P - \dot{\mathbf{x}}^R) \cdot \dot{\mathbf{x}}^R \tag{127a}$$

$$= -(1 + \cos \beta) \tag{127b}$$

Notice from Equation 123 that B lies in the range $0 < B < B/2$. Thus, the curvature must satisfy the relation:

$$1 < \left|\int_{-\infty}^{\infty} [\boldsymbol{\kappa}(s) \cdot \dot{\mathbf{x}}^R]ds\right| < 2 \tag{128}$$

for the fragment-transfer reaction AX + B → XB. Furthermore, small skew angles, which occur when m_X is much less than m_A and m_B, require larger components in the $\mathbf{x}^R$ direction of the reaction-path curvature. In general, from this kind of analysis, we expect large reaction-path curvature whenever a light atom or fragment is transferred between two heavy moieties.

As an example of a small skew angle system, consider the transfer of a hydrogen atom between two heavy atoms such as chlorine. For this symmetric reaction the reaction-path curvature becomes very large in the region around the saddle point (see Figure 2C). In the asymptotic reactant and product valleys the motion along the reaction path corresponds to the motion of a Cl atom relative to an HCl molecule, and the bound motion perpendicular

to the reaction coordinate is the HCl vibration. In these regions the adiabatic separation of the HCl vibration from the slower Cl, HCl translation is expected to be valid. At the saddle point the symmetric, bound motion corresponds to the slow movement of the two Cl atoms relative to each other with the H atom fixed; motion along the reaction coordinate is the faster motion of the hydrogen between two fixed Cl atoms. In this region we expect the vibrationally adiabatic approximation to break down.

When reaction-path curvature is large in the tunneling region, we expect that the vibrationally adiabatic model used for the MCPSAG and SCSAG transmission coefficients breaks down there. For this situation we use more general semiclassical ground-state (SG) transmission probabilities $P^{SG}(E)$. For large-curvature atom-diatom systems with collinear tunneling paths we have presented a nonadiabatic approach,[44,49] the large-curvature ground-state (LCG) tunneling method, that is similar to models employed by Ovchinnikova[174] and Babamov and Marcus.[175] The physical picture of the LCG method is that the reactants approach adiabatically from $s = -\infty$ to the turning point on the adiabatic potential energy curve and then retreat back to $s = -\infty$. All along this path (from $s = -\infty$ to the turning point and back out), using the Cl + HCl reaction as an example, there is a probability that the hydrogen will tunnel from one Cl atom to the other. The tunneling is assumed to occur along the most direct path between the reactant and product valleys with no vibrational adiabaticity relative to the reaction-coordinate motion. For the collinear Cl + HCl reaction on the potential surface of Reference 49, the tunneling path for an energy of 7.8 kcal/mol is shown in Figure 2C as the straight line between the MEP in the reactant and product channels. For the symmetric example considered here the tunneling motion corresponds to the Cl atoms remaining fixed with the hydrogen atom tunneling from one Cl to the other. With this picture in mind we now present a more detailed description of a more general method for calculating transmission coefficients for large-curvature systems. When it is necessary to make the distinction, the method presented here will be called LCG3 (large-curvature ground-state approximation, version 3). The LCG3 method is based on the same physical model as the LCG and LCG2 methods of References 44 and 49, but it does not reduce exactly to either of them, even for the special case of atom-diatom reactions with collinear tunneling paths. It has been changed to allow for easier applicability to polyatomic systems and also to be similar to a special case of the least-action ground-state (LAG) method discussed below. Numerical calculations on the Cl + HCl reaction and several other reactions have shown, however, that the LCG, LCG2, and LCG3 methods yield similar results.

We will present the LCG3 and LAG models for the special case of symmetric or almost thermoneutral reactions for which only the ground states of reactants and products are important at the low temperatures for which the transmission coefficients differ significantly from unity. For less symmetric reactions one would calculate the ground-state transmission coefficient in the exoergic direction by summing the state-to-state reaction probabilities over all important states of the products.

For a tunneling energy E such that E is less than the maximum V^{AG} of the ground-state adiabatic potential, the two outermost turning points (s_0 and s_1) on the adiabatic ground-state potential are defined by

$$V_a^G(s_i) = E \quad , \quad i = 0,1 \tag{129}$$

where $V_a^G(s) < E$ for $s < s_0$ and $s > s_1$. If $T_{tun}(\bar{s}_0)$ is the amplitude for tunneling at the location $\bar{s}_0$ along the reaction path, then the total amplitude for tunneling on the way in is obtained by averaging the amplitudes for tunneling at each $\bar{s}_0$ between $\bar{s}_0 = -\infty$ and s_0:

$$T_0(E) = \int_{-\infty}^{s_0} V_R^{-1}(E,\bar{s}_0)\, \tau^{-1}(\bar{s}_0)\, T_{tun}(\bar{s}_0)\, d\bar{s}_0 \tag{130}$$

where the adiabatic approximation to the local speed along the reaction coordinate at s is

$$V_R(E,\bar{s}_0) = \left\{\frac{2}{\mu}[E - V_a^G(\bar{s}_0)]\right\}^{1/2} \tag{131}$$

and $\tau^{-1}(\bar{s}_0)$ is the number of collisions per unit time that the reactants make with the potential wall separating reactants and products. We have not included a survival factor in Equation 130 because we are calculating the primitive semiclassical amplitude which is only valid when the tunneling probability is small. The tunneling path for each $\bar{s}_0$ is a straight line through the mass-weighted coordinates **x** the end points are $\mathbf{x}(\bar{s}_0)$ and $\mathbf{x}(\bar{s}_1)$, i.e., they lie on the MEP. The end point in the product valley is determined by the resonance condition:

$$V_a^G(\bar{s}_0) = V_a^G(\bar{s}_1) \tag{132}$$

The total amplitude for tunneling along the way in and back out would be $2T_0(E)$; however, to ensure the method satisfies microscopic reversibility, we define the total amplitude as

$$T(E) = T_0(E) + T_1(E) \tag{133}$$

where $T_1(E)$ is the amplitude for tunneling from products to reactants averaged over the half collision from $\bar{s}_1 = s_1$ to $\bar{s}_1 = \infty$.

The definition of $\tau(\bar{s}_1)$ is straightforward for a collinear three-atom system at low energy in the limit of very large curvature where the tunneling path is almost perpendicular to the MEP: it is the period of the vibrational motion normal to the reaction coordinate $\bar{s}_0$. The extension to polyatomic systems is not as obvious. One possible extension is that proposed in another context by Slater[176] in which $\tau(\bar{s}_0)$ is expressed as the geometric mean of the periods for the independent normal modes. This does not contain the correct physical picture for systems in which there is only one mode with large curvature and the rest are only spectator modes throughout the tunneling process. For this case, the vibrational period should depend mainly on the one mode that is strongly coupled to the reaction coordinate. To accomplish this we define the vibrational period in terms of the tunneling path, which is given by

$$\mathbf{x}(\xi) = \mathbf{x}_0 + \left(\frac{\xi - \xi_0}{\xi_1 - \xi_0}\right)(\mathbf{x}_1 - \mathbf{x}_0) \tag{134}$$

where $\mathbf{x}_i$ denotes $\mathbf{x}(\bar{s}_i)$ for $i = 0$ or 1, ξ measures the distance along the tunneling path, and ξ_i is the value of ξ at $\bar{s}_i$. This path involves motion in both the normal Q_m and the reaction coordinate(s). In the classically allowed region near the MEP, the normal- and reaction-coordinate motions are treated separately under an adiabatic approximation; therefore, we assume that the vibrational period $\tau(\bar{s}_0)$ depends on only the normal-coordinate motions at $\bar{s}_0$. The tunneling path is projected onto the $(F - 1)$-dimensional hyperplane of bound normal coordinates **Q** perpendicular to the reaction path at $\bar{s}_0$. The normal coordinates along this projected path are given by

$$Q_m^{\perp}(\xi_\perp) = \xi_\perp q_{\perp,m}(\bar{s}_0) \quad , \quad m = 1,\ldots,F - 1 \tag{135}$$

where $\xi_\perp$ measures the distance along the projection of the tunneling path, and the components of a unit vector in the tunneling direction in the bound normal-coordinate space are given by

$$q_{\perp,m}(\bar{s}_0) = \frac{(\mathbf{x}_1 - \mathbf{x}_0) \cdot \mathbf{L}_m^{GT}(\bar{s}_0)}{\left\{\sum_{m=1}^{F-1} [(\mathbf{x}_1 - \mathbf{x}_0) \cdot \mathbf{L}_m^{GT}(\bar{s}_0)]^2\right\}^{1/2}} \quad , \quad m = 1,\ldots,F-1 \tag{136}$$

Notice that $\xi_\perp$ measures a length in the $(F-1)$-dimensional hyperplane and ξ measures a distance in the full 3N-dimensional space. In an harmonic treatment, the square of the frequency for the motion in the projected tunneling direction specified above is given by

$$\omega_\perp^2(\bar{s}_0) = \sum_{m=1}^{F-1} [\omega_m(\bar{s}_0) q_{\perp,m}(\bar{s}_0)]^2 \tag{137}$$

and the vibrational period is given by[177]

$$\tau(\bar{s}_0) = \frac{2\pi}{\omega_\perp(\bar{s}_0)} \tag{138}$$

A more complete treatment is to define $\tau(\bar{s}_0)$ semiclassically:

$$\tau(\bar{s}_0) = (2\mu)^{1/2} \int_{\xi_{\perp,0}}^{\xi_{\perp,1}} \left\{\epsilon_{vib}^{GT}(\mathbf{n} = 0, \bar{s}_0) - \sum_{m=1}^{F-1} V_m[\bar{s}_0, Q_m(\xi_\perp)]\right\}^{-1/2} d\xi_\perp \tag{139}$$

where $\xi_{\perp,0}$ and $\xi_{\perp,1}$ are the turning points of the zero-point motion in the one-dimensional potential

$$\sum_{m=1}^{F-1} V_m[\bar{s}_0, Q_m(\xi_\perp)].$$

Using this prescription, anharmonicity can be easily included in the definition of $\tau(\bar{s}_0)$.

The tunneling amplitude $[T_{tun}(\bar{s}_0)]$ is calculated semiclassically as

$$T_{tun}(\bar{s}_0) = \exp[-\theta(\bar{s}_0)] \tag{140}$$

where $\theta(\bar{s}_0)$ is the one-dimensional imaginary-action integral along the tunneling path. The imaginary-action integral is defined by

$$\theta(\bar{s}_0) = \theta[E_{av}(\bar{s}_0)] = \frac{(2\mu)^{1/2}}{\hbar} \int_{\xi_0}^{\xi_1} [V_{eff}(\xi) - E_{av}(\bar{s}_0)]^{1/2} \hat{\xi} \cdot \hat{z}(\xi) d\xi \tag{141}$$

where

$$E_{av}(\bar{s}_0) = V_a^G(\bar{s}_0) = V_a^G(\bar{s}_1) \tag{142}$$

is the energy available for tunneling, $V_{eff}(\xi)$ is the effective potential for tunneling, $\hat{\xi}$ is the unit vector along the tunneling path, and $\hat{z}(\xi)$ is a unit vector in the dynamical tunneling direction. Notice that part of the energy, namely, $E - V_a^G(\bar{s}_0)$, is assumed to be localized in the reaction coordinate, which is perpendicular to the tunneling direction in the large-curvature limit, and hence unavailable for motion along the tunneling path. Each value of ξ defines a unique point $\mathbf{x}(\bar{s}_0,\xi)$ in the mass-scaled coordinates by Equation 134 and each such point corresponds to at least one point in the curvilinear coordinates $[s(\bar{s}_0,\xi),\mathbf{Q}(\bar{s}_0,\xi)]$.

A unique value for $s(\bar{s}_0,\xi)$ is determined as follows. First we define $s(\bar{s}_0,\xi_0) = \bar{s}_0$, then for some ξ near ξ_0 a root search is performed to find the value of s such that the vector from $\mathbf{x}(s)$ to $\mathbf{x}(\bar{s}_0,\xi)$ is normal to the vector $\mathbf{v}(s)$ at s. This process is repeated using the value of s at ξ to begin the root search at $\xi + \Delta\xi$ and thereby to construct a single-valued and continuous function $s(\bar{s}_0,\xi)$. [In practice, this root search is carried out in terms of $s(\alpha,\gamma)$ described below as a special case corresponding to $\alpha = 1$]. The system is considered to be in the adiabatic region of the potential if the normal coordinates $\mathbf{Q}(\bar{s}_0,\xi)$ are within their outer turning points, i.e.,

$$\text{sign}\{t_m[s(\bar{s}_0,\xi)]\}Q_m(\bar{s}_0,\xi) < |t_m[s(\bar{s}_0,\xi)]| \quad , \quad m = 1,\ldots,F-1 \tag{143}$$

and if $[s(\bar{s}_0,\xi),\mathbf{Q}(\bar{s}_0,\xi)]$ lies within the locally single-valued region of the curvilinear coordinates, i.e.,

$$\sum_{m=1}^{F-1} B_{mF}[s(\bar{s}_0,\xi)]Q_m(\bar{s}_0,\xi) < 1 \tag{144}$$

The first point in going from $\bar{s}_0$ at which either Equation 143 or 144 is not satisfied is called ξ_0'. Similarly, the first point in going from $\bar{s}_1$ at which either Equation 143 or 144 is not satisfied is called ξ_1'. For $\xi_0 < \xi < \xi_0'$ and for $\xi_1 > \xi > \xi_1'$, the system is assumed to behave adiabatically in the $(s,\mathbf{Q})$ coordinates and the effective potential $V_{\text{eff}}(\bar{s}_0,\xi)$ is set equal to $V_a^G[s(\bar{s}_0,\xi)]$ and $\hat{z}$ is set equal to the unit vector along the MEP at $s(\bar{s}_0,\xi)$. For $\xi_0' < \xi < \xi_1'$, the tunneling is assumed to occur directly along the path defined by Equation 134: $\hat{z}$ is set equal to $\hat{\xi}$ and the effective potential is approximated by

$$V_{\text{eff}}(\bar{s}_0,\xi) = V[\mathbf{x}(\bar{s}_0,\xi)] + V_{\text{corr}}(\xi_0') + \left(\frac{\xi - \xi_0'}{\xi_1' - \xi_0'}\right)[V_{\text{corr}}(\xi_1') - V_{\text{corr}}(\xi_0')] \tag{145}$$

The first term is the actual potential energy surface and $V_{\text{corr}}(\xi_i')$ corrects for the zero-point energy in the modes which are still within their turning points:

$$V_{\text{corr}}(\xi_i') = \sum_{\substack{m=1 \\ Q_m<t_m}}^{F-1} \{\epsilon_{\text{vib},m}^{GT}[n_m = 0, s(\xi_i')] - V_m[s(\xi_i'),Q_m(\xi_i')] + V_m[s(\xi_i'), 0]\} \tag{146}$$

The reason for using linear interpolation between ξ_0' and ξ_1' is that the zero-point energy in the modes which are still within their turning points is not uniquely defined there. It is possible for ξ_0' to be larger than ξ_1', in which case the two adiabatic regions (the one near $\bar{s}_0$ and the one near $\bar{s}_1$) overlap. In this overlap region there are two distinct values of $s(\xi)$, one obtained from the procedure described above, starting at $\bar{s}_0$, and the other obtained by starting at $\bar{s}_1$. The ambiguity is resolved by choosing the value of $s(\xi)$ variationally, i.e., the contriubtion to the phase integral is taken to be the minimum of the two values of the integrand evaluated at the two values of $s(\xi)$.

The primitive expression for the tunneling probability is given by

$$P_{\text{prim}}^{LCG3}(E) = [T(E)]^2 \tag{147}$$

Because of the integration over s in Equation 130, $P_{\text{prim}}^{LCG3}(E)$ is not bounded by one. To remove this inconsistency we propose the following uniform expression which goes to 1/2 at $E = V^{AG}$:

$$P^{LCG3}(E) = \left\{1 + {}^1/_2\left[\frac{1}{P^{LCG3}_{prim}(V^{AG})} - 1\right]\frac{P^{LCG3}_{prim}(E)}{P^{LCG3}_{prim}(V^{AG})}\right\}\Big/\left[1 + \frac{1}{P^{LCG3}_{prim}(E)}\right], \quad E_0 < E < V^{AG} \tag{148a}$$

Note that in the deep tunneling region, for which $P^{LCG3}_{prim}(E)$ is very small, $P^{LCG3}(E)$ tends to $P^{LCG3}_{prim}(E)$.

For $E > V^{AG}$, nonclassical reflection is included by the zero-curvature parabolic uniformization scheme of Equation 118, i.e.,[159]

$$P^{LCG3}(E) = \begin{cases} 1 - P^{MEPSAG}(2V^{AG} - E), & V^{AG} < E < 2V^{AG} - E_0 \\ 1, & E > 2V^{AG} - E_0 \end{cases} \tag{148b}$$

The transmission coefficient $\kappa^{CVT/LCG3}(T)$ is then obtained from the tunneling probability as in Equations 85a to c.

Thus, to obtain a transmission coefficient, the major numerical effort is involved in the integrals of Equations 85a to c and 141. Each of these integrals is calculated by repeated Gauss-Kronrod quadrature, typically with two subintervals with about 61 to 81 quadrature points in each.

For systems with small to intermediate reaction-path curvature (such as $H + H_2$), adiabatic models such as the MCP and SC approximations, which are based physically on nearly optimum tunneling paths defined with respect to the MEP, provide a reasonably accurate description of the tunneling process. In both of these models tunneling is basically in the reaction-coordinate direction and the effective tunneling path is at or near the path of outer turning points for the bound vibrational motions coupled by reaction-path curvature to the reaction coordinate, i.e., for those motions with nonzero B_{mF}. In systems with large reaction-path curvature (such as Cl + HCl), a reasonable model is that the tunneling occurs along the shortest path between the reactant and product valleys, leading to the LC method. In this method, tunneling is basically in the vibrational direction. The reactions Cl + HD and $O + H_2$ are examples of systems with intermediate reaction-path curvature; for these types of systems the optimum tunneling path must be intermediate to the two paths mentioned above. To treat all three kinds of systems on a consistent basis we have developed a least-action ground-state (LAG) tunneling method that chooses the best tunneling paths from sequences of parametrized paths: the choice of paths is based upon a least-action principle — the paths are chosen to give the least exponential damping in the tunneling region. The model includes both the vibrational and the reaction-coordinate contributions to the tunneling probability.

We first consider a case where there are only two reaction-coordinate turning points for the adiabatic potential curve: we call these s_0 and s_1. The sequence of tunneling paths for a given available energy is specified by a set of basis paths depending on a single parameter α such that $\alpha = 0$ yields the MEP and $\alpha = 1$ corresponds to the large-curvature tunneling path for this available energy. We choose a set of basis paths as

$$\mathbf{x}(\alpha,\gamma) = (1 - \alpha)\mathbf{x}[s(0,\gamma)] + \alpha\{\mathbf{x}(s_0) + \gamma[\mathbf{x}(s_1) - \mathbf{x}(s_0)]\} \tag{149}$$

where γ is a progress variable along the path such that at $\gamma = 0, \mathbf{x}(\alpha,0) = \mathbf{x}(s_0)$ and at $\gamma = 1, \mathbf{x}(\alpha,1) = \mathbf{x}(s_1)$, and

$$s(0,\gamma) = s_0 + \gamma(s_1 - s_0) \tag{150}$$

where s_0 and s_1 are defined by Equation 129. Thus, along the MEP;

$$\gamma = (s - s_0)/(s_1 - s_0) \qquad \alpha = 0 \tag{151}$$

Examples of the basis paths $\mathbf{x}(\alpha,\gamma)$ for the Cl + HD reaction on the Stern-Persky-Klein[18,19] extended LEPS potential and for the H + H_2 reaction on the Porter-Karplus surface no. 2[168] are given in Figures 2A and 2B, respectively. For the Cl + HD reaction basis paths for a total energy of 8.0 kcal/mol are shown for α = 0, 1/3, 2/3, and 1. For the H + H_2 reaction, the MEP (α = 0) and the basis path for the α value corresponding to the least exponential damping (α = 0.432) are shown for a total energy of 8.8 kcal/mol.

For a given α, the imaginary-action integral for available energy $E_{av}(\bar{s}_0)$ is defined by

$$\theta(\alpha,\bar{s}_0) = \frac{(2\mu)^{1/2}}{\hbar} \int_0^1 \hat{\xi}(\alpha,\gamma) \cdot \hat{z}(\alpha,\gamma) \frac{\partial \xi(\alpha,\gamma)}{\partial \gamma} \{V_{eff}(\alpha,\gamma) - V_a^G(\bar{s}_0)\}^{1/2} \, d\gamma \tag{152}$$

where $\xi(\alpha,\gamma)$, the distance along the tunneling path, is found by numerical triangulation. Notice that $V_a^G(\bar{s}_0)$ is equal to the available energy. [Notice also that, as discussed below, although the tunneling path is always determined by the basis path, it is not always the same as the basis path, in which case $\xi(\alpha,\gamma)$ must be computed as the distance along the tunneling path, not the basis path]. Notice also that in the LCG method the progress variable is ξ whereas in the LAG method the progress variable is γ, and ξ is a function of α and γ. The unit vectors, $\hat{\xi}$ and $\hat{z}$, have the same definitions as in the LCG method and $V_{eff}(\alpha,\gamma)$ is also defined in a similar manner as in the LCG method. For a fixed α, each γ can be associated with a unique value of the curvilinear coordinates $[s(\alpha,\gamma),\mathbf{Q}(\alpha,\gamma)]$ in the same manner as described for the LCG method. [In the root search for $s(\alpha,\gamma)$, the value of $s(\alpha,\gamma)$ is used to begin the root search at $s(\alpha,\gamma + \Delta\gamma)$. The value of $\Delta\gamma$ is the spacing between points in the quadrature grid for Equation 152.] The system is assumed to be in the adiabatic region of the potential if all the normal coordinates lie within their turning points (Equation 143) and if the point lies within the locally single-valued region (Equation 144). In adiabatic regions the effective potential is set equal to the ground-state adiabatic potential, and the tunneling path is given by the basis path (Equation 149). Since the tunneling path is no longer restricted to be a straight-line path (as was the case in the LCG method), the unit vector $\hat{\xi}(\alpha,\gamma)$ is computed numerically. It is defined by

$$\hat{\xi}(\alpha,\gamma) = \frac{d\mathbf{x}(\alpha,\gamma)}{d\gamma} \Big/ \left| \frac{\partial \mathbf{x}(\alpha,\gamma)}{\partial \gamma} \right| \tag{153}$$

where the derivative is computed from a quadratic fit of $\mathbf{x}(\alpha,\gamma)$ as a function of γ. The two critical values of γ which bound the nonadiabatic region of the potential are defined in terms of ξ_0' and ξ_1' described previously by

$$\xi[\alpha,\gamma_i'(\alpha)] = \xi_i' \quad , \quad i = 0,1 \tag{154}$$

For γ between these two values, the tunneling path is no longer defined by Equation 149, but instead, is taken to be the shortest path between the points $\mathbf{x}[\alpha,\gamma_0'(\alpha)]$ and $\mathbf{x}[\alpha,\gamma_1'(\alpha)]$:

$$\mathbf{x}(\alpha,\gamma) = \mathbf{x}[\alpha,\gamma_0'(\alpha)] + \left[\frac{\gamma - \gamma_0'(\alpha)}{\gamma_1'(\alpha) - \gamma_0'(\alpha)}\right]\{\mathbf{x}[\alpha,\gamma_1'(\alpha)] - \mathbf{x}[\alpha,\gamma_0'(\alpha)]\},$$

$$\gamma_0'(\alpha) < \gamma < \gamma_1'(\alpha) \tag{155}$$

Along this path the effective potential is defined by Equations 145 and 146.

The optimum tunneling path is the one which minimizes the imaginary-action integral $\theta(\alpha,\bar{s}_0)$. Starting with a grid of 11 equally spaced points in α, the smallest value and two closest values of $\theta(\alpha,\bar{s}_0)$ are fit to a quadratic in α. A new value of $\theta(\alpha,\bar{s}_0)$ is computed at the value of α corresponding to the minimum of the fit. The value of α that gives the minimum in $\theta(\alpha,\bar{s}_0)$, $\tilde{\alpha}$, is obtained by repeating this procedure until either $\theta(\alpha,\bar{s}_0)$ is converged to a relative change of 10^{-4} or α changes by less than 10^{-8}.

Equations 149 to 155 all apply for a given $\bar{s}_0$ and $\bar{s}_1$, although the dependence of $\mathbf{x}(\alpha,\gamma)$, $s(\alpha,\gamma)$, $\hat{\xi}(\alpha,\gamma)$, $\hat{z}(\alpha,\gamma)$, $V_{eff}(\alpha,\gamma)$, $Q(\alpha,\gamma)$, $\xi(\alpha,\gamma)$, $\gamma_0'(\alpha)$ and $\gamma_1'(\alpha)$ on $\bar{s}_0$ and $\bar{s}_1$ and of $\theta(\alpha,\bar{s}_0)$ on $\bar{s}_1$ is only implicit in the notation used here. When there are only two reaction-coordinate turning points, $\bar{s}_0$ and $\bar{s}_1$ are themselves unique functions of a single variable E_{av}. We now consider a case where there are four or more reaction-coordinate turning points for the adiabatic potential curve. The LAG procedure described above is carried out using the two outermost turning points s_0 and s_1, as also used in the LCG method. This corresponds to a direct tunneling process from the reactant to the product valley. When there are four or more reaction-coordinate turning points, the amplitude for this direct process is compared with the amplitude for a process in which the tunneling takes place sequentially through the multiple barriers. The amplitude for the sequential process is obtained by carrying out the above LAG procedure for each pair of turning points and taking the product of the amplitudes for tunneling through the individual barriers. The amplitude for tunneling is taken to be the maximum of the direct and sequential values. For the sequential process with four turning points there will be different optimum α values associated with the segments close to reactants and products; we call these $\tilde{\alpha}_0$ and $\tilde{\alpha}_1$. In this case $\theta(\tilde{\alpha}_0,\bar{s}_0)$ becomes $\theta(\tilde{\alpha}_0,\tilde{\alpha}_1,\bar{s}_0)$. For six or more turning points this becomes $\theta(\tilde{\alpha}_0,\tilde{\alpha}_1\tilde{\alpha}_2,\bar{s}_0)$ and so forth for sequential tunneling, but it remains $\theta(\tilde{\alpha},\bar{s}_0))$ with $\tilde{\alpha} = \tilde{\alpha}_0 = \tilde{\alpha}_1 = \ldots$ for a direct tunneling process. The general case will hence be denoted $\theta(\tilde{\alpha}_0,\ldots,\bar{s}_0)$.

For direct (nonsequential) tunneling and $\alpha = 1$, the tunneling paths are the LCG paths. In this case, the tunneling direction may be nearly normal to the reaction-coordinate motion and there is a possibility of tunneling with each vibration against the potential in the bound normal-coordinate direction. For this case the tunneling amplitude should be constructed using an expression similar to Equation 130. For $\alpha = 0$, the tunneling path is the MEP and tunneling at values of s less than the turning point s_0 should not be included. A primitive expression for the tunneling probability which interpolates between these two mechanisms is constructed as follows. The amplitude for tunneling due to the component of vibrational motion in the direction of the tunneling path when the reaction coordinate is in the ranges $\bar{s}_0 = -\infty$ to s_0 and $\bar{s}_1 = s_1$ to $+\infty$ is given by

$$T^{LAG}(E) = T_0^{LAG}(E) + T_1^{LAG}(E) \tag{156}$$

where

$$T_0^{LAG}(E) = \int_{-\infty}^{s_0} \tau^{-1}(\bar{s}_0)V_R^{-1}(E,\bar{s}_0)\exp[-\theta(\tilde{\alpha}_0,\bar{s}_0)]\sin\chi(\tilde{\alpha}_0,\bar{s}_0)d\bar{s}_0 \tag{157}$$

and $\chi(\tilde{\alpha}_0,\bar{s}_0)$ is the angle between the tunneling path for $\alpha = \tilde{\alpha}_0$ and the MEP at $s = \bar{s}_0$. A similar expression is used for $T_1^{LAG}(E)$. The angle $\chi(\tilde{\alpha}_0,\bar{s}_0)$ is given by

$$\cos\chi(\tilde{\alpha}_0,\bar{s}_0) = \mathbf{v}(\bar{s}_0)\cdot\hat{\xi}(\bar{s}_0) \tag{158}$$

The total probability for tunneling at an energy E is obtained by adding the tunneling contributions from vibrating against the barrier to the contribution for tunneling at the reaction-coordinate turning point. This yields:

$$P_{prim}^{LAG}(E) = [T^{LAG}(E)]^2 + \{[\cos \chi(\tilde{\alpha}_0,s_0) + \cos \chi(\tilde{\alpha}_1,s_1)]/2\}^2 \exp[-2\theta(\tilde{\alpha}_0,\ldots,s_0)] \quad (159)$$

Notice that the last argument in the last term is s_0 which is the value of $\tilde{s}_0$ for all the energy being available, i.e., it is the reaction-coordinate turning point for $V_a^G(s)$ at total energy E. A uniform expression for $P^{LAG}(E)$ similar to the expression for the LCG method (Equation 147) is used, and Equation 148b is used to include nonclassical reflection in the LAG method. The transmission coefficient is obtained from the tunneling probabilities by Equation 85a to c, yielding $\kappa^{CVT/LAG}(T)$.

We can now see more clearly how large-curvature approximations in the LAG method lead to the LCG3 method. Along the LCG3 path used in Equations 141 to 146, $s(\xi) = s[\alpha = 1,\gamma(\xi)]$. Furthermore, in the large-curvature limit $\chi(\tilde{\alpha},\tilde{s}_0) = \pi/2$ so Equations 156 to 159 reduce to Equations 130, 133, 140, and 147.

The LAG method provides a physically motivated model for including tunneling in systems with small, medium, or large reaction-path curvature. The method smoothly interpolates between the MEP method in the limit of zero curvature and the LCG3 method in the limit of large curvature. For large-curvature systems, the optimum tunneling paths are very near $\alpha = 1$. For example, for the Cl + HCl reaction at a tunneling energy of 7.8 kcal/mol, the optimum path is for $\alpha = 0.9$; the probability for tunneling along this path is given by $\exp[-2\theta(\tilde{\alpha},\tilde{s}_0)]$ and is 5.9×10^{-4}, whereas for $\alpha = 1$ the probability is 4.8×10^{-4}. The LCG3 and LAG transmission coefficients agree well; at 200 K they are 41.3 and 43.2, respectively, compared to the accurate value of 90.9 and at 300 K they are 10.0 and 10.2, respectively, compared to the accurate value of 15.9. The Cl + HD reaction has intermediate reaction-path curvature and for this system the optimum tunneling paths lie in the range of α from 0.3 to 0.6 for energies at which the probabilities range from 10^{-7} to 10^{-2}. At 8 kcal/mol the probabilities for tunneling along the $\alpha = 0$, 1/3, 2/3, and 1 paths are 1.1×10^{-5}, 3.7×10^{-4}, 1.5×10^{-4}, and 1.1×10^{-5}, respectively. The optimum path has $\alpha = 0.444$ with a tunneling probability of 5.4×10^{-4}. These values can be compared to the probability of tunneling along the MCP of 1.0×10^{-4}. The transmission coefficients for this system at 200 K are 2.0, 3.8, and 7.9 for the MCP, LAG, and accurate quantal methods; at 300 K these values are 1.7, 2.8, and 3.2, respectively. The H + H_2 reaction is a system for which the MCP and SC methods were quite successful, as discussed above. Figure 2A indicates that the MCP and optimum tunneling path ($\alpha = 0.432$) are quite close near the conventional transition state. For the portion of this path which lies between the MEP and MCP the contribution to the tunneling integral θ will be very close to that obtained from the MCP over a comparable portion of the path because both methods use the adiabatic potential in this region. At 8.8 kcal/mol the tunneling probabilities for the MCP and $\alpha = 0.432$ path are quite close: 2.7×10^{-4} and 3.9×10^{-4}, respectively. The transmission coefficients at 200 K are 29, 46, and 45 by the MCP, LAG, and accurate quantal methods; at 300 K these values are 5.1, 7.3, and 8.7, respectively.

V. IMPROVED CANONICAL VARIATIONAL THEORY AND MICROCANONICAL VARIATIONAL THEORY

So far we have emphasized canonical variational theory, in which a single generalized transition state is optimized for a canonical ensemble. Microcanonical variational theory is more complete because it recognizes the conservation of total energy. In μVT a separate generalized transition state is optimized for each total energy (in principle one could also consider a fixed-energy, fixed total angular momentum ensemble, but we shall not do this here). In improved canonical variational theory the generalized transition state is optimized

microcanonically for energies up to the microcanonical variational threshold energy and canonically for higher energy contributions. This means that ICVT has the same threshold as μVT, but the calculations are almost as simple as for CVT. In particular, we choose the generalized transition state at the maximum of $V_a^G(s)$ for energies below this maximum; then for each temperature we choose a single dividing surface for all higher energies. This single dividing surface is found as in CVT except that the canonical ensemble is truncated from below at the threshold energy. In this section we give detailed expressions for the ICVT and μVT rate constants, analogous to the expressions for the CVT rate constant in Sections II and III.

As in Section III, we consider general polyatomic systems, we assume electronic, vibrational, and rotational energies are separable, we treat vibrations quantum mechanically, and we eventually treat rotation classically. At the beginning of the derivations, however, we treat rotation as quantized.

In improved canonical variational theory we enforce the vibrationally adiabatic ground-state threshold for all contributions to the generalized transition state partition function. For this purpose it is convenient to define the vibrational-rotational partition function of the generalized transition state by

$$Q_{vr}^{GT}(T,s) = Q_{vib}^{GT}(T,s)Q_{rot}^{GT}(T,s) \tag{160}$$

to denote the collection of vibrational quantum numbers by the array $\mathbf{n} = \{n_m, m = 1,2,\ldots,F - 1\}$, and to give each rotational state a unique label k. As in CVT, the vibrational-rotational partition function is based on the ground electronic state. The adiabatic potential curve for the quantum state with quantum numbers $(\mathbf{n},k)$ may be written:

$$V_a(\mathbf{n},k,s) = V_{MEP}(s) + \epsilon_{int}^{GT}(\mathbf{n},k,s) \tag{161}$$

where $\epsilon_{int}^{GT}(\mathbf{n},k,s)$ is the vibrational-rotational energy of quantum state $(\mathbf{n},k)$ of the generalized transition state at s:

$$\epsilon_{int}^{GT}(\mathbf{n},k,s) = \epsilon_{vib}^{GT}(\mathbf{n},s) + \epsilon_{rot}^{GT}(k,s) \tag{162}$$

The contribution to $Q_{vr}^{GT}(T,s)$ from each quantum state is $\exp\{-\beta[\epsilon_{int}^{GT}(\mathbf{n},k,s)]\}$. To eliminate the contribution from below the vibrationally adiabatic ground-state threshold, we must replace this exponential by $\exp\{-\beta[V^{AG} - V_{MEP}(s)]\}$ whenever V^{AG} exceeds $V_a(\mathbf{n},k,s)$.[34]

It is convenient to define cutoff partition functions[21] by

$$Q_{vr}^{GT}(T,s;\epsilon) = \sum_{\mathbf{n}}{}' \sum_{k}{}' \exp\{-\beta[\epsilon_{int}^{GT}(\mathbf{n},k,s)]\} \tag{163}$$

and

$$Q_{rot}^{GT}(T,s;\epsilon) = \sum_{k}{}' \exp\{-\beta[\epsilon_{rot}^{GT}(k,s)]\} \tag{164}$$

where the primes on the summations mean we include states only if their energy (vibrational-rotational energy in Equation 163 or rotational energy in Equation 164) is less than the argument ϵ following the semicolon. We also define cutoff sum of vibrational-rotational states and sum of rotational states functions for the generalized transition state by

$$N_{vr}^{GT}(\epsilon,s) = \sum_{\mathbf{n}}{}' \sum_{k}{}' 1 \tag{165}$$

and

$$N_{rot}^{GT}(\epsilon,s) = \sum_{k}{}' 1 \tag{166}$$

where the primes denote that only those levels for which $\epsilon_{int}^{GT}(\mathbf{n},k,s)$ or $\epsilon_{rot}^{GT}(k,s)$ is less than ϵ are included. Thus, $N_{vr}^{GT}(\epsilon,s)$ and $N_{rot}^{GT}(\epsilon,s)$ are the number of vibrational-rotational or rotational states with $\epsilon_{int}^{GT}(\mathbf{n},k,s)$ or $\epsilon_{rot}^{GT}(k,s)$ less than ϵ. Notice that no degeneracy factors occur in Equations 163 to 166 because every state has a unique index. In accordance with the prescription of the previous paragraph, we define an improved generalized transition state partition function by

$$Q_{vr}^{IGT}(T,s) = Q_{vr}^{GT}(T,s) - Q_{vr}^{I}(T,s) \tag{167}$$

where we have also defined:

$$Q_{vr}^{I}(T,s) = Q_{vr}^{GT}[T,s; V^{AG} - V_{MEP}(s)] - \exp\{-\beta[V^{AG} - V_{MEP}(s)]\} \times N_{vr}^{GT}[V^{AG} - V_{MEP}(s),s] \tag{168}$$

Using the assumed separability of vibration and rotation this becomes

$$Q_{vr}^{I}(T,s) = \sum_{\mathbf{n}}{}' (\exp[-\beta\epsilon_{vib}^{GT}(\mathbf{n},s)]Q_{rot}^{GT}[T,s; V^{AG} - V_{MEP}(s) - \epsilon_{vib}^{GT}(\mathbf{n},s)] - \exp\{-\beta[V^{AG} - V_{MEP}(s)]\}N_{rot}^{GT}[V^{AG} - V_{MEP}(s) - \epsilon_{vib}^{GT}(\mathbf{n},s),s]) \tag{169}$$

The classical approximations to Equations 164 and 166, analogous to Equations 45 and 46 for the complete (noncut-off) partition function, are

$$Q_{rot}^{GT}(T,s;\epsilon) = \begin{cases} 2\Gamma_{\beta\epsilon}\left(\frac{3}{2}\right)\left[\left(\frac{2}{\hbar^2\beta}\right)^3 I_A(s)I_B(s)I_C(s)\right]^{1/2}, \text{ nonlinear GTS} & (170a) \\ 2\Gamma_{\beta\epsilon}(1)\,\frac{I(s)}{\hbar^2\beta}, \text{ linear GTS} & (170b) \end{cases}$$

and

$$N_{rot}^{GT}(\epsilon,s) = \begin{cases} \frac{4}{3}\left[\left(\frac{2\epsilon}{\hbar^2}\right)^3 I_A(s)I_B(s)I_C(s)\right]^{1/2}, \text{ nonlinear GTS} & (171a) \\ 2\epsilon I(s)/\hbar^2, \text{ linear GTS} & (171b) \end{cases}$$

where $\Gamma_z(p)$ is the incomplete gamma function defined by

$$\Gamma_z(p) = \int_0^z w^{p-1}\exp(-w)dw \tag{172}$$

Equations 170 and 171 are derived in Appendix 2 by introducing a cutoff into the standard classical expression[14a,178,179] for the rotational partition function.

Combining Equations 167 and 169 to 171, the final expression for the improved generalized TST rate constant for quantum mechanical vibration and classical rotation is

$$k^{IGT}(T,s) = \frac{\sigma}{\beta h \Phi^R(T)} Q^{IGT}(T,s) \exp[-\beta V_{MEP}(s)] \tag{173}$$

where

$$Q^{IGT}(T,s) = Q^{GT}(T,s) - Q^{GT}_{el}(T,s) \sum_{\mathbf{n}}{}' c_{\mathbf{n}}(s) \tag{174}$$

$$c_{\mathbf{n}}(s) = \begin{cases} \dfrac{[2^5 I_A(s) I_B(s) I_C(s)]^{1/2}}{\hbar^3} \left(\Gamma_{\beta\epsilon_{\mathbf{n}}(s)}\left(\dfrac{3}{2}\right) \beta^{-3/2} \exp[-\beta \epsilon^{GT}_{vib}(\mathbf{n},s)] \right. \\ \qquad \left. - \dfrac{2[\epsilon_{\mathbf{n}}(s)]^{3/2}}{3} \exp\{-\beta[V^{AG} - V_{MEP}(s)]\} \right), \text{ nonlinear GTS} \qquad (175a) \\ \dfrac{2I(s)}{\hbar^2} \left(\Gamma_{\beta\epsilon_{\mathbf{n}}(s)}(1) \beta^{-1} \exp[-\beta \epsilon^{GT}_{vib}(\mathbf{n},s)] - \epsilon_{\mathbf{n}}(s) \right. \\ \qquad \left. \times \exp\{-\beta[V^{AG} - V_{MEP}(s)]\} \right), \text{ linear GTS} \qquad (175b) \end{cases}$$

and

$$\epsilon_{\mathbf{n}}(s) = V^{AG} - V_{MEP}(s) - \epsilon^{GT}_{vib}(\mathbf{n},s) \tag{176}$$

The prime on the sum in Equation 174 denotes that it includes only those vibrational levels for which $\epsilon_{\mathbf{n}}(s)$ is positive. Finally, $k^{ICVT}(T)$ is defined as

$$k^{ICVT}(T) = \min_s k^{IGT}(T,s) \tag{177}$$

The microcanonical variational rate constant may be written as

$$k^{\mu VT}(T) = \frac{\sigma Q^{GT}_{el}(T) I^{\mu VT}_{vr}(T)}{h \Phi^R(T)} \tag{178}$$

where

$$I^{\mu VT}_{vr}(T) = \int_0^\infty \exp(-\beta E)\, N^{\mu VT}_{vr}(E)\, dE \tag{179}$$

and

$$N^{\mu VT}_{vr}(E) = \min_s N^{GT}_{vr}(E,s) \tag{180}$$

Here $Q^{GT}_{el}(T,s)$ is assumed independent of s in the bottleneck region and $N^{GT}_{vr}(E,s)$ is the sum of vibrational-rotational states with total energy less than E, i.e., the number of vibrational-rotational states with $V_a(\mathbf{n},k,s)$ less than E. Again we assume separable vibration and rotation, which yields:

$$N_{vr}^{GT}(E,s) = \sum_{\mathbf{n}} \theta[E - V_{MEP}(s) - \epsilon_{vib}^{GT}(\mathbf{n},s)]N_{rot}^{GT}[E - V_{MEP}(s) - \epsilon_{vib}^{GT}(\mathbf{n},s),s] \quad (181)$$

For $N_{rot}^{GT}(\epsilon,s)$ we use the classical approximation given by Equations 171a and b.

In order to use the μVT one must calculate the sum $N_{vr}^{GT}(E,s)$ over the vibration-rotation states or the approximation of Equation 181 to this sum. Many techniques for the evaluation of this sum have been proposed, with special reference to unimolecular reactions.[94,180-190] The most popular are the semiempirical method of Whitten and Rabinovitch[180-183] and the direct-count method.[183,186-188] It is possible to include Morse anharmonicity and hindered rotors in direct counts, but the methods that are efficient for large counts still involve the INM approximation. These techniques can also be used for bimolecular reactions. The most important difference is that $N_{vr}^{GT}(E,s)$ is usually required at relatively lower energies for a bimolecular case; hence, for a given number of atoms, $N_{vr}^{GT}(E,s)$ is a smaller number, and greater accuracy in its evaluation may be both desirable and possible.

One possibility for evaluating Equation 181 when it is small is to use the INM approximation of Section III.B for the vibrational energy levels and direct summation. However, this may become unwieldy as E and $N_{vr}^{GT}(E,s)$ become large. If so, direct Monte Carlo evaluation of the classical anharmonic sum-of-states integral and use of a sum-of-states analog to the Pitzer-Gwinn partition-function approximation for the ratio of the anharmonic to the harmonic sum is one alternative.[101,113-115,120-126] Another alternative is the inversion of the Laplace transform that relates $N_{vr}^{GT}(E,s)$ to $Q_{vr}^{GT}(T,s)$.[94,183,189] This may be especially useful if $Q_{vr}^{GT}(T,s)$ is calculated without the INM approximation.

Since microcanonical variational theory is equivalent to the adiabatic theory of reactions,[21,58] μVT calculations could also be carried out in an adiabatic framework. This method has been used for collinear atom-diatom reactions,[21,58] but it is more difficult to apply in general because the adiabatic state correlations become more complicated when noncollinear reactions are considered.[81-83,160,191-207]

Inclusion of tunneling effects in ICVT and μVT can be accomplished very similarly to the procedure described in Section IV for CVT.[34] Thus,

$$k^{ICVT/SG}(T) = \kappa^{SG}(T)\, k^{ICVT}(T) \quad (182)$$

and

$$k^{\mu VT/SG}(T) = \kappa^{SG}(T)\, k^{\mu VT}(T) \quad (183)$$

where, by analogy to Equations 85a to c,

$$\kappa^{SG}(T) = \frac{\int_0^\infty P^{SG}(E) \exp(-\beta E)dE}{\int_{VAG}^\infty \exp(-\beta E)dE} \quad (184a)$$

$$= \kappa^{CVT/SG}(T) \frac{\exp\{-\beta V_a^G[s_*^{CVT}(T)]\}}{\exp(-\beta V^{AG})} \quad (184b)$$

Here, as introduced between Equations 128 and 129, $P^{SG}(E)$ represents a general semiclassical ground-state transmission probability. The ratio in Equation 184b accounts for the different thresholds in ICVT and μVT as compared to that of CVT, i.e., for the different denominators in Equations 85b and 184a.

For some reactions it may be desirable to go beyond the ground-state approximation for the transmission coefficient. Procedures for calculating excited-state tunneling probabilities in the adiabatic theory of reactions are discussed elsewhere.[58,87] (A statistical-diabatic model has also been considered.[207]) As an example of how excited-state tunneling probabilities may be included in the calculation of the rate constant, we consider microcanonical variational theory. We write the μVT rate constant expression in adiabatic theory form as[58]

$$k^{VA}(T) = \frac{\sigma Q_{el}^{GT}(T,s) \int_0^\infty \exp(-\beta E) N^{VA}(E)\, dE}{h\Phi^R(T)} \tag{185}$$

where

$$N^{VA}(E) = \sum_{\mathbf{n}} \sum_{k} P^{VA}(\mathbf{n},k,E) \tag{186}$$

and $P^{VA}(\mathbf{n},k,E)$ is the vibrationally and rotationally adiabatic transmission probability for state $(\mathbf{n},k)$. If $P^{VA}(\mathbf{n},k,E)$ is approximated semiclassically, it becomes $P^{SA}(\mathbf{n},k,E)$; a special case is $P^{SAG}(E)$, considered in Section IV, which corresponds to $(\mathbf{n},k)$ being the ground state. If we approximate $P^{VA}(\mathbf{n},k,E)$ by its generalized transition state value $\theta[E - V_a(\mathbf{n},k,s)]$, then $N^{VA}(E)$ and $k^{VA}(T)$ reduce to $N^{\ddagger}(E)$ and $k^{\ddagger}(T)$ when s is set to zero, and Equations 185 and 186 reduce to microcanonical variational TST when s is chosen at the maximum of $V_a(\mathbf{n},k,s)$. Instead, however, we can include tunneling and nonclassical reflection effects by calculating $P^{SA}(\mathbf{n},k,E)$ as a one-dimensional tunneling probability using methods similar to those described in Section IV for $P^{SG}(E)$, but with two important differences. First, in adiabatic approximations (or adiabatic regions for methods like the LCG approximation), $V_a^G(s)$ is replaced by $V_a(\mathbf{n},k,s)$. Second, the tunneling path [or $\mu_{eff}^{SC}(s)$ in the SC approximation] is a function of $(\mathbf{n},k)$. Equation 185 was first suggested by the authors in the context of bimolecular reactions,[58] and an identical expression has been suggested by Miller[208] in the context of unimolecular reactions. A generalization of the above treatment is to write:

$$k^{\mu VT/S} = \frac{\sigma Q_{el}^{GT}(T,s) \int_0^\infty \exp(-\beta E) N^{S}(E)\, dE}{h\Phi^R(T)} \tag{187}$$

and

$$N^{S}(E) = \sum_{\mathbf{n}} \sum_{k} P^{S}(\mathbf{n},k,E) \tag{188}$$

where $P^S(\mathbf{n},k,E)$ is the most accurate available semiclassical approximation to the reaction probability of state $(\mathbf{n},k)$ at total energy E. Equation 187 allows for general state-dependent semiclassical transmission corrections to microcanonical variational theory. If $P^S(\mathbf{n},k,E)$ is replaced by the exact reaction probability, then we obtain the exact equilibrium rate constant. This kind of comparison of the TST expression to the exact result is discussed in more detail in Appendix 1.

VI. RECROSSING CORRECTIONS

So far we have discussed using the transmission coefficient to include quantal effects on reaction-coordinate motion. Another kind of effect that one can attempt to include in the

transmission coefficient is the breakdown of TST itself. In particular, if one has a theoretical rate constant [$k^Z(T)$] that one believes is more accurate than conventional TST or hybrid CVT, one can define a corresponding transmission coefficient by

$$\kappa^{\ddagger/Z}(T) = k^Z(T)/k^{\ddagger}(T) \tag{189}$$

or

$$\kappa^{CVT/Z}(T) = k^Z(T)/k^{CVT}(T) \tag{190}$$

In general, this is not too useful since accurate $k^Z(T)$ values are not usually available. However, there have been some practical approaches suggested for calculating transmission coefficients that include, to some degree, estimates of the breakdown of the fundamental assumption of TST. These approaches are based on a TST model, but they include some estimate of the effect of classical recrossing of the conventional or generalized transition state dividing surface. The approaches to be considered are (1) the unified statistical approach, (2) an analytical mechanics approach due to Miller, (3) reduced-dimensionality transmission coefficients, and (4) the unified dynamical model. Method 1 is a statistical theory and is discussed in Section VI.A; methods 2 to 4 are dynamical and are discussed in Section VI.B.

A. Unified Statistical Model

The unified statistical (US) model was first suggested by Miller,[209] rederived by Pollak and Pechukas,[210] and extended in various ways by the authors,[35,58,211] Chesnavich et al.,[212] and Miller.[213] In this section we review some of this work and also present some new extensions. The US model interpolates between μVT in the limit of direct reactions with only one bottleneck and the statistical phase-space theory[13,214] in the limit of complex-forming reactions with two bottlenecks. The US model was first derived by applying the Hirschfelder-Wigner branching analysis[215] in a microcanonical ensemble. The US model rate constant is given by

$$k^{US}(T) = \frac{\sigma Q_{el}^{GT}(T,s)}{h\Phi^R(T)} \int_0^\infty \exp(-\beta E) N_{vr}^{US}(E)\, dE \tag{191}$$

where

$$N_{vr}^{US}(E) = N_{vr}^{\mu VT}(E)\, R^{US}(E) \tag{192}$$

In Equation 192, $N_{vr}^{\mu VT}(E)$ is the microcanonical variational TST approximation to the cumulative reaction probability as given by Equation 180, and $R^{US}(E)$ is the US model recrossing factor. The recrossing factor is defined by

$$R^{US}(E) = [1 + N_{vr}^{\mu VT}(E)/N_{vr}^{min}(E) - N_{vr}^{\mu VT}(E)/N_{vr}^{max}(E)]^{-1} \tag{193}$$

where $N_{vr}^{min}(E)$ is the second-lowest minimum of $N_{vr}^{GT}(E,s)$ as a function of s, and $N_{vr}^{max}(E)$ is the highest maximum of $N_{vr}^{GT}(E,s)$ that lies between the two lowest minima. If there is only one minimum in $N_{vr}^{GT}(E,s)$, then $R^{US}(E)$ is unity, and the US model reduces to μVT.

The same analysis can be applied to a canonical ensemble to give the canonical unified statistical model (CUS). A classical version for collinear atom-diatom reactions was presented previously;[211] here we present the equations for general bimolecular polyatomic reactions with quantized vibrations. The canonical-ensemble average of the flux through a dividing surface at s for a temperature T is proportional to the generalized transition state partition function:

$$q_{vr}^{GT}(T,s) = Q_{vr}^{GT}(T,s) \exp[-\beta V_{MEP}(s)] \quad (194)$$

where $Q_{vr}^{GT}(T,s)$ has its zero of energy at the overall zero of energy at the minimum of the potential well of the reactant. Applying the Hirschfelder-Wigner branching analysis[215] in the canonical ensemble we obtain:

$$k^{CUS}(T) = k^{CVT}(T)\, R^{CUS}(T) \quad (195)$$

where the recrossing factor is defined by

$$R^{CUS}(T) = [1 + q_{vr}^{CVT}(T)/q_{vr}^{max}(T) - q_{vr}^{CVT}(T)/q_{vr}^{min}(T)]^{-1} \quad (196)$$

In Equation 196, $q_{vr}^{CVT}(T)$ is evaluated at the highest maximum of the generalized free energy of activation curve $\Delta G^{GT,0}(T,s)$ as discussed in Section II, $q_{vr}^{max}(T)$ is evaluated at the second-highest maximum of $\Delta G^{GT,0}(T,s)$, and $q_{vr}^{min}(T)$ is evaluated at the lowest minimum between the two highest maxima of $\Delta G^{GT,0}(T,s)$. [Note that in Equation 6 of Reference 211, $q_C^{CVT}(T)$ should be deleted from the numerator; its presence in the numerator is a typographical error].

Both the US and CUS expressions for the rate constant incorporate quantum effects in the bound degrees of freedom orthogonal to the reaction path, but treat motion along the reaction coordinate classically. First we consider including quantum effects on reaction-coordinate motion in the microcanonical US model. The adiabatic model provides a consistent method of including quantum mechanical tunneling effects into μVT through a multiplicative factor $\kappa^{\mu VT/SAG}(T)$. Let us consider the case where the ground-state adiabatic barrier has two maxima. For this case Miller[209] has shown that Equations 192 and 193 can be obtained from a WKB treatment of transmission through the double-barrier potential. Therefore, a consistent method of including tunneling effects in the US model at low energies (where only one adiabatic state is open) is to replace the cumulative reaction probabilities in Equations 192 and 193 by WKB tunneling probabilities through the individual barriers. At sufficiently low energies this yields a ground-state reaction probability of

$$P^{WKBUSG}(E) = p_1 p_2/[p_1 + p_2 - p_1 p_2] \quad (197)$$

where

$$p_i = 1/[1 + \exp(2\theta_i)] \quad , \quad i = 0,1 \quad (198)$$

and θ_i are the WKB imaginary-action integrals through each of the single barriers of the double-barrier potential. This expression is derived from a uniform expression for tunneling through a double-barrier potential,[216,217]

$$P_{uniform}(E) = p_1 p_2/[1 + (1 - p_1)(1 - p_2) + 2\sqrt{1 - p_1}\sqrt{1 - p_2}\cos 2\phi] \quad (199)$$

where the angle ϕ is related to the phase integral for the classically allowed motion in the well between the two potential barriers. For the case of a symmetric system with p_1 very much less than one, Equation 197 is equal to $p_1/2$. However, under these same conditions, the uniform expression (Equation 199) goes like p_1^2 when the system is not near a resonance. At these low energies, the physical picture for the US model is that p_1 is the probability of tunneling through the first barrier into the well between the two barriers. The system is trapped in this well and the branching ratio for going on to products vs. returning to reactants is just p_2:p_1. The uniform expression has this physical picture only near a resonance, i.e., at an energy corresponding to a bound state in the well between the two barriers. At energies

not near a resonance the system is not trapped in the potential well and the probability of reaction is proportional to the product of the tunneling probabilities through the separate barriers. We prefer the latter picture of the tunneling process and therefore abandon the uniform semiclassical approach to putting tunneling effects into the US model.

An alternative approach for including quantum effects on reaction-coordinate motion in the US model is suggested by the form of Equation 192, in which the cumulative reaction probability is written as the μVT one multiplied by a recrossing factor $R^{US}(E)$. Note that $N_{vr}^{\mu VT}(E)$ is zero for energies below the ground-state adiabatic barrier maximum and that $R^{US}(E)$ reduces to unity for these energies. As previously suggested,[58] we use this recrossing factor to correct the adiabatic expression for the cumulative reaction probability, thus providing a quantally unified statistical approximation:

$$N_{vr}^{QUS}(E) = N_{vr}^{VA}(E)\, R^{US}(E) \tag{200}$$

where $N^{VA}(E)$ is given by Equation 186. Alternatively, we could have used the semiclassical approximation to $N_{vr}^{VA}(E)$ in this expression. Equation 200 has the desirable features of approaching the VA limit at low tunneling energies as $R^{US}(E)$ goes to one and approaching the US limit for high energies where tunneling effects are no longer important. Another method of including tunneling that also has these correct limits is[35]

$$k^{US/SAG}(T) = k^{US}(T)\, \kappa^{SAG}(T) \tag{201}$$

where the transmission coefficient $\kappa^{SAG}(T)$ is discussed in Section V.

It is more problematic to incorporate reaction-coordinate quantum effects into the CUS model. In the same spirit as above, $k^{CUS}(T)$ could be corrected by multiplying Equation 195 by a ground-state transmission coefficient for the CVT method, yielding:

$$k^{CUS/SAG}(T) = k^{CUS}(T)\, \kappa^{CVT/SAG}(T) \tag{202}$$

However, this does not have a satisfactory limit at low temperatures. For sufficiently low temperature the free energy of activation curve approaches the ground-state adiabatic potential curve and $k^{CVT}(T)$ approaches $k^{\mu VT}(T)$. However, the CUS recrossing factor $R^{CUS}(T)$ does not necessarily go to one in this low-temperature limit and we do not recover the correct VA limit.

To test the quantized CUS and CUS/SCTSAG models, we compared their predictions to accurate quantal rate constants for 23 collinear atom-diatom systems. These comparisons have not been published previously; we summarize them here. For the 23 systems studied, the CUS recrossing corrections are usually negligible at temperatures below 1000 K, but the quantized CUS theory does provide a useful correction to variational TST in a few cases at high temperature. For the cases studied, the CUS recrossing factors improve the accuracy more often than they worsen it. One case for which the recrossing factor worsens the accuracy is a model HFH system,[90] which has two symmetrically located saddle points separated by a shallow local minimum. For this system, the ratios of CVT/SCTSAG and CUS/SCTSAG rate constants to the accurate quantum mechanical one at 100 K are 0.53 and 0.27, respectively. This is an example of a system in which $R^{CUS}(T)$ incorrectly approaches one half at low temperatures. Even for this system, though, the CUS recrossing factor improves the accuracy at 7000 K. Another case where the CUS/SCTSAG model is less accurate than the CVT/SCTSAG one is the H + H_2 system on surface no. 2 of Porter and Karplus.[168] For this system the ratios of CVT:SCTSAG and CUS:SCTSAG rate constants to the accurate quantal one at 2400 K are 0.97 and 0.58, respectively.

We have also applied the CUS and CUS/SCTSAG models to many atom-diatom reactions in three dimensions. For these cases we find that the CUS recrossing corrections are generally small (less than 20%), but they may be important for accurate calculations of kinetic isotope effects. The general smallness of the US correction to VTST is encouraging, although of course the actual recrossing effects will sometimes be larger than those predicted by the US model.

B. Dynamical Approaches

A model that incorporates recrossing effects on more dynamical grounds has been proposed by Miller.[218] In this model, a dynamical approximation is made that is different (and, one would hope, better) than the fundamental dynamical approximation of conventional TST. Alternatively, this approach can be viewed as employing a TST-type approximation in a curvilinear coordinate system rather than in a coordinate system obtained by a linear transformation from cartesians. We first review the purely classical version of the theory and then discuss the incorporation of quantum effects. Miller first derived the expression for the classical cumulative reaction probability for a dividing surface located at the saddle point; however, a general expression when the dividing surface is at a general location s is

$$N_C^{CC}(E,s) = \kappa_C^{CC}(E,s)\, N_C^{GT}(E,s) \tag{203}$$

where the curvature correction term $\kappa_C^{CC}(E,s)$ has the properties:

$$\kappa_C^{CC}(E,s) \begin{cases} = 1 & , \quad E < E^C(s) \\ < 1 & , \quad E > E^C(s) \end{cases} \tag{204}$$

and $E^C(s)$ is a critical energy given (within the harmonic independent normal-mode approximation) by

$$E^C(s) = V_{MEP}(s) + (\mu/2)\left\{\sum_{m=1}^{F-1} [B_{mF}(s)/\omega_m(s)]^2\right\}^{-1} \tag{205}$$

Miller chose the saddle point location s = 0 for evaluating $N_C^{GT}(E,s)$ in Equation 203, but suggested that a better approximation to N_C^{CC} may be obtained by evaluating $\kappa_C^{CC}(E,s)$ at the value of s corresponding to the maximum of curvature. The dynamical approximation suggested by Miller does not provide an upper bound to the exact classical rate constant and, therefore, it is not totally justified to variationally optimize s to minimize $N_C^{CC}(E,s)$. Instead we suggest that a better approximation may be obtained by evaluating Equation 203 at the value of s that minimizes $N_C^{GT}(E,s)$. In this way one would obtain a recrossing correction factor evaluated at the μVT dividing surface, which is the best GTS dividing surface for a given energy. A problem, however, is that this recrossing correction factor is based upon the reaction-path curvature evaluated at just one point along the reaction coordinate, and it may be highly sensitive to the location at which the recrossing factor is evaluated.

Miller has also given an expression for the canonical rate constant with the recrossing correction evaluated at the saddle point. As in the microcanonical case, a general expression for the canonical case can be derived for any location of the dividing surface. We suggest that a good approximation may be to evaluate the general expression at the CVT generalized dividing surface to give:

$$k_C^{CC}(T) = \kappa_C^{CC}(T)\, k_C^{CVT}(T) \tag{206}$$

where the recrossing correction factor is given by[218]

$$\kappa_C^{CC}(T) = {}^1/_2 + \text{erf}[\{E^C[s_*^{CVT}(T)] - V_{MEP}[s_*^{CVT}(T)]\}/kT]/2 \qquad (207)$$

Miller's transmission coefficient, like the US and CUS corrections, is always between 0.5 and 1.0. We know that for many reactions the exact transmission coefficient in classical mechanics for conventional TST is less than 0.5 and that Miller's correction is inadequate.[21,50,211,219] Miller has pointed out that quantization of the bound degrees of freedom is difficult but can be accomplished. We expect that the recrossing correction will be very different in a quantized world. As we have pointed out previously,[36] variational effects can be very large in a quantized world at low temperatures whereas they would be negligible in a classical world.

The form of the recrossing correction factor given in Equation 207 indicates that it depends upon the dimensionality of the system only through the critical energy E^C. Miller has pointed out that only modes which are coupled to the reaction coordinate contribute to determining E^C. This would seem to indicate that reduced-dimensionality calculations can be useful for calculating recrossing corrections for the full-dimensional system. However, as has been pointed out elsewhere,[34] corrections for quantum effects along the reaction coordinate must include effects from all the bound degrees of freedom, even if only within an adiabatic framework. The effect of dimensionality on transmission coefficients will then depend on the character of the transition state and the character of the modes removed when dimensionality is reduced.

An approach that attempts to include quantal effects more directly is the use of accurate quantal reduced-dimensionality transmission coefficients. In this approach one calculates $\kappa^{\ddagger/Z}(T)$ by Equation 189 where $k^{\ddagger}(T)$ is a reduced-dimensionality TST rate constant and $k^Z(T)$ is the accurate quantal result for the same reduced-dimensionality problem. So far, applications of this approximation have been limited to atom-diatom problems with collinear reaction paths, where the reduced-dimensionality problem is taken to be the purely collinear collision. Exact collinear transmission coefficients for atom-diatom collisions were first calculated by Truhlar and Kuppermann,[148] and collinear transmission coefficients have been used to obtain three-dimensional rate constants and cross sections for several reactions by Kuppermann[220] and by Bowman and co-workers.[221-227] This kind of transmission coefficient is expected to exhibit systematic errors because of the neglect of the contribution of the bending zero-point energy to the shape of the effective potential barrier for the tunneling dynamics. Because of this, the two mathematical-dimensional exact collinear transmission coefficients are expected to provide less accurate three-dimensional rate constants than one mathematical-dimensional approaches like the SCSAG approximation discussed in Section IV. A better procedure is to solve the two mathematical-dimensional collinear tunneling problem with an effective Hamiltonian that includes the effect of the bending degrees of freedom. Transmission coefficients computed this way were first reported by Mortensen,[228] and more recently this idea has been used by Bowman and Lee.[227] A similar approach has been applied by Hayes and Walker[229] in their bend-corrected rotating linear model. When recrossing is negligible, reaction-path curvature is small, and the system is approximately adiabatic in the bottleneck region, these methods are expected to be comparable in accuracy to SCSAG for thermal rate constants. However, they may be more accurate than SCSAG when recrossing is significant or when reaction-path curvature is large. So far, though, although the success of the LCG and LAG methods for a few test cases is encouraging, the two mathematical-dimensional approximations have not been applied to large-curvature systems, and there is not enough experience with such systems to draw general conclusions about these approaches.

In contrast to the reduced-dimensionality methods, the unified dynamical (UD) model[39] includes recrossing effects from classical trajectories calculated in the full-dimensional space. Consistent with variational TST, quantum effects on reaction-coordinate motion are included

by the use of semiclassical adiabatic transmission coefficients or more general semiclassical methods. This model can be viewed as a method of including quantum tunneling effects into quasiclassical trajectory calculations as well as a method for including recrossing effects into variational TST. The UD model is an attempt to improve upon the variational theory of reaction rates as employed by Keck and Anderson and co-workers.[21,24-26,230-232] The method they employed yields purely classical rate constants from trajectories started in the strong interaction region. In the UD method we use a quantized Keck (QK) method (similar to the approach taken by Smith[233]) in which the initial conditions are selected from a quasiclassical ensemble: i.e., the bound degrees of freedom orthogonal to the reaction coordinate are quantized in the same manner as described for the generalized TST calculations.

The QK reaction probabilities $P^{QK}(\mathbf{n},k,E)$ are calculated for each adiabatic state $(\mathbf{n},k)$. The trajectories are started from a dividing surface which is orthogonal to the reaction coordinate and located at the maximum $s^{\ddagger}_{*}(\mathbf{n},k)$ of the adiabatic potential curve $V_a(\mathbf{n},k,s)$. For energies above the adiabatic barrier maximum $V^{A}(\mathbf{n},k)$, the initial conditions for the trajectories are selected from a microcanonical ensemble located on the dividing surface such that the energy in each of the bound modes equals $\epsilon^{GT}_{vib,m}[n_m,s^{\ddagger}_{*}(\mathbf{n},k)]$. Each trajectory is integrated forward (toward products) and backward (toward reactants) from the dividing surface and given a weight:

$$W(\mathbf{x}_0,\mathbf{p}_0) = [1 - (-1)^{M(\mathbf{x}_0,\mathbf{p}_0)}]/2M(\mathbf{x}_0,\mathbf{p}_0) \tag{208}$$

where $M(\mathbf{x}_0,\mathbf{p}_0)$ is the total number of times the trajectory crosses the dividing surface, and $\mathbf{p}_0$ is a vector of initial momentum components conjugate to $\mathbf{x}_0$, the starting position of the trajectory. The probability for reaction from state $(\mathbf{n},k)$, $P^{QK}(\mathbf{n},k,E)$, is obtained from the proper phase-space average of these weights.

The dividing surface is a hyperplane in the multidimensional space. For each vibrational mode in the dividing surface, a transformation is made to the action-angle variables (q_m,N_m). The reaction probability is then given by

$$P^{QK}(\mathbf{n},k,E) = (2\pi)^{-(F-1)} \int_0^{2\pi} \cdots \int_0^{2\pi} W(\mathbf{q},\mathbf{N})\, d\mathbf{q} \tag{209}$$

where the numbers $n_m = N_m - {}^1/_2$, $m = 1,2,\ldots,F-1$, are required to be integers. In each mode the transformation between the angle variable and the normal coordinate is given by

$$q_m(Q_m) = \frac{\displaystyle\int_{Q_{m<}}^{Q_m} \{\epsilon^{GT}_{vib,m}[n_m,s^{\ddagger}_{*}(\mathbf{n},k)] - V_{eff,m}[Q'_m,s^{\ddagger}_{*}(\mathbf{n},k)]\}^{-1/2}\, dQ'_m}{4\pi\hbar \displaystyle\int_{Q_{m<}}^{Q_{m>}} \{\epsilon^{GT}_{vib,m}[n_m,s^{\ddagger}_{*}(\mathbf{n},k)] - V_{eff,m}[Q'_m,s^{\ddagger}_{*}(\mathbf{n},k)]\}^{-1/2}\, dQ'_m} \tag{210}$$

where the effective potential $V_{eff,m}[Q'_m,s^{\ddagger}_{*}(\mathbf{n},k)]$ is the actual one-dimensional potential for mode m in the dividing surface with all other normal coordinates set to zero, and $Q_{m<}$ and $Q_{m>}$ are the turning points in this potential. In the calculations of $P^{QK}(\mathbf{n},k,E)$ the integral over the angle q_m is done by Gauss quadrature and a value of Q_m for each q_m is determined from Equation 210 by a root search procedure. The vibrational energy level is determined from the anharmonic approximation to the effective potential.

As an example of an application of the above method, we consider a collinear atom-diatom reaction in which case $F = 2$ and the dividing surface is one dimensional, and near the reaction coordinate, the dividing surface is a straight line perpendicular to the reaction coordinate. However, the effective potential along this straight line need not necessarily

have a turning point on the dissociative side of the reaction coordinate. Consistent with the Morse I approximation, which assumes that the bound mode dissociates to three separated atoms, the dividing surface is defined to be this straight line only to the point at which the potential is a local maximum. Beyond this point, the dividing surface is defined as a straight line which goes out to the dissociative three-atom limit parallel to the bisector of the skew angle. In this manner the dividing surface is made up of either one or two straight-line segments such that the effective potential along the dividing surface has the correct dissociation limit.

The momenta in the Q_m and s directions are determined by energy conservation and are given by

$$P_m^2 = 2\mu\{\epsilon_{vib,m}^{GT}[n_m,s^\ddagger(\mathbf{n},k)] - V_{eff}[Q_m,s^\ddagger(\mathbf{n},k)]\} \tag{211}$$

and

$$p_s^2 = 2\mu\{E - V_a[\mathbf{n},k,s^\ddagger(\mathbf{n},k)]\} \tag{212}$$

Specifying the momentum P_m in this manner yields a value for the action integral which is only approximately equal to $n_m + {}^1/_2$ as required by the quasiclassical condition. This procedure is used to ensure that the adiabatic barrier maximum implicit in the trajectory calculations is the same as that used in the tunneling calculation that is incorporated into the UD method as discussed below.

Another problem arises in this procedure because the dividing surface is not a periodic-orbit dividing surface[234-236] (PODS). If a dividing surface were chosen to be a PODS, a trajectory started on the dividing surface with no momentum normal to the surface would remain in the surface forever and never recross it. If the PODS is not straight, this same trajectory recrosses our dividing surface an infinite number of times. Similarly, a trajectory which is slightly perturbed from the PODS would never recross the PODS, but would recross our dividing surface many times before leaving the interaction region. This becomes a critical problem in trying to evaluate the amount of recrossing for energies near the adiabatic barrier maximum where the momentum in the reaction-coordinate direction is very small. To perform the calculations at these energies it is necessary to specify criteria for defining when a recrossing corresponds to a "true" recrossing, i.e., one which would have recrossed the PODS. Alternatively, the QK probabilities at these energies could be obtained by extrapolation from higher energies where this is not a problem.

For energies below the adiabatic barrier maximum, tunneling may be accounted for by any of the previously mentioned tunneling methods. First consider a semiclassical adiabatic model in which a primitive expression for the tunneling probability is given by

$$P_{prim}^{SA}(\mathbf{n},k,E) = \exp[-2\theta^{SA}(\mathbf{n},k,E)] \tag{213}$$

We wish to define a uniform expression for the UD reaction probability which includes tunneling for energies below $V^\wedge(\mathbf{n},k)$ and includes nonclassical reflection and classical recrossing corrections for energies above $V^\wedge(\mathbf{n},k)$. Defining the quantal threshold energy for state $(\mathbf{n},k)$ as

$$\epsilon_{thr}(\mathbf{n},k) = \max[V_a(\mathbf{n},k,s = -\infty), \quad V_a(\mathbf{n},k,s = +\infty)] \tag{214}$$

such an expression is given by

$$P^{UD/SA}(\mathbf{n},k,E) = \begin{cases} \{2/P^{QK}[\mathbf{n},k,V^A(\mathbf{n},k)] - 1 + 1/P^{SA}_{prim}(\mathbf{n},k,E)\}^{-1}, \\ \qquad \epsilon_{thr}(\mathbf{n},k) < E \leq V^A(\mathbf{n},k) \\ (1 - \{1 + 1/P^{SA}_{prim}[\mathbf{n},k,2V^A(\mathbf{n},k) - E]\}^{-1})P^{QK}(\mathbf{n},k,E), \\ \qquad V^A(\mathbf{n},k) \leq E \leq 2V^A(\mathbf{n},k) - \epsilon_{thr}(\mathbf{n},k) \\ P^{QK}(\mathbf{n},k,E),\ 2V^A(\mathbf{n},k) - \epsilon_{thr}(\mathbf{n},k) < E \end{cases} \tag{215}$$

For very low energies $P^{UD/SA}(\mathbf{n},k,E)$ reduces to the primitive tunneling probability $P^{SA}_{prim}(\mathbf{n},k,E)$; at $E = V^A(\mathbf{n},k)$, $P^{SA}_{prim}(\mathbf{n},k,E)$ becomes one and the UD/SA probability goes to $P^{QK}(\mathbf{n},k,V^A(\mathbf{n},k)]/2$; for energies in the range $V^A(\mathbf{n},k) \leq E \leq 2V^A(\mathbf{n},k) - \epsilon_{thr}(\mathbf{n},k)$, the UD/SA probability is equal to the probability obtained from the quasiclassical Keck method multiplied by a probability for nonclassical reflection. Instead of using semiclassical adiabatic tunneling probabilities, more general tunneling probabilities, such as quantum mechanical probabilities for tunneling through the adiabatic barriers, could be used in Equation 215. To provide the correct limiting value near the adiabatic barrier maximum, these more general probabilities must be replaced by a primitive-type expression that goes to one at the adiabatic barrier maximum. A general prescription to define a primitive-type tunneling probability corresponding to a general tunneling probability $P(\mathbf{n},k,E)$ is given by

$$P_{prim}(\mathbf{n},k,E) = ([P(\mathbf{n},k,E)]^{-1} - \{P[\mathbf{n},k,V^A(\mathbf{n},k)]\}^{-1} + 1)^{-1} \tag{216}$$

At low energies, where the probability becomes small, the first term inside the brackets dominates and the primitive expression reduces to the general one, while at the barrier maximum the first two terms inside the brackets cancel and the primitive expression becomes one.

For calculating thermally averaged quantities we consider the thermal rate constant for the ground electronic surface in the following equation. The tunneling method is left general and denoted by Y. Satte-selected thermal rate constants are obtained from the reaction probability by

$$k^{UD/Y}(\mathbf{n},k,T) = \sigma[h\Phi^R_{rel}(T)]^{-1}\exp[\beta V_a(\mathbf{n},k,s = -\infty)] \times \int_{\epsilon_{thr}(\mathbf{n},k)}^{\infty} \exp(-\beta E)P^{UD/Y}(\mathbf{n},k,E)\, dE \tag{217}$$

where $\Phi^R_{rel}(T)$ is the partition function per unit volume for the asymptotic reactant relative translational motion. The thermal rate constant, including electronic surface factors, is then given by

$$k^{UD/Y}(T) = Q^{GT}_{el}(T)[Q^R_{el}(T)Q^R_{vr}(T)]^{-1} \sum_{\mathbf{n},k} \exp[-\beta V_a(\mathbf{n},k,s = -\infty)]k^{UD/Y}(\mathbf{n},k,T) \tag{218}$$

where

$$Q^R_{el}(T)Q^R_{vr}(T) = Q^A(T)Q^B(T) \tag{219}$$

At low temperatures, where the thermal rate constant is dominated by the ground state, a UD transmission coefficient can be defined by

$$\kappa^{UD/YG}(T) = k^{UD/Y}(\mathbf{n} = 0,k = 0,T)/k^{A}(\mathbf{n} = 0,k = 0,T) \tag{220}$$

where

$$k^{A}(\mathbf{n} = 0,k = 0,T) = \frac{\sigma\exp(-\beta V^{AG})}{h\beta\Phi^{R}_{rel}(T)\exp[-\beta V^{G}_{a}(s = -\infty)]} \tag{221}$$

It is useful to define approximate expressions in which the rotational degrees of freedom are treated classically, as in the μVT expressions given in Section V. Also, since tunneling effects are most important at low temperatures and therefore may often be adequately described by tunneling through the ground state, Equation 218 may be approximated by

$$k^{UD/Y}(T) = \{\exp[-\beta V_a(\mathbf{n} = 0,k = 0,s = -\infty)]k^{UD/Y}(\mathbf{n} = 0,k = 0,T) + \sum_{(\mathbf{n},k)\neq(\mathbf{0},0)} \exp[-\beta V_a(\mathbf{n},k,s = -\infty)]k^{QK}(\mathbf{n},k,T)\}/Q^{R}_{vr}(T) \tag{222}$$

where $k^{QK}(\mathbf{n},k,T)$ is defined in terms of $P^{QK}(\mathbf{n},k,T)$ of Equation 209 analogously to Equation 217.

VII. COMPARISON TO TRAJECTORY CALCULATIONS

The accurate calculation of chemical reaction rates by quantum mechanical collision theory is a very complicated rearrangement scattering problem that involves too many open channels to be generally practical. One alternative to a quantal calculation is a trajectory calculation.[2-5,232,237] In a trajectory calculation, one may directly sample from a thermal distribution of energies rather than numerically average a cross section computed as a function of energy and the relevant quantum numbers. However, a trajectory calculation suffers from the difficulty of incorporating quantal effects at the most critical stage of the reaction. Although quantization can be easily enforced in the initial or final asymptotic region, it requires complicated classical S matrix calculations to enforce it in both places or to include barrier penetration.[238-240] In addition, both quantal scattering theory and trajectory calculations require the whole potential energy surface as input. In contrast, conventional TST with unit transmission coefficient enforces bound-mode quantization at the transition state and requires only a knowledge of the saddle point region of the potential energy surface. The three most serious deficiencies of conventional TST are (1) neglect of barrier penetration, i.e., tunneling, (2) neglect of classical recrossing effects, and (3) the assumption of a separable reaction coordinate. Variational TST with vibrationally adiabatic transmission coefficients, as discussed in this chapter, provides a practical and consistent improvement with respect to the first two difficulties. In variational TST with SC transmission coefficients, the required knowledge of the potential energy surface is intermediate between that required for full scattering calculations and that required for conventional TST; what is required is a knowledge of the MEP and a normal-mode analysis at a sequence of points along it. More general semiclassical ground-state transmission coefficients, like the LCG or LAG approximations, require information about the surface farther from the MEP.

Another important difference between trajectory calculations and generalized TST for thermal rate constants is caused by the differing amounts of vibrational nonadiabaticity at the critical point in the interaction region. The quantization scheme we use for generalized TST assumes complete quantization of bound degrees of freedom in the generalized transition state. This is in accordance with the standard practice of using quantized partition functions in conventional TST. Trajectory calculations, on the other hand, involve some nonadiabat-

icity, i.e., even though a trajectory may be started with zero-point energies for all degrees of freedom of the reactants, some reactive trajectories have less than the local zero-point energy in their bound degrees of freedom when they pass through the conventional or generalized transition state. The true quantum mechanical dynamics also involve some vibrational nonadiabaticity, so trajectory calculations cannot automatically be faulted in this regard.[241] However, the evidence so far is that trajectory calculations involve too much vibrational nonadiabaticity, so that the extent of their agreement with accurate quantal calculations is sometimes helped by a cancellation of errors, i.e., the overestimation of vibrational nonadiabaticity partly compensates for the neglect of tunneling. (One of the motivations for the unified dynamical theory discussed in the previous section is to incorporate quantization at the dynamical bottleneck while simultaneously including quantal tunneling and classical recrossing effects.) The tendency to overestimate vibrational nonadiabaticity in a trajectory calculation is understandable since the finite, and often large, energy-level spacings in quantum mechanics promote adiabaticity to a greater extent than classical mechanical dynamical factors do. For a similar reason, the vibrational adiabaticity assumption is expected to be best for high-frequency stretches and worst for low-frequency modes like bends. Even for bends, however, accurate three-dimensional quantum mechanical calculations[6] indicate that vibrational adiabaticity is useful for a quantitative understanding of the value of the threshold energy. For collinear reactions, the nature of vibrational adiabaticity of stretching vibrations in the threshold region is even better understood. Although there is definite evidence of vibrational nonadiabaticity in the accurate transition state wavefunction for the H + H_2 reaction,[242] it can be mimicked to some extent by tunneling calculations such as the Marcus-Coltrin path and SC approximation models discussed in Section IV, which predict more tunneling than the MEP vibrationally adiabatic separable tunneling model. However, even though there have been important advances in our ability to model multidimensional tunneling reactions in the last few years, the present models must still be applied with caution when they are applied to systems very different than the ones for which they have been tested.

VIII. CONCLUDING REMARKS

Since conventional TST is very widely discussed in the literature, and other reviews are available that discuss various applications of variational TST,[3,5,20,36,39,46,47,243] we have emphasized in this chapter the computational formalism of variational TST, especially for polyatomic systems and with emphasis on the methods used in our group.

In 1966, Bunker[10] reviewed the existing evidence for the correctness of TST. He warned users of the theory not to oversimplify the potential energy surface, the vibrational analysis, or the tunneling correction. He concluded that if these cautions are observed, "we may rely on the theory to provide a bimolecular rate prediction within a factor of 10 of the truth". At that time he also concluded that there was little evidence to support the assumption of TST that an equilibrium distribution of activated complexes was maintained kinematically by bimolecular collsions.

Recent research has reemphasized Wigner's collisional approach[16] to TST, and numerous dynamical studies have led to a greater understanding of how the quasiequilibrium assumption may be justified by the directness of reactive trajectories in the threshold region or by vibrational adiabaticity. We have detailed tests of conventional and variational TST against accurate quantal dynamics for many collinear and two three-dimensional quantal systems. The importance of variationally optimizing the transition state dividing surface has been demonstrated, and reliable tunneling models have been developed and refined. We now have much more confidence in our ability to make dynamical predictions of thermal reaction rates than was possible at the time of Bunker's statement, and we expect in most cases to be able

to predict the thermal rate constant to within a factor of two or better of the accurate quantal result for a given potential energy surface. In fact, there is probably no reaction for which our inability to accurately calculate the rate constant for a given potential energy surface leads to greater errors than the errors caused by the inexactness of the potential energy surface.

ACKNOWLEDGMENTS

The work at the University of Minnesota was supported in part by the U.S. Department of Energy, Office of Basic Energy Sciences, under contract DE-AC02-79ER10425. The work at Chemical Dynamics Corporation was supported by the U.S. Army through the Army Research Office under contract DAAG-29-81-C-0015.

APPENDIX 1: COLLISIONAL DERIVATION OF TRANSITION STATE THEORY

In this appendix we consider the general bimolecular reaction Equation 1a. Let $S(\alpha,E_{rel})$ be the state-selected, fixed-energy cross section for initial internal state α and initial relative translational energy E_{rel}. The label α denotes the set of vibrational-rotational quantum numbers $(\mathbf{n},k)$ for both reactants. The final states of the products are not specified, i.e., this cross section is summed over the state-to-state cross sections for all final states. The state-selected rate constant at relative translational temperature T is related to the state-selected reaction cross section $S(\alpha,E_{rel})$ by a Maxwell-Boltzmann average over initial relative translational energies at temperature T:[1,15,244,245]

$$k(\alpha,T) = \left(\frac{1}{\pi\mu}\right)^{1/2}(2\beta)^{3/2}\int_0^\infty S(\alpha,E_{rel})E_{rel}\exp(-\beta E_{rel})\,dE_{rel} \qquad (223)$$

where μ is the reduced mass for relative motion of the reactants. The thermal rate constant is in turn related to $k(\alpha,T)$ by

$$k(T) = [Q^R_{ins}(T)]^{-1}\sum_\alpha d_\alpha\, k(\alpha,T)\exp[-\beta\epsilon^R_{int}(\alpha)] \qquad (224)$$

where $\epsilon^R_{int}(\alpha)$ and $Q^R_{int}(T)$ are the internal energy of the reactants in state α and the reactant internal partition function at temperature T, respectively, so that

$$Q^R_{int}(T) = \sum_\alpha d_\alpha \exp[-\beta\epsilon^R_{int}(\alpha)] \qquad (225)$$

where d_α is the degeneracy of state α. Note that $\epsilon^R_{int}(\alpha)$ is the sum of the internal energies of A and B, and d_α and $Q^R_{int}(T)$ are products of quantities referring to A and B.

$$S(\alpha,E_{rel}) = \frac{\sigma\pi h^2}{p^2}\sum_\ell\sum_{m\ell} P_{\alpha\ell m_\ell}(E_{rel}) \qquad (226)$$

where

$$E_{rel} = p^2/2\mu \qquad (227)$$

ℓ and m_ℓ are quantum numbers for initial orbital angular momentum of relative motion and its component with respect to a space-fixed axis, and $P_{\alpha\ell m_\ell}(E_{rel})$ is a reaction probability. Combining Equations 223, 224, 226, and 227 yields:

$$k(T) = \frac{\sigma}{Q^R_{int}(T)} \frac{h^2}{(2\pi\mu kT)^{3/2}} \sum_\alpha d_\alpha \sum_\ell \sum_{m_\ell} \int_0^\infty P_{\alpha\ell m_\ell}(E_{rel}) \times \exp\{-\beta[\epsilon^R_{int}(\alpha) + E_{rel}]\}\, dE_{rel} \quad (228)$$

The total partition function per unit volume for reactants is

$$\Phi^R(T) = \Phi^R_{rel}(T)\, Q^R_{int}(T) \quad (229)$$

where

$$\Phi^R_{rel}(T) = (2\pi\mu kT)^{3/2}/h^3 \quad (230)$$

and where, as in Section II, we work in the center-of-mass system so that the translational part of $\Phi^R(T)$ includes only relative motion. Using Equations 229 and 230, we can rewrite Equation 228 as

$$k(T) = \frac{\sigma}{\beta h \Phi^R(T)} \sum_\alpha d_\alpha \sum_\ell \sum_{m_\ell} \bar{P}_{\alpha\ell m_\ell}(T) \exp[-\beta\epsilon^R_{int}(\alpha)] \quad (231)$$

where

$$\bar{P}_{\alpha\ell m_\ell}(T) = \int_0^\infty P_{\alpha\ell m_\ell}(E_{rel}) \exp(-\beta E_{rel})\beta dE_{rel} \quad (232)$$

Equation 231 is equivalent to Equation 45 of Reference 220, and it is exact. Earlier collision-theory formulations for three-dimensional reactions were given by Eliason and Hirschfelder[1] and Christov[246-251] and formulations for collinear reactions were given by Mortensen[228] and in Reference 148. See also References 145, 252, and 253. A useful alternative form of Equation 231 is

$$k(T) = \frac{\sigma}{\beta h \Phi^R(T)} \sum_\alpha d_\alpha \sum_\ell \sum_{m_\ell} \int_{\epsilon^R_{int}(\alpha)}^\infty P_{\alpha\ell m_\ell}(E) \exp(-\beta E)\beta dE \quad (233)$$

where the reaction probability is considered as a function of the total energy given by

$$E = \epsilon^R_{int}(\alpha) + E_{rel} \quad (234)$$

Now we make the TST assumption. Consider a reaction coordinate s such that $s = -\infty$ corresponds to reactants and $s = s_*$ to the generalized transition state. Let $\epsilon^{GT}_{int}(\alpha,s)$ represent the adiabatic vibrational-rotational eigenvalues. Now in Equation 233 we make the transition state assumption:

$$P_{\alpha\ell m_\ell}(E) \simeq \theta[E - V_{MEP}(s_*) - \epsilon^{GT}_{int}(\alpha,s_*)] \quad (235)$$

where θ denotes a Heaviside step function. Then Equation 233 becomes

$$k(T) = \frac{\sigma}{\beta h \Phi^R(T)} \exp[-\beta V_{MEP}(s_*)] \sum_\alpha \sum_\ell \sum_{m_\ell} d_\alpha \exp[-\beta\epsilon^{GT}_{int}(\alpha,s_*)] \quad (236)$$

Since α,ℓ, m_ℓ are a complete set of indexes, this is equivalent to Equation 8 without the classical approximation. If, instead, we make the better approximation:

$$P_{\alpha\ell m_\ell}(E) \simeq \theta\{E - \max_s[V_{MEP}(s) + \epsilon_{int}^{GT}(\alpha,s)]\} \tag{237}$$

then we obtain the more accurate Equation 185.

APPENDIX 2: CUTOFF CLASSICAL ROTATIONAL PARTITION FUNCTION AND SUM OF STATES

In this appendix we derive the classical approximations to the cut-off rotational partition function and the cut-off sum of rotational states function. These quantities are needed for the ICVT and μVT formalisms of Section V and are defined by Equations 164 and 166, respectively.

First consider the cut-off rotational partition function for a nonlinear generalized transition state. Introducing an energy cut-off ϵ into the usual classical expression[14,178,179] for the partition function yields:

$$Q_{rot}^{GT}(T,s;\epsilon) = \frac{1}{\pi\hbar^3} \prod_{\substack{i=A,B,C \\ \epsilon_{rot}\le\epsilon}} \int_{-\infty}^{\infty} \exp[-\beta J_i^2/2I_i(s)]\, dJ_i \tag{238}$$

where the J_i are the components of rotational angular momentum around the principal axes, and

$$\epsilon_{rot} = \sum_{i=A,B,C} J_i^2/[2I_i(s)] \tag{239}$$

To evaluate this we convert to spherical polar coordinates with radius:

$$R_J = \epsilon_{rot}^{1/2} \tag{240}$$

The angular integrals give 4π so that Equation 238 reduces to

$$Q_{rot}^{GT}(T,s;\epsilon) = \frac{4[8I_A(s)I_B(s)I_C(s)]^{1/2}}{\hbar^3} \int_0^{\epsilon^{1/2}} R_J^2 \exp(-\beta R_J^2)\, dR_J \tag{241}$$

Evaluation of the remaining one-dimensional integral yields Equation 170a.

The cut-off sum of rotational states is then easily obtained by the relation:

$$N_{rot}^{GT}(\epsilon,s) = \lim_{\beta\to 0} Q_{rot}^{GT}(T,s;\epsilon) \tag{242}$$

This yields Equation 171a. The reader should note that the result of Equation 171a differs from Equation 6-45 of Reference 94, which is apparently in error by a factor of π.

The derivations for a linear generalized transition state are similar. The linear transition state analog of Equation 238 is

$$Q_{rot}^{GT}(T,s;\epsilon) = \frac{2}{\hbar^2} \int_0^{(2I\epsilon)^{1/2}} J \exp[-\beta J^2/2I(s)]\, dJ \tag{243}$$

Evaluation of the integral yields Equation 170b. Use of Equation 242 then yields Equation 171b.

APPENDIX 3: GLOSSARY OF ABBREVIATIONS

AG:	adiabatic ground-state (threshold energy)
C:	(as a subscript, C denotes a purely classical quantity)
CUS:	canonical unified statistical (model)
CVT:	canonical variational theory
G:	ground state
GT:	generalized transition state
GTS:	generalized transition state
ICVT:	improved canonical variational theory
INM:	independent normal modes (approximation)
LAG:	least-action ground state (transmission coefficient)
LCG:	large-curvature (approximation) ground state (transmission coefficient)
MCP:	Marcus-Coltrin path
MEP:	minimum energy path
R:	reactant
S:	semiclassical
SA:	semiclassical adiabatic
SAG:	semiclassical adiabatic ground state (transmission coefficient)
SC:	small-curvature approximation for tunneling and nonclassical reflection
SCT:	small-curvature approximation for tunneling only
SG:	semiclassical ground state (transmission coefficient)
TST:	transition state theory
UD:	unified dynamical (model)
VA:	vibrationally rotationally adiabatic
VTST:	variational transition state theory; i.e., CVT, ICVT, or μVT
μVT:	microcanonical variational theory
$\ddagger$:	conventional TST

REFERENCES

1. **Eliason, M. A. and Hirschfelder, J. O.,** General collision theory treatment for the rate of bimolecular, gas phase reactions, *J. Chem. Phys.*, 30, 1426, 1959.
2. **Truhlar, D. G. and Muckerman, J. T.,** Reactive scattering cross sections: quasiclassical and semiclassical methods, in *Atom-Molecule Collision Theory: A Guide for the Experimentalist*, Bernstein, R. B., Ed., Plenum Press, N.Y., 1979, 505.
3. **Truhlar, D. G.,** Accuracy of trajectory calculations and transition state theory for thermal rate constants of atom transfer reactions, *J. Phys. Chem.* 83, 188, 1979.
4. **Truhlar, D. G. and Wyatt, R. E.,** History of H_3 kinetics, *Annu. Rev. Phys. Chem.*, 27, 1, 1976.
5. **Walker, R. B. and Light, J. C.,** Reactive molecular collisions, *Annu. Rev. Phys. Chem.*, 31, 401, 1980.
6. **Schatz, G. C. and Kuppermann, A.,** Quantum mechanical reactive scattering for three-dimensional atom plus diatom systems. II. Accurate cross sections for H + H_2, *J. Chem. Phys.*, 65, 4668, 1976.
7. **Schatz, G. C.,** The quantum dynamics of H + H_2(v = 1): a coupled states study of cross sections and rate constants, *Chem. Phys. Lett.*, 94, 183, 1983.
8. **Glasstone, S., Laidler, K. J., and Eyring, H.,** *Theory of Rate Processes*, McGraw-Hill, N.Y., 1941, 10.
9. **Johnston, H. S.,** *Gas Phase Reaction Rate Theory*, Ronald Press, N.Y., 1966, 119.
10. **Bunker, D. L.,** *Theory of Gas Phase Reaction Rates*, Pergamon Press, Oxford, 1966, 9.
11. **Laidler, K. J.,** *Theories of Chemical Reaction Rates*, McGraw-Hill, N.Y., 1969, 42.
12. **Weston, R. E., Jr. and Schwartz, H. A.,** *Chemical Kinetics*, Prentice-Hall, Englewood Cliffs, N.J., 1972, 95.

13. **Nikitin, E. E.,** *Theory of Elementary Atomic and Molecular Processes in Gases*, Clarendon Press, Oxford, 1974, chap. 1, section 50.
14. **Rapp, D.,** *Statistical Mechanics*, Holt, Rinehard & Winston, N.Y., 1972, chaps. 4, 5, and 11.
15. **Smith, I. W. M.,** *Kinetics and Dynamics of Elementary Gas Reactions*, Butterworths, London, 1980.
16. **Wigner, E.,** The transition state method, *Trans. Faraday Soc.*, 34, 29, 1938.
17. **Pechukas, P. and McLafferty, F. J.,** On transition-state theory and the classical mechanics of collinear collisions, *J. Chem. Phys.*, 58, 1622, 1973.
18. **Stern, M. J., Persky, A., and Klein, F. S.,** Force field and tunneling effects in the H-H-Cl reaction system. Determination from kinetic-isotope-effect measurements, *J. Chem. Phys.*, 58, 5697, 1973.
19. **Baer, M.,** An exact quantum mechanical study of the isotopic collinear reactive systems H_2 + Cl and D_2 + Cl, *Mol. Phys.*, 27, 1429, 1974.
20. **Truhlar, D. G. and Garrett, B. C.,** Variational transition state theory, *Acc. Chem. Res.*, 13, 440, 1980.
21. **Garrett, B. C. and Truhlar, D. G.,** Generalized transition state theory. Classical mechanical theory and applications to collinear reactions of hydrogen molecules, *J. Phys. Chem.*, 83, 1052, 1979; 83, 3058, 1979; 87, 4553, 1983.
22. **Wigner, E.,** Calculation of the rate of elementary association reactions, *J. Chem. Phys.*, 5, 720, 1937.
23. **Horiuti, J.,** On the statistical mechanical treatment of the absolute rate of chemical reaction, *Bull. Chem. Soc. Jpn.*, 13, 210, 1938.
24. **Keck, J. C.,** Variational theory of chemical reaction rates applied to three-body recombinations, *J. Chem. Phys.*, 32, 1035, 1960.
25. **Keck, J. C.,** Variational theory of reaction rates, *Adv. Chem. Phys.*, 13, 85, 1967.
26. **Jaffe, R. L., Henry, J. M., and Anderson, J. B.,** Variational theory of reaction rates: application to F + $H_2 \rightleftarrows$ HF + H, *J. Chem. Phys.*, 59, 1128, 1973.
27. **Miller, W. H.,** Quantum mechanical transition state theory and a new semiclassical model for reaction rate constants, *J. Chem. Phys.*, 61, 1823, 1974.
28. **Pechukas, P.,** Statistical approximations in collision theory, in *Dynamics of Molecular Collisions*, Part B, Miller, W. H., Ed., Plenum Press, N.Y., 1976, 269.
29. **Garrett, B. C. and Truhlar, D. G.,** Criterion of minimum state density in the transition state theory of bimolecular reactions, *J. Chem. Phys.*, 70, 1593, 1979.
30. **Garrett, B. C. and Truhlar, D. G.,** Generalized transition state theory. Bond energy-bond order method for canonical variational calculations with applications to hydrogen atom transfer reactions, *J. Am. Chem. Soc.*, 101, 4534, 1979.
31. **Garrett, B. C. and Truhlar, D. G.,** Generalized transition state theory. Canonical variational calculations using the bond energy-bond order method for bimolecular reactions of combustion products, *J. Am. Chem. Soc.*, 101, 5207, 1979.
32. **Garrett, B. C. and Truhlar, D. G.,** Variational transition state theory. Primary kinetic isotope effects for atom transfer reactions, *J. Am. Chem. Soc.*, 102, 2559, 1980.
33. **Garrett, B. C. and Truhlar, D. G.,** Generalized transition state theory. Calculations for the reactions D + H_2 and H + D_2 using an accurate potential energy surface: explanation of the kinetic isotope effect, *J. Chem. Phys.*, 72, 3460, 1980.
34. **Garrett, B. C., Truhlar, D. G., Grev, R. S., and Magnuson, A. W.,** Improved treatment of threshold contributions in variational transition state theory, *J. Phys. Chem.*, 84, 1730, 1980; 87, 4554, 1983.
35. **Garrett, B. C., Truhlar, D. G., and Grev, R. S.,** Application of variational transition state theory and the unified statistical model to H + $Cl_2 \rightarrow$ HCl + Cl, *J. Phys. Chem.*, 84, 1749, 1980.
36. **Garrett, B. C., Truhlar, D. G., and Grev, R. S.,** Determination of the bottleneck regions of potential energy surfaces for atom transfer reactions by variational transition state theory, in *Potential Energy Surfaces and Dynamics Calculations*, Truhlar, D. G., Ed., Plenum Press, N.Y., 1981, 587.
37. **Garrett, B. C., Truhlar, D. G., and Magnuson, A. W.,** Variational transition state theory and vibrationally adiabatic transmission coefficients for kinetic isotope effects in the Cl-H-H reaction system, *J. Chem. Phys.*, 74, 1029, 1981.
38. **Garrett, B. C., Truhlar, D. G., and Magnuson, A. W.,** New semiempirical method of modeling potential energy surfaces for generalized TST and application to kinetic isotope effects in the Cl-H-H system, *J. Chem. Phys.*, 76, 2321, 1982.
39. **Truhlar, D. G., Isaacson, A. D., Skodje, R. T., and Garrett, B. C.,** The incorporation of quantum effects in generalized transition state theory, *J. Phys., Chem.*, 86, 2252, 1982; 87, 4554, 1983.
40. **Bondi, D. K., Clary, D. C., Connor, J. N. L., Garrett, B. C., and Truhlar, D. G.,** Kinetic isotope effects in the Mu + H_2 and Mu + D_2 reactions: accurate quantum calculations for the collinear reactions and variational transition state theory predictions for one and three dimensions, *J. Chem. Phys.*, 76, 4986, 1982.
41. **Blais, N. C., Truhlar, D. G., and Garrett, B. C.,** Temperature dependence of the activation energy, *J. Chem. Phys.*, 76, 2768, 1982.

42. **Clary, D. C., Garrett, B. C., and Truhlar, D. G.,** Comparison of variational transition state theory and quantum sudden calculations of three-dimensional rate coefficients for the reactions D(H) + BrH → DBr(HBr) + H, *J. Chem. Phys.*, 78, 777, 1983.
43. **Blais, N. C., Truhlar, D. G., and Garrett, B. C.,** Quasiclassical trajectory (and variational transition state theory) study of the rates and temperature-dependent activation energies of the reactions Mu + H_2 (completely thermal) and H, D, and Mu + H_2($v = 0$, $j = 2$), *J. Chem. Phys.*, 78, 2373, 1983.
44. **Garrett, B. C., Truhlar, D. G., Wagner, A. F., and Dunning, T. H., Jr.,** Variational transition state theory and tunneling for a heavy-light-heavy reaction using an *ab initio* potential energy surface. ^{37}Cl + H(D)^{35}Cl → H(D)^{37}Cl + ^{35}Cl, *J. Chem. Phys.*, 78, 4400, 1983.
45. **Rai, S. N. and Truhlar, D. G.,** Variational transition state theory calculations for an atom-radical reaction with no saddle point: O + OH_2, *J. Chem. Phys.*, 79, 6046, 1983.
46. **Pechukas, P.,** Transition state theory, *Annu. Rev. Phys. Chem.*, 32, 159, 1981.
47. **Pechukas, P.,** Recent developments in transition state theory, *Ber. Bunsenges. Phys. Chem.*, 86, 372, 1982.
48. **Isaacson, A. D. and Truhlar, D. G.,** Polyatomic canonical variational theory for chemical reaction rates. Separable-mode formalism with application to OH + H_2 → H_2O + H, *J. Chem. Phys.*, 76, 1380, 1982.
49. **Bondi, D. K., Connor, J. N. L., Garrett, B. C., and Truhlar, D. G.,** Test of variational transition state theory with a large-curvature tunneling approximation against accurate quantal reaction probabilities and rate coefficients for three collinear reactions with large reaction-path curvature: Cl + HCl, Cl + DCl, and Cl + MuCl, *J. Chem. Phys.*, 78, 5981, 1983.
50. **Truhlar, D. G., Runge, K., and Garrett, B. C.,** Variational transition state theory and tunneling calculations of potential energy surface effects on the reaction of O(^3P) with H_2, *Proc. 20th Int. Symp. Combustion*, Combustion Institute, Pittsburgh, in press.
51. **Parr, C. A.,** Harmonic-Quartic Vibrations in Reaction-Rate Theory, in Ph.D. thesis, California Institute of Technology, Pasadena, 1969, 292.
52. **Bron, J. and Hacker, S. O.,** The anharmonicity correction for kinetic isotope effect calculations, *Can. J. Chem.*, 51, 2765, 1973.
53. **Bron, J.,** Anharmonicity correction for kinetic isotope effect calculations involving hydrogen isotopes, *J. Chem. Soc. Faraday Trans. II*, 70, 240, 1974.
54. **Garrett, B. C. and Truhlar, D. G.,** Importance of quartic anharmonicity for bending partition functions in transition-state theory, *J. Phys. Chem.*, 83, 1915, 1979.
55. **Garrett, B. C. and Truhlar, D. G.,** Reliable *ab initio* calculation of a chemical reaction rate and a kinetic isotope effect: H + H_2 and D + D_2, *Proc. Natl. Acad. Sci. U.S.A.*, 76, 4755, 1979.
56. **Pacey, P. D.,** Participation of two-dimensional hindered internal rotations in activated complexes, *J. Chem. Phys.*, 77, 3540, 1982.
57. **Wilson, E. B., Jr., Decius, J. C., and Cross, P. C.,** *Molecular Vibrations*, McGraw-Hill, N.Y., 1955, 19.
58. **Garrett, B. D. and Truhlar, D. G.,** Generalized transition state theory. Quantum effects for collinear reactions of hydrogen molecules, *J. Phys. Chem.*, 83, 1079, 1979; 84, 682, 1980.
59. **Truhlar, D. G. and Kuppermann, A.,** Exact tunneling calculations, *J. Am. Chem. Soc.*, 93, 1840, 1971.
60. **Schaefer, H. F.,** Potential beneath the surface, *Chem. Br.*, 11, 227, 1975.
61. **Fukui, K., Kato, S., and Fujimoto, H.,** Constituent analysis of the potential gradient along a reaction coordinate. Method and an application to CH_4 + T reaction, *J. Am. Chem. Soc.*, 97, 1, 1975.
62. **Russegger, P. and Brickman, P.,** Quantum states of intramolecular nuclear motion with large amplitudes: pseudorotation of trigonal bipyramidal molecules, *J. Chem. Phys.*, 62, 1086, 1975.
63. **Russegger, P.,** Photoisomerization about carbon-nitrogen double bonds. I. Kinetic and potential energy for ground and excited states of methylenimine, *Chem. Phys.*, 34, 329, 1978.
64. **Russegger, P.,** Vibrational wavefunctions for the thermal and photochemical syn-anti isomerization of imines, *Chem. Phys.*, 41, 299, 1979.
65. **Russegger, P.,** Vibrational nonadiabatic model calculations on the unimolecular cis-trans isomerization of dideuteroethylene, *Ber. Bunsenges. Phys. Chem.*, 85, 330, 1981.
66. **Setser, D. W.,** Unimolecular reactions of polyatomic molecules, radicals, and ions, in *Chemical Kinetics*, Polanyi, J. C., Ed., Medical and Technical Publishing, Oxford, 1972, 1.
67. **Szwarc, M.,** Discussion on the paper by H. Eyring et al., in *The Transition State, A Symposium Held at Sheffield, 3-4 April 1962*, Chemical Society, London, 1962, 25.
68. **Tweedale, A. and Laidler, K. J.,** Vibrationally adiabatic model for the dynamics of H + H_2 systems, *J. Chem. Phys.*, 53, 2045, 1970.
69. **Margenau, H. and Murphy, G. M.,** *The Mathematics of Physics and Chemistry*, Van Nostrand Reinhold, N.Y., 1943, 476.
70. **McIver, J. W. and Komornicki, A.,** Rapid geometry optimization for semiempirical molecular orbital methods, *Chem. Phys. Lett.*, 10, 303, 1971.

71. **Pulay, P.,** Direct uses of the gradient for investigating molecular energy surfaces, in *Applications of Electronic Structure Theory*, Vol. 2, Schaefer, H. F., Ed., Plenum Press, N.Y., 1977, 153.
72. **McIver, J. W. and Komornicki, A.,** Structure of transition states in organic reactions. General theory and an application to the cyclobutane-butadiene isomerization using a semiempirical molecular orbital method, *J. Am. Chem. Soc.*, 94, 2625, 1972.
73. **Pauling, L. and Wilson, E. B.,** *Introduction to Quantum Mechanics with Applications to Chemistry*, McGraw-Hill, N.Y., 1935, 282.
74. **Ishida, K., Morokuma, K., and Komornicki, A.,** The intrinsic reaction coordinate. An *ab initio* calculation for HNC → NCH and $H^- + CH_4 \rightarrow CH_4 + H^-$, *J. Chem. Phys.*, 66, 2153, 1977.
75. **Cerjan, C. J. and Miller, W. H.,** On finding transition states, *J. Chem. Phys.*, 75, 2800, 1981.
76. **Miller, W. H., Handy, N. C., and Adams, J. E.,** Reaction path Hamiltonian for polyatomic molecules, *J. Chem. Phys.*, 72, 99, 1980.
77. **Landau, L. D. and Lifshitz, E. M.,** *The Classical Theory of Fields*, Pergamon Press, Oxford, 1975, 16.
78. **Herzberg, G.,** *Molecular Spectra and Molecular Structure. II. Infrared and Raman Spectra of Polyatomic Molecules*, Van Nostrand Reinhold, Princeton, 1945, 505.
79. **Osamura, Y., Yamaguchi, Y., Saxe, P., Vincent, M. A., Gaw, J. F., and Schaefer, H. F., III,** Unified theoretical treatment of analytic first and second energy derivatives in open-shell Hartree-Fock theory, *J. Chem. Phys.*, 72, 131, 1982.
80. **Truhlar, D. G., Kilpatrick, N. J., and Garrett, B. C.,** Reaction-path interpolation models for variational transition state theory, *J. Chem. Phys.*, 78, 2438, 1983.
81. **Gaedtke, H. and Troe, J.,** Berechnung Spezifischer Geschwindigkeitskonstanten k(E) für Zerfallsreaktionen. I. Pyrolyse und Photolyse Von NO_2, *Ber. Bunsenges. Phys. Chem.*, 77, 24, 1973.
82. **Quack, M. and Troe, J.,** Specific rate constants of unimolecular processes. II. Adiabitic channel model, *Ber. Bunsenges. Phys. Chem.*, 78, 240, 1974.
83. **Quack, M. and Troe, J.,** Unimolecular processes. V. Maximum free energy criterion for the high-pressure limit of dissociation reactions, *Ber. Bunsenges. Phys. Chem.*, 81, 329, 1977.
84. **Hase, W. L.,** Theoretical critical configuration for ethane decomposition and methyl radical recombination, *J. Chem. Phys.*, 57, 730, 1972.
85. **Herzberg, G.,** *Molecular Spectra and Molecular Structure. I. Spectra of Diatomic Molecules*, Van Nostrand Reinhold, Princeton, 1950, 101.
86. **Abramowitz, M. and Stegun, I. A.,** *Handbook of Mathematical Functions*, National Bureau of Standards, Washington, D.C., 1964.
87. **Garrett, B. C. and Truhlar, D. G.,** Accuracy of tunneling corrections to transition state theory for thermal rate constants of atom transfer reactions, *J. Phys. Chem.*, 83, 200, 1979; 83, 3058, 1979.
88. **Garrett, B. C., Truhlar, D. G., Grev, R. S., and Walker, R. B.,** Comparison of variational transition state theory and the unified statistical model with vibrationally adiabatic transmission coefficients to accurate collinear rate constants for T + HD → TH + D, *J. Chem. Phys.*, 73, 235, 1980.
89. **Garrett, B. C., Truhlar, D. G., Grev, R. S., Magnuson, A. W., and Connor, J. N. L.,** Variational transition state theory, vibrationally adiabatic transmission coefficients, and the unified statistical model tested against accurate quantal rate constants for collinear F + H_2, H + F_2, and isotopic analogs, *J. Chem. Phys.*, 73, 1721, 1980.
90. **Garrett, B. C., Truhlar, D. G., Grev, R. S., Schatz, G. C., and Walker, R. B.,** Reaction probabilities, resonances, and thermal rate constants for the collinear reactions H + FH and D + FD on a low-barrier surface: close-coupling and tunneling calculations, variational transition state theory, and the unified statistical model, *J. Phys. Chem.*, 85, 3806, 1981.
91. **Skodje, R. T., Truhlar, D. G., and Garrett, B. C.,** A general small-curvature approximation for transition-state-theory transmission coefficients, *J. Phys. Chem.*, 85, 3019, 1981.
92. **Clary, D. C.,** Exchange reactions of hydrogen halides with hydrogenic atoms, *Chem. Phys.*, 71, 117, 1982.
93. **Baer, M., Halavee, U., and Persky, A.,** The collinear Cl + XY system (X,Y = H, D, T). A comparison between quantum mechanical, classical, and transition state theory results, *J. Chem. Phys.*, 61, 5122, 1974.
94. **Forst, W.,** *Theory of Unimolecular Reactions*, Academic Press, N.Y., 1973, chap. 6.
95. **Truhlar, D. G.,** Oscillators with quartic anharmonicity: approximate energy levels, *J. Mol. Spectrosc.*, 38, 415, 1971.
96. **Schatz, G. C. and Elgersma, H.,** A quasi-classical trajectory study of product vibrational distributions in the OH + H_2 → H_2O + H reaction, *Chem. Phys. Lett.*, 73, 21, 1980.
97. **Walch, S. P. and Dunning, T. H.,** A theoretical study of the potential energy surface for OH + H_2, *J. Chem. Phys.*, 72, 1303, 1980.
98. **Crawford, B. L., Jr.,** The partition functions and energy levels of molecules with internal torsional motions, *J. Chem. Phys.*, 8, 273, 1940.

99. **Wilson, E. B., Jr.,** The present status of the statistical method of calculating thermodynamic functions, *Chem. Rev.*, 27, 17, 1940.
100. **Pitzer, K. S. and Gwinn, W. D.,** Thermodynamic functions for molecules with internal rotation, *J. Chem. Phys.*, 9, 485, 1941.
101. **Pitzer, K. S. and Gwinn, W. D.,** Energy levels and thermodynamic functions for molecules with internal rotation. I. Rigid frame with attached tops, *J. Chem. Phys.*, 10, 428, 1942.
102. **Li, J. C. M. and Pitzer, K. S.,** Energy levels and thermodynamic functions for molecules with internal rotation. IV. Extended tables for molecules with small moments of inertia, *J. Phys. Chem.*, 60, 466, 1956.
103. **Cohen, N.,** A simple analytic approximation for contributions of hindered internal rotors to bimolecular rate coefficients calculated by transition state theory, Aerospace Report ATR-82(7888)-2, Aerospace Corporation, El Segundo, Calif., January 1982.
104. **Isaacson, A. D., Truhlar, D. G., Scanlon, K., and Overend, J.,** Tests of approximation schemes for vibrational energy levels and partition functions for triatomics: H_2O and SO_2, *J. Chem. Phys.*, 75, 3017, 1981.
105. **Morino, Y., Kuchitsu, K., and Yamamoto, S.,** The anharmonic constants and average structure of ammonia, *Spectrochim. Acta*, 24A, 335, 1968.
106. **Kassel, L. S.,** Mathematical methods for computing thermodynamic functions from spectroscopic data, *J. Chem. Phys.*, 1, 576, 1933.
107. **Gordon, A. R.,** The calculation of thermodynamic quantities from spectroscopic data for polyatomic molecules: the free energy, entropy, and heat capacity of steam, *J. Chem. Phys.*, 2, 65, 1934.
108. **Kassel, L. S.,** The calculation of thermodynamic functions from spectroscopic data, *Chem. Rev.*, 18, 277, 1936.
109. **Stockmayer, W. H., Kavanagh, G. M., and Mickley, H. S.,** The thermodynamic properties of gaseous sulfur trioxide, *J. Chem. Phys.*, 12, 408, 1944.
110. **Wagman, D. D., Kilpatrick, J. E., Pitzer, K. S., and Rossini, F. D.,** Heats, equilibrium constants, and free energies of formation of the acetylene hydrocarbons through the pentynes, to 1500 K, *J. Res. Natl. Bur. Stand.*, 35, 467, 1945.
111. **Pennington, R. E. and Kobe, K. A.,** Contributions of vibrational anharmonicity and rotation-vibration interaction to thermodynamic functions, *J. Chem. Phys.*, 22, 1442, 1954; errors in the equations of Pennington and Kobe have been pointed out by Gordon, J. S. and Robinson, R., in *Kinetics, Equilibria, and Performance of High-Temperature Systems*, Bahn, G. S., Ed., Gordon & Breach, N.Y., 1963, 39; Durand, J. L., p. 185.
112. **Woolley, H. W.,** Calculation of thermodynamic functions for polyatomic molecules, *J. Res. Natl. Bur. Stand.*, 56, 105, 1956.
113. **Doll, J. D. and Myers, L. E.,** Semiclassical Monte Carlo methods, *J. Chem. Phys.*, 71, 2880, 1979.
114. **Hase, W. L.,** Overview of unimolecular dynamics, in *Potential Energy Surfaces and Dynamics Calculations*, Truhlar, D. G., Ed., Plenum Press, N.Y., 1981, 1.
115. **Isaacson, A. D. and Truhlar, D. G.,** The accuracy of the Pitzer-Gwinn method for partition functions of anharmonic vibrational modes, *J. Chem. Phys.*, 75, 4090, 1981.
116. **Rapp, D.,** *Statistical Mechanics*, Holt, Rinehart & Winston, New York, 1972, chaps. 4, 5, and 11.
117. **Nielsen, H. H.,** The vibration-rotation energies of molecules and their spectra in the infra-red, *Encycl. Phys.*, 37/1, 173, 1959.
118. **Bron, J. and Wolfsberg, M.,** Effect of vibrational anharmonicity on hydrogen-deuterium exchange equilibria involving ammonia molecules, *J. Chem. Phys.*, 57, 2862, 1962.
119. **Bron, J.,** Zero point energy of linear triatomic molecules, *J. Chem. Soc. Faraday Trans. II*, 70, 871, 1974.
120. **Bunker, D. L.,** Monte Carlo calculation of triatomic dissociation rates, *J. Chem. Phys.*, 37, 393, 1962.
121. **Hase, W. L. and Buckowski, D. G.,** Monte Carlo sampling of a microcanonical ensemble of classical harmonic oscillations, *Chem. Phys. Lett.*, 74, 284, 1980.
122. **Noid, D. W., Koszykowski, M. L., Tabor, M., and Marcus, R. A.,** Properties of vibrational energy levels in the quasiperiodic and stochastic regimes, *J. Chem. Phys.*, 72, 6169, 1980.
123. **Adams, J. E. and Doll, J. D.,** Desorption from solid surfaces via generalized Slater theory, *J. Chem. Phys.*, 74, 1467, 1981.
124. **Adams, J. E. and Doll, J. D.,** A Monte Carlo evaluation of thermal desorption rates, *J. Chem. Phys.*, 74, 5332, 1981.
125. **Adams, J. E.,** Vibrational predissociation of $Ar \cdot BCl_3$: a Monte-Carlo study, *J. Chem. Phys.*, 78, 1275, 1983.
126. **Farantos, S. C., Murrell, J. N., and Hajduk, J. C.,** Monte Carlo calculations of classical density of states for non-separable polyatomic potential energy surfaces, *Chem. Phys.*, 68, 109, 1982.
127. **Feit, M. D. and Fleck, J. A., Jr.,** Solution of the Schrödinger equation by a spectral method. II. Vibrational energy levels of triatomic molecules, *J. Chem. Phys.*, 78, 301, 1983.

128. **Saenz, A. W. and O'Rourke, R. C.,** Number of states and the magnetic properties of an electron gas, *Rev. Mod. Phys.*, 27, 381, 1965.
129. **Witschel, W.,** Calculation of the vibrational partition function of polyatomic molecules including Fermi or Darling-Dennison resonance, *Chem. Phys. Lett.*, 2, 349, 1968.
130. **Witschel, W., Großwendt, B., and Bohmann, J.,** Level densities for polyatomic molecules, *Physik. Tech. Bund. Mitt.*, 87, 3, 1977.
131. **Bohmann, J. and Witschel, W.,** Isotopic mass dependence of the dissociation equilibria of diatomic molecules, *J. Chem. Soc. Faraday Trans. II*, 74, 2238, 1978.
132. **Witschel, W. and Bohmann, J.,** On the statistical mechanics of quartic type oscillators, application of variational and perturbation methods, *J. Phys. A*, 13, 2735, 1980.
133. **Witschel, W.,** A statistical variation-perturbation method for the partition function of anharmonic oscillators, *Phys. Lett.*, 77A, 107, 1980.
134. **Bohmann, J. and Witschel, W.,** On the operator formulation of the polyatomic molecule partition function, *Z. Naturforsch.*, 38A, 167, 1983.
135. **Witschel, W.,** Exact results for the statistical thermodynamics of the asymmetric single and double well anharmonic oscillator, *Chem. Phys. Lett.*, 86, 558, 1982.
136. **Girardeau, M. and Mazo, R. M.,** Variational methods in statistical mechanics, *Adv. Chem. Phys.*, 24, 187, 1973.
137. **Bohmann, J. and Witschel, W.,** On a flexible double minimum potential, *Z. Naturforsch.*, 34a, 1106, 1979.
138. **Witschel, W.,** Analytic results for a partition function of a generalized anharmonic oscillator, *Z. Naturforsch.*, 36a, 481, 1981.
139. **Wigner, E. P.,** Über das Übershrieten von Potentialschwellen bei Chemischen Reaktionen, *Z. Phys. Chem. Abt. B*, 19, 203, 1932.
140. **Rapp, D.,** *Statistical Mechanics*, Holt, Rinehart, & Winston, New York, 1972, chaps. 4, 5, and 11.
141. **Skodje, R. T. and Truhlar, D. G.,** Parabolic tunneling calculations, *J. Phys. Chem.*, 85, 624, 1981.
142. **Marcus, R. A.,** On the analytical mechanics of chemical reactions. Quantum mechanics of linear collisions, *J. Chem. Phys.*, 45, 4493, 1966.
143. **Marcus, R. A.,** On the analytical mechanics of chemical reactions. Classical mechanics of linear collisions, *J. Chem. Phys.*, 45, 4500, 1966.
144. **Marcus, R. A.,** Analytical mechanics of chemical reactions. III. Natural collision coordinates, *J. Chem. Phys.*, 49, 2610, 1968.
145. **Marcus, R. A.,** On the theory of chemical reaction cross sections. II. Application to the H + H_2 reaction, *J. Chem. Phys.*, 46, 959, 1967.
146. **Marcus, R. A.,** Local approximation of potential energy surfaces permitting separation of variables, *J. Chem. Phys.*, 41, 610, 1964.
147. **Truhlar, D. G. and Kuppermann, A.,** A test of transition state theory against exact quantum mechanical calculations, *Chem. Phys. Lett.*, 9, 269, 1971.
148. **Truhlar, D. G. and Kuppermann, A.,** Exact and approximate quantum mechanical reaction probabilities and rate constants for the collinear H + H_2 reaction, *J. Chem. Phys.*, 56, 2232, 1972.
149. **Truhlar, D. G., Kuppermann, A., and Adams, J. T.,** Exact quantum mechanical reaction probabilities and rate constants for the isotopic collinear H + H_2 reactions, *J. Chem. Phys.*, 59, 395, 1973.
150. **Marcus, R. A.,** Activated complex theory: current status, extensions, and applications, *Techniques of Chemistry*, Vol. 6, Weissberger, A. and Lewis, E. S., Eds., Wiley - Interscience, N.Y., 1974, 13.
151. **Marcus, R. A. and Coltrin, M. E.,** A new tunneling path for reactions such as H + $H_2 \rightarrow H_2$ + H, *J. Chem. Phys.*, 67, 2609, 1977.
152. **Kemble, E. C.,** *The Fundamental Principles of Quantum Mechanics with Elementary Applications*, Dover, N.Y., 1937.
153. **Heading, J.,** *An Introduction to Phase Integral Methods*, Methuen, London, 1961.
154. **Marcus, R. A.,** Generalization of Activated-complex theory. III. Vibrational adiabaticity, separation of variables, and a connection with analytical mechanics, *J. Chem. Phys.*, 43, 1598, 1965.
155. **Connor, J. N. L.,** On the analytical description of resonance tunneling reactions, *Mol. Phys.*, 15, 37, 1968.
156. **Miller, W. H.,** Semiclassical theory for non-separable systems: construction of "good" action-angle variables for reaction rate constants, *Faraday Discuss. Chem. Soc.*, 62, 40, 1977.
157. **Garrett, B. C. and Truhlar, D. G.,** Semiclassical tunneling calculations, *J. Phys. Chem.*, 83, 2921, 1979.
158. **Wyatt, R. E.,** Quantum mechanics of the H + H_2 reaction: investigation of vibrational adiabatic models, *J. Chem. Phys.*, 51, 3489, 1969.
159. **Skodje, R. T., Truhlar, D. G., and Garrett, B. C.,** Vibrationally adiabatic models for reactive tunneling, *J. Chem. Phys.*, 77, 5955, 1983.

160. **Gray, S. K., Miller, W. H., Yamaguchi, K., and Schaefer, H. F., III,** Reaction path Hamiltonian: tunneling effects in the unimolecular isomerization HNC → HCN, *J. Chem. Phys.*, 73, 2733, 1980.
161. **Marcus, R. A.,** Analytical mechanics of chemical reactions. IV. Classical mechanics of reactions in two dimensions, *J. Chem. Phys.*, 49, 2617, 1968.
162. **George, T. F. and Miller, W. H.,** Classical S-matrix theory of reactive tunneling: linear H + H_2 collisions, *J. Chem. Phys.*, 57, 2458, 1972.
163. **Kuppermann, A., Adams, J. T., and Truhlar, D. G.,** Streamlines of probability current density and tunneling fractions for the collinear H + H_2 → H_2 + H reaction, *Abstr. Pap. 8th Int. Conf. Phys. Electron. At. Collisions*, Institute of Physics, Belgrade, 1973, 149.
164. **Adams, J. T., Kuppermann, A., and Truhlar, D. G.,** Probability current densities, probability densities, and tunneling coefficients for the collinear H + H_2 exchange reaction, unpublished manuscript.
165. **Kuppermann, A.,** Accurate quantum calculations of reactive systems, *Theor. Chem. Adv. Perspect.*, 6A, 79, 1981.
166. **Chapman, S., Garrett, B. C., and Miller, W. H.,** Semiclassical transition state theory for nonseparable systems: application to the collinear H + H_2 reaction, *J. Chem. Phys.*, 63, 2710, 1975.
167. **Kronrod, A. S.,** *Nodes and Weights of Quadrature Formulas*, Consultants Bureau, N.Y., 1965.
168. **Porter, R. N. and Karplus, M.,** Potential energy surface for H_3, *J. Chem. Phys.*, 40, 1105, 1964.
169. **Cohen, N. and Westberg, K. R.,** Chemical kinetic data sheets for high-temperature chemical reactions, Aerospace Report ATR-82(7888)-3, Aerospace Corporation, El Segundo, Calif., July 1982.
170. **McConnell, A. J.** *Applications of the Absolute Differential Calculus*, Blackie & Son, London, 1931, chap. XIII.
171. **Craig, H. V.,** *Vector and Tensor Analysis*, McGraw-Hill, N.Y., 1943, chap. VIII.
172. **Sokolnikoff, I. S.,** *Tensor Analysis*, John Wiley & Sons, N.Y., 1951, section 49.
173. **Thomas, T. Y.,** *Concepts from Tensor Analysis and Differential Calculus*, Academic Press, N.Y., 1965, chap. IV.
174. **Ovchinnikova, M. Ya.,** The tunneling dynamics of the low temperature H exchange reactions, *Chem. Phys.*, 36, 85, 1979.
175. **Babamov, V. K. and Marcus, R. A.,** Dynamics of hydrogen atom and proton transfer reactions. Symmetric case, *J. Chem. Phys.*, 74, 1790, 1981.
176. **Slater, N. B.,** *The Theory of Unimolecular Reactions*, Cornell University Press, Ithaca, N.Y., 1959.
177. **Goldstein, H.,** *Classical Mechanics*, Addison-Wesley, Reading, Mass., 1965, 294.
178. **Hill, T. L.,** *An Introduction to Statistical Thermodynamics*, Addison-Wesley, Reading, Mass., 1960, chap. 6.
179. **Mayer, J. E. and Mayer, M. G.,** *Statistical Mechanics*, 2nd ed., John Wiley & Sons, N. Y., 1977, chap. 7.
180. **Whitten, G. Z., and Rabinovitch, B. S.,** Approximate and facile approximation for vibrational energy-level sums, *J. Chem. Phys.*, 38, 2466, 1963.
181. **Whitten, G. Z. and Rabinovitch, B. S.,** Approximation for rotation-vibrational energy level sums, *J. Chem. Phys.*, 41, 1883, 1964.
182. **Tardy, D. C., Rabinovitch, B. S., and Whitten G. Z.,** Vibration-rotation energy-level density calculations, *J. Chem. Phys.*, 48, 1427, 1968.
183. **Robinson, P. J. and Holbrook, K. A.,** *Unimolecular Reactions*, Wiley-Interscience, London, 1971, chap. 5.
184. **Forst, W.,** Methods for calculating energy level densities, *Chem. Rev.*, 71, 339, 1971.
185. **Huy, L.-K., Forst, W., and Prášil, Z.,** Anharmonic correction factor for vibrational sum of states, *Chem. Phys. Lett.*, 9, 476, 1971.
186. **Stein, S. E. and Rabinovitch, B. S.,** Accurate evaluation of internal energy level sums and densities including anharmonic oscillators and hindered rotors, *J. Chem. Phys.*, 58, 2438, 1973.
187. **Stein, S. E. and Rabinovitch, B. S.,** Examination of approximations to hindered internal rotation in the calculation of energy level sums, *J. Chem. Phys.*, 60, 908, 1974.
188. **Stein, S. E. and Rabinovitch, B. S.,** On the use of exact state counting methods in RRKM rate calculations, *Chem. Phys. Lett.*, 49, 183, 1977.
189. **Hoare, M. R. and Pal, P.,** Densities of states and the complex partition function, *Mol. Phys.*, 20, 695, 1971.
189a **Astholz, D. C., Troe, J., and Wieters, W.,** Unimolecular processes in vibrationally highly excited cycloheptatrienes. I. Thermal isomerization in shock waves, *J. Chem. Phys.*, 70, 5107, 1979.
190. **Doll, J. D.,** Anharmonic corrections in unimolecular rate theory: a Monte Carlo approach, *Chem. Phys. Lett.*, 72, 139, 1980.
191. **Marcus, R. A.,** Analytical mechanics and almost vibrationally adiabatic chemical reactions, *Discuss. Faraday Soc.*, 44, 7, 1968.

192. **Wyatt, R. E.,** Theory of three-dimensional reactive collisions using natural collision coordinates, *J. Chem. Phyus.*, 56, 390, 1972.
193. **Harms, S. H. and Wyatt, R. E.,** Hindered asymmetric top states for chemical reactions, *J. Chem. Phys.*, 62, 3162, 1975.
194. **Harms, S. H. and Wyatt, R. E.,** Hindered asymmetric top wavefunctions for three-dimensional H + H_2, *J. Chem. Phys.*, 62, 3173, 1975.
195. **Elkowitz, A. B. and Wyatt, R. E.,** Approximate hindered asymmetric top wavefunctions for atom-diatom molecule collisions, *J. Chem. Phys.*, 62, 3683, 1975.
196. **Elkowitz, A. B. and Wyatt, R. E.,** Three-dimensional natural collision coordinate asymmetric top theory of reactions. Application to H + H_2, *J. Chem. Phys.*, 63, 702, 1975.
197. **Harms, S. H., Elkowitz, A. B., and Wyatt, R. E.,** Asymmetric top states for chemical reactions: angular representations, avoided crossings, and bifurcation, *Mol. Phys.*, 31, 177, 1976.
198. **Elkowitz, A. B. and Wyatt, R. E.,** J, conserving approximation for the hydrogen exchange reactions, *Mol. Phys.*, 31, 189, 1976.
199. **Redmon, M. J. and Wyatt, R. E.,** Three-dimensional quantum mechanical studies of the H + H_2 and F + H_2 reactions, *Int. J. Quantum Chem. Symp.*, 9, 403, 1976.
200. **Quack, M. and Troe, J.,** Complex formation in reactive and inelastic scattering: statistical adiabatic channel model of unimolecular processes. III, *Ber. Bunsenges. Phys. Chem.*, 79, 171, 1975.
201. **Quack, M.,** Detailed symmetry selection rules for reactive collisions, *Mol. Phys.*, 34, 477, 1977.
202. **Chiu, Y.-N.,** Vibronic symmetry correlation in molecular combination and dissociation, *J. Chem. Phys.*, 64, 2997, 1976.
203. **Metropoulos, A. and Chiu, Y.-N.,** Rotation-vibration symmetry correlation in bimolecular reactions: building-up principle from molecular fragments, *J. Chem. Phys.*, 68, 5607, 1978.
204. **Morokuma, K. and Kato, S.,** Potential energy characteristics for chemical reactions, in *Potential Energy Surfaces and Dynamics, Calculations*, Truhlar, D. G., Ed., Plenum Press, N.Y., 1981, 243.
205. **Yamashita, K., Yamabe, T., and Fukui, K.,** IRC approach to chemical dynamics: toward mode-selective chemical reactions, *Chem. Phys. Lett.*, 84, 123, 1981.
206. **Yamashita, K., Yamabe, T., and Fukui, K.,** Dynamic behavior of the IRC in chemical laser systems, *Theor. Chim. Acta*, 60, 523, 1982.
207. **Truhlar, D. G. and Isaacson, A. D.,** Statistical-diabatic model for state-selected reaction rates. Theory and application of vibrational-mode correlation analysis to $OH(n_{OH})$ + $H_2(n_{HH}) \rightarrow H_2O$ + H, *J. Chem. Phys.*, 77, 3516, 1982.
208. **Miller, W. H.,** Tunneling corrections to unimolecular rate constants, with application to formaldehyde, *J. Am. Chem. Soc.*, 101, 6810, 1979.
209. **Miller, W. H.,** Unified statistical model for "complex" and "direct" reaction mechanisms, *J. Chem. Phys.*, 65, 2216, 1975.
210. **Pollak, E. and Pechukas, P.,** Unified statistical model for "complex" and "direct" reaction mechanisms: a test on the colinear H + H_2 exchange reaction, *J. Chem. Phys.*, 70, 325, 1979.
211. **Garrett, B. C. and Truhlar, D. G.,** Canonical unified statistical model. Classical mechanical theory and applications to collinear reactions, *J. Chem. Phys.*, 76, 1853, 1982.
212. **Chesnavich, W. J., Bass, L., Su, T., and Bowers, M. T.,** Multiple transition states in unimolecular reactions: a transition-state switching model. Application to the $C_4H_8^+$ system, *J. Chem. Phys.*, 74, 2228, 1981.
213. **Miller, W. H.,** Reaction path Hamiltonian for polyatomic systems: further developments and applications, in *Potential Energy Surfaces and Dynamics Calculations*, Truhlar, D. G., Ed., Plenum Press, N.Y., 1981, 265.
214. **Light, J. C.,** Statistical theory of bimolecular exchange reactions, *Discuss. Faraday Soc.*, 44, 14, 1967.
215. **Hirschfelder, J. O. and Wigner, E.,** Some quantum-mechanical considerations in the theory of reactions involving an activation energy, *J. Chem. Phys.*, 7, 616, 1939.
216. **Child, M. S.,** Measurable consequences of a dip in the activation barrier for an adiabatic chemical reaction, *Mol. Phys.*, 12, 401, 1967.
217. **Connor, J. N. L.,** On the analytical description of resonance tunneling reactions, *Mol. Phys.*, 15, 37, 1968.
218. **Miller, W. H.,** Effect of reaction path curvature and dimensionality on the accuracy of classical transition state theory, *J. Chem. Phys.*, 76, 4904, 1982.
219. **Garrett, B. C. and Truhlar, D. G.,** Improved canonical variational theory for chemical reaction rates. Classical mechanical theory and applications to collinear reactions, *J. Phys. Chem.*, 84, 805, 1980.
220. **Kuppermann, A.,** An exact quantum mechanical transition state theory. I. An overview, *J. Phys. Chem.*, 83, 171, 1979.
221. **Bowman, J. M., Ju, G.-Z., Lee, K.-T., Wagner, A. F., and Schatz, G. C.,** Tests of collinear quasi-classical trajectory transmission coefficient correction to transition state theory, *J. Chem. Phys.*, 75, 141, 1981.

222. **Bowman, J. M., Ju, G.-Z., and Lee, K.-T.,** New approximate quantum cross sections for the H + H_2 reaction, *J. Chem. Phys.*, 75, 5199, 1981.
223. **Lee, K.-T., Bowman, J. M., Wagner, A. F., and Schatz, G. C.,** A comparative study of the reaction dynamics of the $O(^3P) + H_2 \rightarrow OH + H$ reaction on several potential energy surfaces. II. Collinear exact quantum transmission coefficient correction to transition state theory, *J. Chem. Phys.*, 76, 3583, 1982.
224. **Bowman, J. M., Ju, G.-Z., and Lee, K.-T.,** Incorporation of collinear exact quantum reaction probabilities into three-dimensional transition state theory, *J. Phys. Chem.*, 86, 2232, 1982.
225. **Bowman, J. M., Lee, K.-T., and Ju, G.-Z.,** Approximate quantum differential cross sections for the F + H_2 reaction, *Chem. Phys. Lett.*, 86, 384, 1982.
226. **Lee, K.-T. and Bowman, J. M.,** Approximate quantum differential cross sections for the F + HD → HF + D and DF + H reactions, *J. Phys. Chem.*, 86, 2289, 1982.
227. **Bowman, J. M. and Lee, K.-T.,** Reduced dimensionality quantum calculations of integral cross sections for $H + H_2(v = 1) \rightarrow H_2(v' = 0), H_2(v' = 1) + H$, *Chem. Phys. Lett.*, 94, 363, 1983.
228. **Mortensen, E. M.,** Permeabilities and transmission coefficients for various isotopic reactions of the type $H + H_2 \rightarrow H_2 + H$, *J. Chem. Phys.*, 48, 4029, 1968.
229. **Hayes, E. F. and Walker, R. B.,** Reactive differential cross sections in the rotating linear model: is there a resonance in the F + $H_2(v = 0)$ reaction?, *J. Chem. Phys.*, in press.
230. **Anderson, J. B. and Kung, R. T. V.,** Vibrational population inversion in hydrogen iodide from H + I_2 → HI + I, *J. Chem. Phys.*, 58, 2477, 1973.
231. **Anderson, J. B.,** A test of the validity of the combined phase-space/trajectory method, *J. Chem. Phys.*, 52, 2446, 1975.
232. **Porter, R. N.,** Molecular trajectory calculations, *Annu. Rev. Phys. Chem.*, 25, 317, 1974.
233. **Smith, I. W. M.,** Combining transition state theory with quasiclassical trajectory calculations. I. Collinear collisions, *J. Chem. Soc. Faraday Trans. II*, 77, 747, 1981.
234. **Pollak, E. and Pechukas, P.,** Transition states, trapped trajectories, and classical bound states embedded in the continuum, *J. Chem. Phys.*, 69, 1218, 1978.
235. **Pechukas, P. and Pollak, E.,** Transition state theory is exact if the transition state is unique, *J. Chem. Phys.*, 71, 2062, 1979.
236. **Pollak, E., Child, M. S., and Pechukas, P.,** Classical transition state theory: a lower bound to the reaction probability, *J. Chem. Phys.*, 72, 1669, 1980.
237. **Truhlar, D. G. and Dixon, D. A.,** Direct-mode chemical reactions: classical theories, in *Atom-Molecule Collision Theory: A Guide for the Experimentalist*, Bernstein, R. B., Ed., Plenum Press, N.Y., 1979, 595.
238. **Miller, W. H.,** Classical-limit quantum mechanics and the theory of molecular collisions, *Adv. Chem. Phys.*, 25, 69, 1974.
239. **Miller, W. H.,** Classical S-matrix in molecular collisions, *Adv. Chem. Phys.*, 30, 77, 1975.
240. **Child, M. S.,** Semiclassical effects in heavy-particle collisions, *Adv. At. Molec. Phys.*, 14, 225, 1978.
241. **Marcus, R. A.,** Energy distributions in unimolecular reactions, *Ber. Bunsenges. Phys. Chem.*, 81, 190, 1977.
242. **Bowman, J. M., Kuppermann, A., Adams, J. T. and Truhlar, D. G.,** A direct test of the vibrationally adiabatic theory of chemical reactions, *Chem. Phys. Lett.*, 20, 229, 1973.
243. **Hase, W. L.,** Unimolecular variational transition state theory, *Acc. Chem. Res.*, 16, 258, 1983.
244. **Greene, E. F. and Kuppermann, A.,** Chemical reaction cross sections and rate constants, *J. Chem. Educ.*, 45, 361, 1968.
245. **Ross, J., Light, J. C., and Schuler, K. E.,** Rate coefficients, reaction cross sections, and microscopic reversibility, in *Kinetic Processes in Gases and Plasmas*, Hochstim, A. R., Ed., Academic Press, N.Y., 1969, 281.
246. **Christov, S. G.,** Quantum-mechanical theory of reaction rates, *Ber. Bunsenges. Phys. Chem.*, 76, 507, 1972.
247. **Christov, S. G.,** On the quantum-mechanical and classical treatment of chemical kinetics, *Ber. Bunsenges. Phys. Chem.*, 78, 537, 1974.
248. **Christov, S. G. and Parlapanski, M.,** Quantum effects and isotopic effects in chemical kinetics, *Int. J. Chem. Kinet.*, 11, 665, 1979.
249. **Christov, S. G.,** Collision theory test of bimolecular and unimolecular reactions and its experimental test, *Int. J. Quantum Chem.*, 18, 253, 1980.
250. **Christov, S. G.,** Collision theory treatment of monomolecular and bimolecular gas reactions, *Int. J. Quantum Chem.*, 12, 495, 1977.
251. **Christov, S. G.,** The exact transition-state theory and its relations to collision theory, *J. Res. Inst. Catalysis Hokkaido Univ.*, 28, 119, 1980.
252. **Eyring, H., Walter, J., and Kimball, G. E.,** *Quantum Chemistry*, John Wiley & Sons, N.Y., 1944, chap. 16; see Reference 12 of Reference 21 for a list of errors in this derivation.
253. **Truhlar, D. G.,** The adiabatic theory of chemical reactions, *J. Chem. Phys.*, 53, 2041, 1976.

Errata for "Generalized Transition State Theory"

This section contains all known errata to the GTST book chapter (Ref. 5 in Sect. 21) by D. G. Truhlar, A. D. Isaacson, and B. C. Garrett.

1. p. 71, line 1: $V[x_{i\gamma}])$ should be $V([x_{i\gamma}])$.

2. p. 71, third line after eq. (6): "coordinate(s)" should be "coordinate (s)".

3. p. 77, Fig. caption line 3: "1 molecule and per centimeter, anharmonicity" should be "1 molecule per centimeter, and anharmonicity".

4. p. 78, second line after eq. (15): $\nabla V(R)_j'$ should be $\nabla V(R_j')$.

5. p. 81, eq. (31): $x_{i'\gamma'}$ should be $x_{i'\beta'}$.

6. p. 82, eq. (35), line 1: $(m_A + m_B)^{-1}$ should be M^{-1} where M is the total mass.

7. same equation, line 2: insert "μ_f" in numerator.

8. p. 83, line 2: $Q^{GT,0}(T,s)$ should be $Q^{GT}(T,s)$.

9. p. 83, line 8: $\Phi_V^R(T)$ should be $\Phi_C^R(T)$.

10. p. 83, second line from the bottom: Δ should be ΔG.

11. p. 84, first line after eq. (42): ΔG_C^{GT} should be $\Delta G_C^{GT,0}$

12. p. 88, line 16: "accurage" should be "accurate".

13. p. 94, eq.(85c): add "β" before "V" in first exponential.

14. p. 95, line after eq. (91): "MED" should be "MEP".

15. p. 97, eq. (98) should read

$$B_{mF} = -\sum_{i=1}^{N}\sum_{\gamma}\frac{d\left\{\left[sign(s)\right]v_{i\gamma}(s)\right\}}{ds}L_{i\gamma,m}^{GT}(s)$$

or

$$B_{mF} = -\sum_{i=1}^{N}\sum_{\gamma}\frac{dv_{i\gamma}(s)}{d|s|}L^{GT}_{i\gamma,m}(s)$$

16. p. 97, second line after eq. (98): $B_{mF(s)}$ should be $-B_{mF(s)}$.

17. p. 97, third line after eq. (98): $1 - \kappa(s) \bullet \mathbf{Q}(s)]^2$ should be $[1 - \kappa(s) \bullet \mathbf{Q}(s)]^2$.

18. p. 97, second and third lines after eq. (100): "μ" should not be a subscript.

19. p. 97, third line after eq. (101): $[\hbar/\mu\omega_m(s)]1/2$ should be $[\hbar/\mu\omega_m(s)]^{1/2}$.

20. p. 101, in the last sentence, the gradient in the product channel (or reactant channel) should by multiplied by -1.

21. p. 102, line 7: "is $\boldsymbol{x}(s)$" should be "is $\dot{\boldsymbol{x}}(s)$."

22. p. 102, fourth and fifth lines after eq. (126): "$\mathbf{x}$" should be "$\dot{\boldsymbol{x}}$" in three places.

23. p. 102, line after eq. (127b): "B" should be β in two places, and "B/2" should be $\pi/2$. Thus below eq. (127), the inequality should be $0 < \beta < \pi/2$.

24. p. 102, line after eq. (128): "XB" should be "A + XB".

25. p. 102, second line after eq. (128): x^R should be $\dot{x}^R$.

26. p. 103: eq. (130) should be the special case of eq. (157) with $\tilde{\alpha}_0 = 1$, i.e., insert $\sin\left(\chi\left(\tilde{\alpha}_0 = 1, s_0\right)\right)$ before $d\tilde{s}_0$.

27. p. 104, fifth line after eq. (131): "mass-weighted coordinates **x** the" should be "mass-scaled coordinates **x**; the".

28. p. 104, second line after eq. (133): $\tilde{s}_1$ should be $\tilde{s}_0$.

29. p. 104, second line after eq. (134): "zt" should be "at" and "normal" should be "generalized normal coordinates".

30. p. 104, third line after eq. (134): "coordinate(s)" should be "coordinate (s)".

31. p. 104, eq. (135) and following: notice that $q_{\perp,m}$ depends on $\tilde{s}_1$ as well as $\tilde{s}_0$.

32. p. 106, eq. (144): insert a minus sign before the left-hand side because every term in the sum is negative.

33. p. 106, eq. (146): the condition $Q_m < t_m$ should be replaced by eq. (143).

34. p. 106: eq. (147) should be the special case of eq. (159) with $\tilde{\alpha}_0 = \tilde{\alpha}_1 = 1$.

35. p. 110, line 6: 147 should be 148a.

36. p. 117, line 3: "reactant" should be "reactants".

37. p. 117, second line from bottom: $p_2 : p_1$ should be p_2/p_1.

38. p. 118, second line from bottom: ":" should be "/" in two places.

39. p. 121, line below eq. (209): "N_m - 1/2" should be "$(N_m + 1/2)/h$ ".

40. p. 121, eq. (210): $1/4\pi h$ should be π.

41. p. 123, second line above eq. (217): "satte" should be "state".

42. Ref. 58, line 1: "B.D." should be "B.C.".

43. Ref. 71, line 2: "Vol. 2" should be "Vol. 4 of Modern Theoretical Chemistry".

44. Ref. 192, line 2: "*Phyus*" should be "*Phys*".

45. Ref. 231, line 2: "52" should be "62".